The Role of Phospholamban and Sarcolipin in Skeletal Muscle Disease

by

Val Andrew M. Fajardo

A thesis
presented to the University of Waterloo
in fulfillment of the
thesis requirement for the degree of
Doctor of Philosophy
in
Kinesiology

Waterloo, Ontario, Canada, 2015
©Val Andrew M. Fajardo

AUTHOR'S DECLARATION

This thesis consists of material all of which I authored or co-authored: see Statement of Contributions included in the thesis. This is a true copy of the thesis, including any required final revisions, as accepted by my examiners.

I understand that my thesis may be made electronically available to the public.

Val Andrew M. Fajardo

Statement of Contributions

Chapters 2, 3, and 4 of this thesis are presented as manuscripts published or currently in submission, and all manuscripts were a joint effort across several co-authors. The contributions from every author for each of the chapters are listed below.

Chapter 2 – Thesis Study I:

Phospholamban overexpression in mice causes a centronuclear myopathy-like phenotype

Val A. Fajardo[1§], Eric Bombardier[1§], Elliott McMillan[1], Khanh Tran[1], Brennan J. Wadsworth[1], Daniel Gamu[1], Andrew Hopf, Chris Vigna[1], Ian C. Smith[1], Catherine Bellissimo[1], Robin N. Michel[2], Mark A. Tarnopolsky[3,4,5], Joe Quadrilatero[1], A. Russell Tupling[1]*

From the [1]Department of Kinesiology, University of Waterloo, Waterloo, Ontario, Canada, [2]Department of Exercise Science, Concordia University, Montreal, Quebec, Canada, [3]Departement of Kinesiology, [4]Department of Pediatrics, and [5]Department of Medicine, McMaster University, Hamilton, Ontario, Canada.

A.R.T., V.A.F., and E.B. conceived the study idea. V.A.F. coordinated Western blot experiments and with K.T. performed the Western blot analyses. E.B. and C.B. performed the histological and histochemical analysis. E.B., C.B, and E.M performed the immunofluorescence staining experiments. V.A.F., D.G., and A.H., performed SERCA ATPase activity. V.A.F. and C.V. performed Ca^{2+} uptake measures. E.M. performed proteolytic activity and oxidative stress assays. V.A.F. and E.B. performed plasma creatine kinase analysis. B.J.W. and I.C.S. conducted soleus contractile analysis. V.A.F. conducted treadmill running. J.Q. and A.R.T. contributed reagents, materials, and analysis tools. M.T. provided the muscle biopsies from CNM patients. A.R.T. and V.A.F. wrote the manuscript that was reviewed by all authors.

Chapter 3 – Thesis Study II (currently in submission in Brain and Behaviour as of Sept. 11, 2015):

Diaphragm assessment in mice overexpressing phospholamban in slow-twitch type I muscle fibres

Val Andrew Fajardo[1], Ian Curtis Smith[1], Eric Bombardier[1], Paige J Chambers[1], Joe Quadrilatero[1], A. Russell Tupling[1]

From the [1]Department of Kinesiology, University of Waterloo, Waterloo, Ontario, Canada

V.A.F. and A.R.T. conceived the study idea. V.A.F. performed Western blot analyses on SERCA isoforms, SLN, PLN, and dynamin 2. V.A.F. performed SERCA activity and Ca^{2+} uptake assays on diaphragm, gluteus minimus and soleus muscles. I.C.S. conducted the *in vitro* contractility experiments. V.A.F. performed the histological/histochemical/immunofluorescence experiments and E.B. analyzed the images. P.J.C. performed nuclear fraction isolation and NFAT Western blots. J.Q. provided materials and equipment. V.A.F. and A.R.T. wrote the manuscript that was approved by all authors.

Chapter 4 – Thesis Study IV (currently in submission in Journal of Biological Chemistry as of Dec. 14, 2015):

Sarcolipin is vital for muscle growth and remodelling and counters disease pathology

Val A. Fajardo, Dan Gamu, Bradley A. Rietze, Catherine Bellissimo, Andrew Mitchell, Darin Bloemberg, Paige J. Chambers, Frenk Kwon, Eric Bombardier, Joe Quadrilatero, A. Russell Tupling*

Department of Kinesiology, University of Waterloo, 200 University Ave., Waterloo, ON, N2L 3G1 Canada

A.R.T. and V.A.F. conceived the study idea. V.A.F., D.G, D.B., P.J.C., and F.K. performed Western blot analyses. V.A.F. performed SERCA ATPase, Ca^{2+} uptake, TEM, serum creatine kinase, and *in vitro* contractility experiments. D.G. performed CLAMS analyses for daily food intake and ambulation. A.M. performed the proteolytic activity assays. V.A.F., B.A.R., and C.B. performed histological, histochemical, and immunofluorescent staining. B.A.R. and E.B. analyzed fibre type distribution and cross-sectional area. V.A.F. and P.J.C. performed the simultaneous plantaris mechanical overload and soleus tenotomy surgeries, and C.B. conducted the cardiotoxin injections. V.A.F. designed the breeding strategy for generating the Pln^{OE}/Sln^{KO} and mdx/Sln^{KO} mice, which was carried out by V.A.F., C.B., F.K., and P.J.C. J.Q. and A.R.T contributed reagents, materials, and analysis tools. A.R.T. and V.A.F. wrote the manuscript that was reviewed by all authors.

Abstract

Sarcolipin (SLN) and phospholamban (PLN) are two small proteins that physically interact with and inhibit the sarco(endo)plasmic reticulum Ca^{2+}-ATPase (SERCA) pump. Results from our laboratory and others have shown that, under conditions of high-fat feeding, SLN is recruited in skeletal muscles to uncouple SERCA-mediated Ca^{2+} transport from ATP hydrolysis thereby increasing energy expenditure by the SERCA pumps and combating obesity. Since, PLN is considered structurally and functionally homologous with SLN, we initially questioned whether PLN could also uncouple the SERCA pump, increase energy expenditure, and combat the obesigenic effects of a high-fat diet. To this end, we purchased commercially available mice that overexpressed PLN (Pln^{OE}); however, the surprising discovery of pathology within their soleus muscles shifted the focus from metabolism to myopathy.

In the first study of this thesis, the overall objectives were to characterize the Pln^{OE} mouse model with respect to SERCA and muscle function, and to diagnose the disease found in their skeletal muscles. Since the Pln^{OE} mice were designed to overexpress PLN specifically in their type I skeletal muscle fibres, the analyses of this study was restricted to the postural muscles, soleus and gluteus minimus, that normally contain approximately 55-65% and 27% type I fibre proportions, respectively. As a result of the 6-to-7-fold upregulation in the inhibitory PLN protein, reductions in SERCA's apparent affinity for Ca^{2+} (-0.16 K_{Ca} in *p*Ca units, $P \leq 0.05$), maximal activity (-15-28%, $P \leq 0.05$), and Ca^{2+} uptake (-20-74%, $P \leq 0.05$) in the soleus and gluteus minimus muscles from Pln^{OE} mice were observed. Reductions in the rates of relaxation (-*d*F/*d*t, -60%, $P \leq 0.05$) in isolated soleus muscles assessed *in vitro* further support the decrements in SERCA function. With respect to

the myopathy, the soleus muscles exhibited muscle weakness and progressive atrophy, which was associated with an overall enhancement of all the major proteolytic pathways existing in skeletal muscle (caspase-3, cathepsin, calpain, and proteasome, $P \leq 0.05$) and oxidative stress revealed with dichlorofluoroscein fluorescence assays ($P \leq 0.05$) and protein nitrosylation ($P \leq 0.05$). Moreover, results from histological, histochemical, and immunofluorescent analyses of the Pln^{OE} soleus and gluteus minimus muscles revealed greater central nuclei, type I fibre predominance and hypotrophy, and central aggregation of oxidative activity, suggesting that the myopathy found in these muscles resembled the rare congenital disease centronuclear myopathy (CNM). Interestingly, preliminary findings from muscle biopsies from three CNM patients and five healthy controls revealed that, in CNM, SERCA function is significantly impaired (-53% maximal activity, $P \leq 0.05$) and is associated with a trending increase in PLN expression ($P = 0.08$); however future experiments with more CNM patients that are genetically related are required to further examine PLN's potential role in CNM. Nevertheless, the results from study I demonstrate, for the first time, the importance of PLN in skeletal muscle health and disease, and have uncovered a novel model for CNM to test novel mechanisms and therapeutic strategies.

In study II, the diaphragm muscles from Pln^{OE} mice were examined because these types of investigations that assess respiratory function in animal models of CNM are limited. Since the diaphragm muscles typically comprise of 10% type I fibres, it was hypothesized that the diaphragm muscles would also display impaired SERCA function, muscle weakness, and CNM pathology. The results from this study; however, indicate that although SERCA's affinity for Ca^{2+} was significantly lower in the Pln^{OE} diaphragm compared with wild-type (-0.07 K_{Ca} in pCa units, $P \leq 0.05$), SERCA function was not impaired to the extent seen in the

Pln^{OE} soleus and gluteus minimus muscles with no differences in maximal SERCA activity and only a 15% reduction in Ca^{2+} uptake that did not reach statistical significance ($P = 0.08$). Moreover, there was very little pathology in the *Pln*^{OE} diaphragm with no impairments in *in vitro* force contractility and only type I fibre hypotrophy being evident with no central nuclei, type I fibre predominance, or central aggregation of oxidative activity. Thus, the diaphragm muscles appear to confer resistance to *Pln*^{OE}-induced myopathy and understanding the underlying mechanisms may lead to novel therapeutic strategies.

One interesting possibility that was tested in this thesis involved the potential role of SLN, which was upregulated according to disease severity in the *Pln*^{OE} mice as SLN was increased 7-9 fold ($P \leq 0.05$) in the *Pln*^{OE} gluteus minimus and soleus muscles; but only increased 2.5-fold ($P \leq 0.05$) in the *Pln*^{OE} diaphragm. Similar patterns of SLN expression were previously observed in the dystrophic *mdx* and *mdx*/*utrophin*-null mouse models where SLN was found upregulated to a greater extent in the *mdx*/*utrophin*-null mouse which exhibits far worse dystrophic pathology. The question of whether this increase in SLN represents a maladaptive or adaptive role in myopathy was the focus of study III in this thesis. To this end, three separate mouse models of myopathy were tested.

First, the role of SLN in the *Pln*^{OE}-induced myopathy was assessed by generating the *Pln*^{OE}/*Sln*^{KO} mouse. The results from these experiments show that in the absence of *Sln* the *Pln*^{OE} induced myopathy was worsened with greater reductions in *in vitro* soleus force production and muscle mass relative to body weight ($P \leq 0.05$). The exacerbated muscle weakness and atrophy could not be attributed to differences in food intake, daily activity, or muscle proteolysis, and was instead accounted for by a failure to promote type II fibre hypertrophy. In response to *Pln* overexpression and the concomitant reduction in type I fibre

cross-sectional area, the type II fibres hypertrophy ($P \leq 0.05$) and transition towards a slower oxidative fibre population ($P \leq 0.05$) – a result due to the increased load bearing activities of the type II fibres that subsequently activate the Ca^{2+}-dependent serine/threonine phosphatase calcineurin. Without *Sln*, the Pln^{OE}/Sln^{KO} mice had lower activation of calcineurin revealed by greater levels of phosphorylated nuclear factor of activated T-cells (NFAT, $P \leq 0.05$) thereby causing a failure in the type II fibres to hypertrophy and transition to a slow fibre population. Interestingly, similar effects were observed in mechanical overload experiments where WT plantaris muscles exhibited ectopic SLN expression, myofibre hypertrophy and a transition towards a slow-oxidative population ($P \leq 0.05$) as a result of calcineurin activation (61% lower phosphorylation of NFAT, $P \leq 0.05$). In contrast, Sln^{KO} plantaris muscles failed to hypertrophy and transition to a slow-oxidative phenotype as a result of a blunted activation of calcineurin (22% lower phosphorylation of NFAT, $P = 0.11$). Collectively, the results from these experiments suggest that the SLN upregulation in the Pln^{OE} mouse is critical in triggering calcineurin and mediating adaptive muscle remodeling.

The second mouse model of disease used in study III was the tenotomized soleus, which is a model of hindlimb unloading known to cause muscle degeneration. The results from these experiments revealed that in the absence of a 14-fold upregulation of SLN, the soleus muscles exhibited greater muscle atrophy ($P \leq 0.05$), associated with larger percent reductions in myofibre cross-secitonal area (CSA) and an accelerated slow-to-fast fibre type transition. Consistent with SLN's role in activating calcineurin, tenotomy resulted in a significantly lower phophorylation of NFAT in WT soleus (-57%, $P \leq 0.03$), which was blunted in the Sln^{KO} soleus (-32%, $P = 0.06$). Taken together, these results suggests that SLN

upregulation, as result of muscle unloading, is required to amplify calcineurin signaling to counteract/stabilize the effects of muscle atrophy and slow-to-fast fibre type transitions.

Finally, the role of SLN in the *mdx* mouse was determined by generating *mdx*/*Sln*^{KO} mice. Consistent with the findings throughout study III, in the absence of *Sln* the myofibres of the *mdx*/*Sln*^{KO} mice exhibited smaller CSA ($P \leq 0.05$) and a slow-to-fast fibre type transition ($P \leq 0.05$). Since promoting the slow-fibre population is considered a valid therapeutic strategy with the leading mechanistic hypothesis being an induction of utrophin, the slow-to-fast fibre type shift in the *mdx*/*Sln*^{KO} mice is maladaptive. Indeed, this fibre type shift did result in lowered utrophin expression compared with *mdx* ($P \leq 0.05$). Utrophin is a dystrophin homolog that provides compensatory membrane stability in the absence of dystrophin, and its expression is largely controlled by calcineurin. Thus, these results are in support of SLN's role in activating calcineurin and can account for the worsened dystrophic pathology with greater myofibre degeneration revealed by an elevated serum creatine kinase concentration ($P \leq 0.05$) and greater variation in the minimal Feret's diameter ($P \leq 0.05$), an indicator of dystrophic pathology. The increased variability in fibre diameter is likely due to the combined effects of increased degeneration, reduced myofibre cross-sectional area, and impaired regenerative capacity ($P \leq 0.05$) in the absence of *Sln*.

Taken together the results from study III have answered the questioned pertaining to SLN's role in skeletal muscle disease, a question that has remained elusive for many years. These findings clearly demonstrate that SLN is vital in activating muscle growth and remodeling and counters disease pathology by promoting calcineurin signaling. Combined with the findings in the *Pln*^{OE} mouse in study I, the results from study III show that although PLN and SLN are structurally homologous and are both capable of inhibiting SERCA

function, their physiological roles in skeletal muscle may differ. Specifically, increased PLN expression can cause skeletal muscle atrophy and disease whereas increased SLN is required to counter it. Thus, the collective results from this thesis reveal the importance of PLN and SLN in skeletal muscle disease.

Acknowledgements

First, thank you to my wife, Beth, who has been so patient throughout my entire career as a graduate student. It is my hope that all the hard work that I put in to this will be rewarded soon, and I will be able to provide for you and my family. I could not have done this without your tremendous support. You were always there to listen to all my problems and watch all my presentations. It took tremendous courage from you to let me wear Adidas and PUMA everyday.

Thank you to my parents. If you had not brought me here from Philippines I would have never known SERCA, sarcolipin or phospholamban. In all seriousness, everything I am now is a result of how you raised me. I hope that the work that I have done to obtain this PhD makes you proud and is everything you had hoped for when you brought us over to Canada.

Thank you to my in-laws, the Eppendorfs. Despite, having no connection to the Eppendorf Company, you have contributed so much to the success of this thesis by providing your continual support. I apologize for the days in which it seemed as though my mind was elsewhere – it was with sarcolipin and phospholamban. I look forward to our future together as a family, as I know it will be filled with great fun and laughter.

Thank you to my supervisor, Dr. Russ Tupling. Thank you for allowing me to switch gears from metabolism to myopathy. It was an honour and a pleasure working for you. I hope one day, if given the opportunity, that I will be half as good of a supervisor as you. I have learned so many valuable things from you, not just the in the lab, but, perhaps more importantly, in life as well. The way you balance life and school is inspiring, and I hope to achieve that same balance. I'll start with buying a van.

Thank you Dr. Paul LeBlanc for your continual mentorship and friendship. When I get back to the Niagara region then we can officially start counting who wins our golf matches.

To my lab mates past and present: we have accomplished so many great things together. I went into my PhD with the mentality of going in just to get things done; but the value of the friendships I've gained throughout my PhD undoubtedly outweighs any journal publication of any impact. Eric, Chris, Ian, Dan, Anton, and Khanh – thank you for accepting my application into your wolf pack. You are all exceptional role models in science and in life. Paige, Cat, Frenk, Riley, and Emma – you have so much to look forward to in your future with this lab and with Russ. Absorb it all and have fun. I wish you all the best of success in your research!

To my family and friends: I am deeply sorry. I apologize for the times where I chose school over you. Your patience and support has helped me through this PhD and I am so grateful to have you all in my life.

It is clear that I have been blessed throughout my time as a PhD student. I have been blessed with an amazing wife, incredible friends, family, role models, and an exceptional supervisor, that have all helped me along the way. Thank you God.

Dedication

This work is dedicated to my beautiful wife Beth, the strongest woman I know, and the little bun and future buns in the oven...and, of course, Stevie.

Table of Contents

List of Figures

List of Tables

List of Abbreviations

ATP – adenosine triphosphate

ANOVA – analysis of variance

β-MHC – beta myosin heavy chain promoter

CAMKII – Ca^{2+}-calmodulin dependent kinase II

Ca^{2+} - calcium

$[Ca^{2+}]_i$ – intracellular calcium concentration

$[Ca^{2+}]_f$ – free calcium concentration

CCD – central cores disease

CK – creatine kinase

CLAMS – comprehensive laboratory animal monitoring system

CNM – centronuclear myopathy

COX – cytochrome *c* oxidase

CSA – cross-sectional area

CuZnSOD – Copper zinc superoxide dismutase

DNA – deoxyribonucleic acid

DNM2 or Dnm2 – gene encoding dynamin 2 protein in human or mouse

DCF – dichlorofluoroscein

DHPR – dihidropyridine receptors

DMD – Duchenne's muscular dystrophy

-df/dt – Rate of force decay/relaxation

+df/dt – Rate of force production

ECC – excitation-contraction coupling

ECL – enhanced chemiluminescence

K_{Ca} – concentration of Ca^{2+} required to elicit half maximal SERCA activity

MEF2 – myocyte enhancer factor 2

mdx – mouse model for Duchenne's muscular dystrophy

mdx/*Sln*^{KO} – mouse model for Duchenne's muscular dystrophy

mdx/*Utr*$^{-/-}$ – mouse model for Duchenne's muscular dystrophy without utrophin protein

MHC – myosin heavy chain

mMD – multiplie minicores disease

MTM1 or *mtm1* – gene encoding for myotubularin 1 in human or mouse

M1-M10 – SERCA's 10 transmembrane helices

NFAT – nuclear factor of activated T-cells

NADH-TR – nicotinamide adenine dinucleotide tetrazolium reductase

NM – nemaline myopathy

Ny - nitrosylation

OV – mechanical overload induced by soleus and gastrocnemius tenotomy

*p*Ca – negative logarithm of the concentration of Ca^{2+}

PCR – polymerase chain reaction

PGC-1α – Peroxisome proliferator-activated receptor gamma coactivator 1-alpha

PIP3 – phosphoinositide-3 phosphate

PI3K – phosphoinositide-3 kinase

PLN – phospholamban

PLN or *Pln* – gene encoding phospholamban in human or mouse

Pln$^{-/-}$ - mouse model with phospholamban genetically removed

Pln^{OE} – mouse model of PLN overexpression in slow-twitch type I fibres

Pln^{OE}/*Sln*^{KO} – mouse model PLN overexpression in slow-twitch type I fibres without SLN

PVDF – polyvinylidene difluoride

RyR – ryanodine receptor

SDH – succinate dehydrogenase

SDS-PAGE – sodium dodecyl sulfate polyacrylamide gel electrophoresis

Ser16 – serine residue 16 in phospholamban that is subjected to phosphorylation

SERCA – sarco(endo)plasmic reticulum Ca^{2+}-ATPase

SERCA1a – the SERCA isoform found predominantly in fast muscle

SERCA2a – the SERCA isoform found predominantly in slow muscle

SLN – sarcolipin

SLN or *Sln* – gene encoding sarcolipin in human or mouse

Sln^{KO} or $Sln^{-/-}$ - mouse model with sarcolipin genetically removed

SR – sarcoplasmic reticulum

SREBP1 – sterol regulatory binding protein 1

Thr5 – threonine residue 5 in sarcolipin that is subjected to phosphorylation

Thr17 – threonine residue 17 in phospholamban that is subjected to phosphorylation

Tny - tenotomy

t-tubule – transverse tubule

TTN – gene encoding for titin in human

Tukey HSD – Tukey honest significant difference test

Ub - ubiquitin

*V*max – in this context, maximal rates of SERCA activity

WT – wild-type mice

Chapter 1 – Introduction, review of the literature and statement of the problem

Introduction and review of the literature

Ca^{2+} ions in skeletal muscle govern many physiological processes including excitation-contraction coupling (ECC) (1), energy expenditure (2-4), second messenger signaling (5), and apoptosis (6). Therefore, it is easy to understand that the concentration of intracellular free Ca^{2+} ($[Ca^{2+}]_i$) needs to be controlled precisely. The sarcoplasmic reticulum (SR) is largely responsible for the control of $[Ca^{2+}]_i$, although there are important contributions from cytoplasmic buffers, mitochondria, and sarcolemmal proteins (7, 8). The SR tightly regulates resting $[Ca^{2+}]_i$ to a concentration of 30-100 nM while maintaining a lumenal concentration in the millimolar range (8) thereby creating a large intra-extracellular ion gradient (1:10,000) (9, 10). This task is accomplished by the activities of the sarco(endo)plasmic reticulum Ca^{2+}-ATPases (SERCAs or SERCA pumps) and Ca^{2+} release channels (ryanodine receptors; RyRs) both of which are integral SR membrane proteins (1).

The reciprocal action of RyRs and SERCA pumps allows for the SR to exert its control of $[Ca^{2+}]_i$. For example, during ECC in skeletal muscle, an action potential depolarizes the transverse-tubule membrane leading to SR Ca^{2+} release through RyRs by virtue of their direct connection with voltage sensitive dihydropiridine receptors (DHPRs) at the terminal cisternae of the triad (transverse-tubule flanked by two junctional SR membranes). The increased $[Ca^{2+}]_i$, binds to troponin C removing the inhibitory actions of tropomyosin on actin and allowing for the formation of cross bridges and muscle contraction. Conversely, SERCA pumps catalyze the active transport of Ca^{2+} back into the SR, using energy from ATP hydrolysis, thereby returning $[Ca^{2+}]_i$ back to resting level and eliciting muscle relaxation. Even at rest, SERCA pumps act to maintain $[Ca^{2+}]_i$ as they counteract the

natural leak of Ca^{2+} that occurs through RyRs and SERCA pumps themselves. Experiments from our laboratory measuring resting muscle metabolic rate after inhibition of RyR Ca^{2+} leak using $MgCl_2$ revealed a 40-50% reduction in O_2 consumption, which we attributed to a decrease in SERCA ATP usage (4). While this finding prompted further studies to assess SERCA as a control point for energy balance regulation and as a potential target for metabolic alterations to oppose obesity (2, 3), it also highlights SERCA's significant contribution in maintaining resting $[Ca^{2+}]_i$ in skeletal muscle.

SERCAs are 110 kDa integral membrane proteins belonging to a family of cation transporters, namely, P-type ATPases, so called because a phosphorylated intermediate involving an Asp residue is formed during the catalytic cycle (11). Structurally, these pumps consist of 10 transmembrane domains (M1-M10) and three cytoplasmic domains (actuator, nucleotide binding and phosphorylation; together referred to as the headpiece) (12). Two Ca^{2+} binding sites (site I and II) are formed between transmembrane helices M4, M5, M6, and M8 (13, 14). In vertebrates, there are three distinct genes (*ATP2a1*/serca1, *ATP2a2*/serca2, *ATP2a3*/serca3) that produce more than 10 isoforms through alternative splicing (15). Specifically, in adult skeletal muscle, two SERCA isoforms predominate, namely SERCA1a and SERCA2a; the expression of which, has been suggested to be dependent on muscle fiber type (15-18). The SERCA1a isoform consists of 1001 amino acids and is expressed predominately in adult fast-twitch skeletal muscle, whereas SERCA2a is made up of 997 amino acids and is expressed in heart and slow-twitch skeletal muscle (19). However, Western blot analysis from our laboratory on human vastus lateralis single fibres suggests that both SERCA1a and SERCA2a may be present in either type I or type IIa fibres (20).

Phospholamban and Sarcolipin

Phospholamban (PLN) and sarcolipin (SLN) are structural homologs both capable of physically interacting with SERCAs and inhibiting their function. In the heart, SLN and PLN both regulate SERCA2a; however, SLN is expressed greatly in the atria, whereas PLN is expressed predominantly in the ventricles (21-23). In human skeletal muscle, SLN and PLN may regulate both SERCA1a and SERCA2a; however, results from single fibre Western blots on vastus lateralis muscle suggest that SLN may preferentially regulate SERCA1a whereas PLN may preferentially regulate SERCA2a (20). In general, SLN and PLN expression in rodent skeletal muscle is far lower compared to larger mammals (22, 24, 25). Specifically, in rodent skeletal muscle SLN and PLN are found predominantly expressed in soleus muscles (26). In mouse soleus, both SERCA1a and SERCA2a are expressed (4) which suggests that SLN and PLN may regulate either SERCA isoform. Indeed, single fibre Western blotting could determine if SLN and PLN may selectively regulate one specific SERCA isoform similar to that in human skeletal muscle, but is complicated due to limits in both levels of protein and SLN/PLN expression.

SLN is a 31 amino acid single-pass integral SR membrane protein with a transmembrane domain (19 amino acids), a cytoplasmic domain (7 amino acids), and a highly conserved lumenal domain (5 amino acids) (27, 28). On the other hand, PLN is a 52 amino acid single-pass integral SR membrane protein with a transmembrane domain (19 amino acids), a long cytoplasmic domain (30 amino acids), and a short lumenal domain (3 amino acids) (29). Structurally, SLN and PLN are similar in their transmembrane domain

with 7 amino acids being identical (30) and 8 amino acids that are highly conserved as L, I, V or M (31) (**Figure 1**). More importantly, the transmembrane domains of both SLN and PLN share a common binding site in between SERCA transmembrane helices M2, M4, M6 and M9 (30, 32). Highly conserved amino acids between SLN and PLN are also present in the cytoplasmic domain (**Figure 1**).

Figure 1.1. Amino acid sequence alignment of SLN and PLN from mouse. Adapted from (28). Identical amino acids across species are shaded in grey whereas the highly conserved amino acids across species are letters in bold (30).

By physically interacting with either SERCA1a or SERCA2a, both SLN and PLN have been shown to reduce SERCA's affinity for Ca^{2+} in a cell model expression system (33). Specifically, this was depicted as an increased Ca^{2+} requirement to reach half-maximal rates of SERCA Ca^{2+} uptake. In addition, experiments with co-reconstituted proteoliposomes containing SLN or PLN with SERCA1a also depicted a reduction in SERCA affinity for Ca^{2+} through increased Ca^{2+} requirements to reach half-maximal rates of SERCA activity (ATP hydrolysis) (28). The results from these studies are summarized in Table 1. In mice, genetic deletion of *Sln* (*Sln*$^{-/-}$) and *Pln* (*Pln*$^{-/-}$) improved SERCA affinity for Ca^{2+} in the atria (21) and ventricles (34), respectively, and was associated with increased relaxation rates and increased contractility. In skeletal muscle, similar effects were reproduced in our laboratory using the soleus muscles of *Sln*$^{-/-}$ mice (26) and, although enhanced contractility and increased

relaxation rates were also observed in skeletal muscles from *Pln*$^{-/-}$ mice presumably due to improved SERCA Ca^{2+} uptake (35), there have been no studies to date assessing SERCA function in these mice.

Table 1.1. Calculated and reported reductions in SERCA affinity for Ca^{2+} in the presence of SLN or PLN.

	Expression system	ΔK_{Ca}
Ca^{2+}-ATPase	SLN + SERCA1a	-0.20
Proteoliposomes (28)	PLN + SERCA1a	-0.25
Ca^{2+} uptake	SLN + SERCA1a	-0.22
HEK-293 cells (33)	PLN + SERCA1a	-0.36
	SLN + SERCA2a	-0.37
	PLN + SERCA2a	-0.40

The effects of the SLN PLN were compared with SERCA alone in either proteoliposomes or HEK-293 cells. K_{Ca} is the Ca^{2+} concentration required to attain the half-maximal Ca^{2+}-ATPase or uptake activity rate reported in *p*Ca (negative logarithm) units. ΔK_{Ca} were reported in the study of HEK-293 cells and were calculated based on reported averages in the study of proteoliposomes.

The inhibitory actions of SLN and PLN on SERCA can be relieved by phosphorylation (36-40). With respect to PLN in cardiac muscle, the effects of phosphorylation are well established. Specifically, β-adrenergic stimulation causes phosphorylation of PLN residues Ser16 by protein kinase A (PKA) and Thr17 by Ca^{2+}-calmodulin dependent kinase II (CAMKII) that ultimately leads to enhancements in cardiac muscle contraction and relaxation (37). It is unclear whether phosphorylation of PLN regulates its inhibitory action in skeletal muscle as discrepant results from the same laboratory have been reported (35, 41). Specifically, in one study, the use of a β-adrenergic agonist, isoproterenol, reduced half-relaxation time presumably due to PLN phosphorylation and improved SERCA function (35); however, this effect could not be reproduced in a study

7 years later (41). In regards to SLN, experiments in a model of cardiac overexpression of *Sln* in *Pln*$^{-/-}$ mice revealed a reduction of SERCA affinity for Ca^{2+} that was attributed solely to SLN protein, which could be relieved upon isoproterenol treatment (40). In this study, Gramolini and colleagues attributed the β-adrenergic effect to the phosphorylation of SLN at Thr5 by serine/threonine kinase. Moreover, experiments in ventricular myocytes using point mutation of Thr5 support the significance of this phosphorylation site and highlight a role for CAMKII in isoproterenol-mediated phosphorylation (36). It is important to note that whether phosphorylation of SLN can relieve SERCA inhibition in skeletal muscle has not been investigated.

One additional mechanism that may govern SLN- and PLN-mediated inhibition of SERCA is the formation of homo-oligomeric structures that likely prevents physical interactions with the SERCA pumps. PLN is capable of oligomerizing to form a pentameric structure and is visible as a ~20 kDa band using Western blot protocols where muscle homogenates have not been boiled prior to gel loading (26). In contrast, SLN was initially shown to be incapable of oligomerization (33); however, a recent study using fluorescence resonance energy transfer spectroscopy and microscopy, showed that, *in vitro*, SLN is indeed capable of forming homo-oligomers of both low (n=2) and high order (n>2) (42). The presence of these SLN oligomers have yet to be detected through Western blotting of cardiac and skeletal muscle homogenates in our laboratory and is complicated due to the amount of non-specific binding of the SLN antibody occurring above 10 kDa (3).

Divergence between SLN and PLN

Despite the structural and functional similarities in SLN and PLN, there are a few significant differences between these two SERCA-regulatory proteins. For example, along with the transmembrane domain, PLN has a relatively larger cytoplasmic domain that is also capable of interacting with SERCA and is vital for its inhibitory action (43). In addition, we have shown that SLN reduces the apparent coupling ratio of SERCA (3) presumably leading to greater energy released as heat. In support of this, *Sln*$^{-/-}$ mice developed hypothermia when exposed to acute cold temperature (30, 44), and were more susceptible to diet induced obesity when compared to their WT littermates (2, 44). In contrast, results from previous reports examining the role of PLN as an uncoupler of SERCA are more complex. Earlier findings from Dr. Jones' and Dr. Kranias' group have both shown that PLN is capable of uncoupling SERCA2a in cardiac muscles at low $[Ca^{2+}]_i$ (> 6.5 *p*Ca) (45, 46); however, the fact that *Pln*$^{-/-}$ mice did not develop hypothermia after cold exposure led Dr. Periasamy's group to suggest that PLN may not uncouple SERCA like SLN (30). To investigate this theory further, Sahoo and colleagues used HEK-293 cells transfected with a number of mutant SERCA, PLN, and SLN variants and presented 3 major findings. First, although SLN and PLN bind within the same groove in the SERCA transmembrane domain, they may bind to different amino acids. Second, SLN is capable of binding to SERCA even when exposed to high Ca^{2+} levels while PLN cannot. Finally, SLN can bind to SERCA throughout its catalytic cycle while PLN may only bind to SERCA at one point during its catalytic cycle. Thus, the ability of PLN to uncouple SERCA2a in cardiac muscles only at low $[Ca^{2+}]_i$ (45, 46) may be explained by changes in binding affinities as $[Ca^{2+}]_i$ increases (30), and could account for the lack in developed hyperthermia upon cold exposure. Of note, changes in SLN expression in *Pln*$^{-/-}$ mice may also account for these differences observed with cold

exposure; however this was not examined in the study by Sahoo and colleagues. Furthermore, the possibility that PLN can uncouple SERCA2 or SERCA1 in skeletal muscle or its role in offsetting the obesigenic effects of a high-fat diet have not yet been fully investigated.

Superinhibition

Due to specific amino acids found in SLN (V19, I22) and PLN (I47, I48) these two proteins are able to physically bind with each other to form a binary complex (31). Structurally, this binary complex may fit within the SERCA groove formed by transmembrane helices M2, M4, M6 and M9 where individual PLN and SLN molecules normally bind (31, 32). Functionally, when SLN and PLN are expressed together with SERCA in HEK-293 cells (33) or proteoliposomes (28), superinhibition occurs and leads to drastic reductions in SERCA affinity for Ca^{2+} and maximal rates of ATP hydrolysis and Ca^{2+}-uptake (Table 2). It has been proposed that by binding to PLN, SLN inhibits PLN from forming pentamers thereby increasing the amount of PLN monomers capable of inhibiting SERCA (33). While this would explain further reductions in Ca^{2+} affinity, it may not explain reductions in maximal SERCA activity that are tested at high Ca^{2+} concentrations capable of dissociating PLN from SERCA (30). It is possible that the binary complex of SLN-PLN allows for PLN to bind to SERCA throughout the whole catalytic cycle, however this has yet to be investigated.

Table 1.2. Calculated and reported reductions in SERCA affinity for Ca^{2+} and maximal rates of Ca^{2+} ATPase activity and Ca^{2+} uptake during ternary superinhibition.

	SERCA	% ΔVmax	ΔK_{Ca}
Ca^{2+}-ATPase			
Proteoliposomes			
(28)	SERCA1a	-20%	-0.40
Ca^{2+} uptake			
HEK-293 cells	SERCA1a	-32%	-0.93
(33).	SERCA2a	-42%	-1.01

The effects of the superinhibitory complex were compared with SERCA alone in either proteoliposomes or HEK-293 cells. % ΔVmax were calculated based on average values reported in the respective study. K_{Ca} is the Ca^{2+} concentration required to attain the half-maximal Ca^{2+}-ATPase or uptake activity rate reported in *p*Ca (negative logarithm) units. ΔK_{Ca} were reported in the study of HEK-293 cells and were calculated based on reported averages in the study of proteoliposomes.

In addition to mediating ternary superinhibition of SERCA, SLN alone may drastically impair SERCA function when expressed in high concentration (28). When recombinant SLN protein and SERCA1a were reconsitituted into proteoliposomes in a 4.5:1 molar ratio, Gorski and colleagues observed reductions in Ca^{2+} affinity and maximal rate of ATP hydrolysis (-30%). Moreover, progessive increases in SLN/SERCA molar ratio from 0:1 to 20:1 in lipid vesicles resulted in progressive reductions in SERCA mediated Ca^{2+} uptake (47, 48). Therefore, at higher SLN concentrations, SLN may act alone or together with PLN to drastically impair SERCA function. In support of this, forced overexpression of SLN in rat soleus through electroporation, reduced maximal rates of Ca^{2+} uptake by 31% (49). Together these findings may have implications in skeletal muscle myopathy where SERCA function is impaired and SLN protein expression is often upregulated.

SERCA and Ca^{2+} dysregulation in Skeletal Muscle Myopathies

Skeletal muscle myopathy is a broad term that describes a state in which the muscle is suffering. It may result from a number of abnormalities and can be placed into a variety of categories including: channelopathy, mitochondrial and metabolic myopathy, nucleoskeleton myopathy, acquired myopathy and congenital myopathy (50-55). Dysregulated Ca^{2+}-handling is a common feature in most, if not all, skeletal muscle myopathies, and is exemplified clearly in congenital myopathies (56-59). Congenital or inherited muscle myopathies are a genetically heterozygous diverse group of static or progressive muscle diseases that often result in muscle weakness, atrophy, hypotonia, cardiac- and respiratory dysfunction (60-63). These myopathies may be either non-dystrophic or dystrophic where the former are caused by genetic defects in the contractile apparatus of muscle, and are defined by distinctive histochemical or ultrastructural changes on muscle biopsy (60). Conversely, the muscular dystrophies are diseases of muscle membrane or supporting proteins characterized by extensive muscle degeneration/regeneration cycling, fibrosis, inflammation, and often, elevated serum creatine kinase levels (60, 63).

Core myopathies, centronuclear myopathies (CNM), and nemaline myopathies (NM) make up the three most common inherited non-dystrophic myopathies (61, 62). Their differential diagnosis is based on histopathological analyses of skeletal muscle biopsies. In core myopathies, oxidative stains typically using NADH-TR, SDH, and COX stains reveal unstained cores in the sarcomeres of type I fibres (62). Two core myopathies have been defined to date: 1) central cores disease (CCD) where the cores run the length of the myofibre and 2) multiple minicores disease (mMD) that is characterized by smaller multiple cores that do not extend along the myofibre (62). CNMs are characterized by excessive

internalized/centralized nuclei within myofibres without prominent findings of degeneration or regeneration, type I fibre predominance and hypotrophy, and central aggregation of oxidative activity (61, 64). Lastly, nemaline myopathies are diagnosed on the basis of rod-like accumulations of Z-disk-derived material found in either the sarcoplasm or nuclear membranes (62, 65, 66).

It is important to note that these non-dystrophic myopathies do not occur as mutually exclusive events as there are variable levels of overlapping histological phenotypes amongst patients (61, 67). Evidence within the literature suggests that dysregulated Ca^{2+} may be a common factor in their etiology and likely contributes to the overlapping phenotypes. In fact, although a number of genetic defects in a variety of proteins can cause CCD, NM, or CNM, respectively, a mutation in the *RYR1* gene that encodes for the RyR1 protein found in skeletal muscle may result in all three myopathies (59, 61). The *RYR1*-related myopathies are thought to result from abnormal ECC secondary to leaky RyR Ca^{2+} channels and or uncoupled RyR-DHPR interactions, however, how this relates to the histological development of sarcomere lesions remains unclear (68). Nevertheless, with respect to increased RyR leak, one may question why SERCA pumps can no longer compensate for RyR leak during these myopathies as SERCA pumps are able to catalyze the re-uptake of Ca^{2+} leaked from RyR channels in healthy resting skeletal muscle (4). Apart from mutations in *RYR1*, mice lacking nebulin, a giant protein (800 kDa) that spans the entire length of the thin filament, phenotypically recapitulates human NM (69). In the quadriceps muscles of these transgenically modified mice, severe impairments in maximal SERCA Ca^{2+} uptake ($\%\Delta Vmax = -70\%$) were reported when compared to their WT littermates (69). Collectively,

these studies demonstrate SERCA's potential involvement in the pathology of the various non-dystrophic congenital myopathies.

With respect to the dystrophic myopathies, Duchenne's muscular dystrophy (DMD) is the most severe form of muscular dystrophy affecting 1 in 3500 males (70) resulting from an X-linked mutation that renders patients without the dystrophin protein. Without dystrophin, the dystrophin-glycoprotein complex found within the sarcolemmal membrane becomes disarrayed (71) which compromises the structural integrity of the membrane thereby making them more fragile and susceptible to exercise-induced damage. DMD is a progressive muscle-wasting disease and early death often results from respiratory failure and cardiac dysfunction. Studies using muscle biopsies from DMD patients as well as muscles from the *mdx* mouse, which less severely recapitulates the DMD phenotype, have linked $[Ca^{2+}]_i$ overload to the necrosis and muscle degeneration (57, 58, 72, 73). Specifically, $[Ca^{2+}]_i$ overload can promote many detrimental processes that are involved with muscular dystrophy including: activation of proteolytic calpains, activation of caspases, elevating reactive oxygen specie (ROS) production, induction of mitochondrial apoptosis, enhancing inflammation and promoting fibrosis (56, 74-79). While increased membrane fragility would presumably increase sarcolemmal Ca^{2+} permeability and would likely contribute to the $[Ca^{2+}]_i$ overload, there may also be a role for SERCA. In a study using the dystrophic *mdx* mouse and the more phenotypically severe *mdx*/*utrophin*-null (*mdx*/*Utr*$^{-/-}$) mouse, SERCA-mediated Ca^{2+} uptake was far more impaired in the *mdx*/*Utr*$^{-/-}$ mice suggesting that impaired SERCA function is at least associated with an increase in dystrophic pathology (80). Interestingly, many studies have now shown that impaired SERCA contributes to the dystrophic pathology since improving its function by genetic overexpression of SERCA or

heat shock protein 72, which protects SERCA from oxidative damage (81), mitigates the disease and improves muscle contractility and structure (57, 58, 82, 83).

Even in the acute setting, SERCA may have a potential role. For example, corticosteroid treatment of asthmatic patients often leads to acute myopathy characterized by skeletal muscle wasting and weakness (84, 85), and, in a previous study, daily intramuscular injections of triamcinolone for 5 days led to atrophied diaphragm muscles and prolonged half-relaxation times in Wistar rats (86). The slowed relaxation time supports a role for SERCA function and can be accounted for, at least in part, by a down-regulation of *SERCA1a* and *-2a* mRNA (87). Taken together, impaired SERCA function may be involved in congenital myopathies, muscular dystrophies, and even in conditions of acute injury.

SLN and PLN in skeletal muscle myopathies

It is now well established that SLN expression is upregulated under conditions of muscle disease, disuse, and injury (summarized in Table 1.3). What is fascinating about SLN expression in myopathy is that it also seems to increase along with disease severity. This is demonstrated clearly in the muscles from *mdx*/*Utr*$^{-/-}$ mice that display greater fold-inductions of SLN content compared with *mdx* mice (Table 1.3). Thus, it is possible that SLN contributes to the progressive decline in SERCA function that worsened according to disease pathology in the *mdx* and *mdx*/*Utr*$^{-/-}$ mice (88); however the exact role of SLN in muscular dystrophy or any other form of myopathy remains unknown. In contrast to SLN, the pattern of expression of PLN across myopathies has not been studied well (summarized in Table 1.4). Furthermore, the results from the few studies assessing PLN mRNA or protein expression across muscle diseases/conditions, along with unpublished results from our laboratory, show

that unlike SLN, PLN expression does not consistently increase in response to disease, disuse, or injury (Table 1.4).

Table 1.3. Summary of the current literature demonstrating upregulated SLN expression in skeletal muscle disease, disuse, and injury.

Mouse model	Muscle	mRNA/protein	fold-induction	
NM	quadriceps	protein	+20-fold	(69)
	soleus	protein	+1.7-fold*	(69)
(*nebulin* knockout)	EDL	protein	+10-fold*	(69)
CNM				
	tibialis anterior	mRNA	+3.5-fold*	(89)
(*Srpk3* knockout)				
(*miR133a* knockout)	tibialis anterior	mRNA	+35-fold	(90)
(*miR133a* knockout)	tibialis anterior	protein	+3.5-fold*	(90)
Disuse	gastrocnemius	mRNA	+7-fold	(91)
(denervation)	soleus	protein	+20-fold	Unp.
	EDL	protein	ectopic	Unp.
ALS				
	gluteus superficialis	mRNA	+2-fold	(91)
($SOD1^{G93A}$)				
Corticosteroid myopathy	diaphragm	mRNA	+2-fold	(87)
Cardiotoxin injury	d.n.s	mRNA	d.n.s.	(91)
Myotonic dystrophy	quadriceps	mRNA	98.3-fold	(92)
	quadriceps	mRNA	72.8-fold	(92)
(HSA^{LR}20b)	quadriceps	mRNA	42.6-fold	(92)
(HSA^{LR}41)				
($Mbln^{-/-}$)				
Muscular dystrophy	vastus lateralis	mRNA	d.n.s.	(93)
	deltoid	mRNA	d.n.s.	(93)
(human limb girdle)				
(human limb girdle)				
(*mdx*)	soleus	protein	+10-fold	(88)
(*mdx*)	diaphragm	protein	+3-fold	(88)
(*mdx*)	quadriceps	protein	+ectopic	(88)
(*mdx*/$Utr^{-/-}$)	soleus	protein	+20-fold	(88)
(*mdx*/$Utr^{-/-}$)	diaphragm	protein	+8-fold	(88)
	quadriceps	protein	ectopic (2-fold†)	(88)
(*mdx*/$Utr^{-/-}$)				

NM, nemaline myopathy; CNM, centronuclear myopathy; *Srpk3*, gene encoding for serine arginine rich protein-specific kinase-3; *miR133a*, gene encoding for microRNA 133a; ALS, amyotrophic lateral sclerosis disease; $SOD1^{G93A}$, transgenic mouse model with a G93A mutation in the superoxide dismutase gene; HSA^{LR}20b and 41, human skeletal actin long repeat transgenic mouse models of myotonic dystrophy; $Mbln^{-/-}$, muscleblind-like protein knockout mice as a mouse model of myotonic dystrophy; *mdx*, mouse model for DMD; *mdx*/$Utr^{-/-}$, mouse model for DMD. *Fold-induction relative to the control (wild-type or sham condition) calculated from representative images in the respective publications using imageJ software. Unp., unpublished data from R. Tupling laboratory; d.n.s., data not shown, although the upregulation of *Sln* mRNA was suggested but not shown. †Represents a 2-fold increase in SLN protein compared to *mdx* quadriceps.

Table 1.4. Summary of the current literature demonstrating varied PLN expression in skeletal muscle disease, disuse, and injury.

Mouse model	Muscle	mRNA/protein	fold-induction	
NM				
(*nebulin* knockout)	quadriceps	protein	unaltered	(69)
CNM				
(*Srpk3* knockout)	tibialis anterior	mRNA	unaltered	(89)
(*miR133a* knockout)	tibialis anterior	protein	+1.4-fold*	(90)
Disuse				
(denervation)	soleus	protein	+40-fold	Unp.
(denervation)	EDL	protein	ectopic†	Unp.
Corticosteroid myopathy	diaphragm	mRNA	unaltered	(87)
Muscular dystrophy	soleus	protein	-5.8-fold	Unp.
(*mdx*)	diaphragm	protein	unaltered	Unp.
(*mdx*)	diaphragm	protein	+3.3-fold	Unp.
(*mdx*/*Utr*$^{-/-}$)				

NM, nemaline myopathy; CNM, centronuclear myopathy; *Srpk3*, gene encoding for serine arginine rich protein-specific kinase-3; *miR133a*, gene encoding for microRNA 133a,; ALS, amyotrophic lateral sclerosis disease;; *mdx*, mouse model for DMD; *mdx*/*Utr*$^{-/-}$, mouse model for DMD.
*Fold-induction relative to the control (wild-type or sham condition) calculated from representative images using imageJ software.
Unp., unpublished data from R. Tupling laboratory.
†ectopic expression, based on the fact that PLN could not be detected in WT muscle with equal loading. PLN can be detected in non-transforming EDL muscle (Figure 1.2); however, in this case could have been interfered with by the strong antigen:antibody complex signals that compete for the chemiluminescent substrate.

Interestingly, although PLN expression is not consistently upregulated across different skeletal muscle myopathies, overexpression of PLN (*Pln*^{OE}) in rabbit type I fibres leads to a dystrophic-like myopathy in their slow-twitch dominant soleus muscles (~ 90% type I fibres (94)) with severe muscle wasting, fibrosis, fatty infiltration, and skeletal muscle weakness (95). The mouse soleus is comprised of approximately 35% type I fibres (96), and PLN-overexpression in these fibres resulted in reduced muscle mass and muscle cross-sectional area; however, unlike the *Pln*^{OE} rabbit, there were no observed pathological alterations using light microscopy (41). Surprisingly, when we purchased these

commercially available mice to study the role of PLN as an uncoupler of SERCA and its effects on high-fat feeding, we found obvious signs of myopathy in the soleus muscles along with the previously observed muscle atrophy (Figure 1.3a,b). Furthermore, when we examined SLN content, we found that its expression was upregulated approximately 9-fold (Figure 1.3c). Thus, the *Pln*^{OE} mouse is a valuable model to determine the role of PLN and SLN in skeletal muscle myopathy.

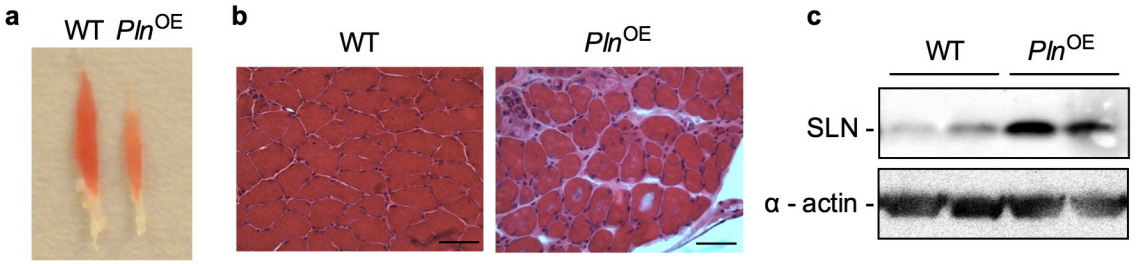

Figure 1.2. Phospholamban overexpressing (*Pln*^{OE}) mice display soleus muscle atrophy, pathology and greater SLN content. **a** Image illustrating soleus muscle atrophy observed in heterozygous *Pln*^{OE} mice compared with wild-type (WT). **b** Representative H&E-stained sections showing muscle pathology in heterozygous *Pln*^{OE} mice. Scale bars are set to 50 μm. **c** Representative Western blot image demonstrating sarcolipin (SLN) up-regulation in soleus muscle homogenates from heterozygous *Pln*^{OE} mice. 25 μg of protein were loaded and α-actin was used as a loading control.

Statement of the problem

This literature review has highlighted the potential impact of SERCA dysfunction on a number of muscle myopathies. SLN and PLN are two small inhibitory proteins that regulate the SERCA pump, and SLN, specifically, is considered a marker of muscle disease given its consistent upregulation in protein and/or mRNA. In contrast, the pattern of PLN expression in skeletal muscle myopathies is less defined and more variable. Nevertheless, PLN overexpression in mice exhibits signs of myopathy and a 9-fold increase in SLN content. This thesis sought to characterize the Pln^{OE} induced myopathy and determine the role of SLN.

Objectives and hypotheses for Thesis Study I

The main objectives for Study I were:

1. Characterize SERCA function in the soleus and gluteus minimus muscles from Pln^{OE} mice.
2. Characterize the myopathic phenotype as non-dystrophic or dystrophic as well as progressive or non-progressive.
3. Characterize the soleus muscle atrophy in the Pln^{OE} muscles and examine the role of the major proteolytic pathways (ie. calpain, caspase-3, cathepsin, and ubiquitin-proteasome).
4. Characterize *in vitro* soleus muscle contractility with respect to force produced and twitch kinetics.
5. Characterize whole body muscle performance with treadmill exercise running.

The specific hypotheses (outcomes) for Study I were:

1. Since PLN and SLN are inhibitors of the SERCA pump, it was hypothesized that maximal SERCA activity, rates of Ca^{2+} uptake, and SERCA's affinity for Ca^{2+} would be reduced in Pln^{OE} soleus and gluteus minimus muscles compared with WT.
   (The data are consistent with the hypothesis as SERCA dysfunction was clearly evident in these muscle types).
2. Consistent with the Pln^{OE} rabbit, it was hypothesized that the myopathy in the Pln^{OE} mice would resemble a dystrophic phenotype with greater central nuclei, greater fibrosis, plasma creatine kinase concentration, and immune cell infiltration.
   (The data are inconsistent with the hypothesis. Although the Pln^{OE} soleus and gluteus minimus muscles displayed some dystrophic features including greater central nuclei, fibrosis, and slightly elevated plasma creatine kinase, the myopathy in these mice was diagnosed as CNM based on the additional findings of type I fibre predominance and hypotrophy and central aggregation of oxidative activity).
3. Based on its Ca^{2+} dependency, it was hypothesized that calpains would display greater activity in the Pln^{OE} mice and would account for the soleus muscle atrophy.
   (The data are consistent with the hypothesis in that calpains were more active; however caspase-3 and cathepsins were also more active, and there was also greater total protein ubiquitinylation).
4. Based on the muscle damage and atrophy observed in the soleus muscles it was hypothesized that they would exhibit lower force production. In addition, it was hypothesized that twitch relaxation rates and rates of force development would be depressed.

(The data are consistent with the hypotheses. Force production, rates of relaxation, and rates of force development were all significantly depressed in the Pln^{OE} muscles).

5. It was hypothesized that Pln^{OE} mice would be more susceptible to fatigue during treadmill exercise compared with WT.

   (The data are consistent with the hypothesis and Pln^{OE} mice had, on average, a shorter time to fatigue during treadmill exercise).

Objectives and hypotheses for Thesis Study II

Based on the diagnosis of a CNM-like phenotype in the Pln^{OE} soleus and gluteus minimus muscles, this study sought to assess the diaphragm muscles, since studies examining respiratory or diaphragm function in animal models of CNM are limited. The main objectives for Study II were:

1. Characterize SERCA function with respect to SERCA activity, Ca^{2+} uptake, and SERCA's apparent affinity for Ca^{2+}.
2. Determine whether the diaphragm muscles displayed the three typical hallmarks of CNM (ie. central nuclei, type I fibre predominance and hypotrophy, and central aggregation of oxidative activity).
3. Determine whether SLN content was increased in the Pln^{OE} diaphragm muscles like the soleus and gluteus minimus muscles.
4. Determine whether the Pln^{OE} diaphragm muscles exhibited muscle weakness and slower twitch kinetics upon *in vitro* contractility assessment.

The specific hypotheses (outcomes) for Study II were:

1. It was hypothesized that SERCA activity, rates of Ca^{2+} uptake and SERCA's apparent affinity for Ca^{2+} would be reduced in the *Pln*^{OE} diaphragm compared with wild-type since these muscles normally comprise of 10% type I fibres that would overexpress PLN.

   (The data are inconsistent with the hypothesis. SERCA's apparent affinity was reduced and but rates of Ca^{2+} uptake were non-significantly different. In addition, maximal rates of SERCA activity were unaltered. Taken together, the level of SERCA impairment was not as pronounced in the *Pln*^{OE} diaphragm compared with the soleus and gluteus minimus muscles).

2. It was hypothesized that similar to the soleus and gluteus minimus muscles the diaphragm muscles would display a CNM-like phenotype.

   (The data are inconsistent with the hypothesis. The diaphragm muscles did not display all of the features commonly observed in CNM with only type I fibre hypotrophy being evident without any elevations in central nuclei, central aggregation of oxidative activity, or type I fibre percent).

3. It was hypothesized that similar to the soleus and gluteus minimus muscles SLN content would be upregulated in the diaphragm muscles as a general marker of muscle disease.

   (The data are consistent with the hypothesis; however SLN was only upregulated 2.5-fold in the *Pln*^{OE} diaphragm compared with the 7-9-fold increase observed in the soleus and gluteus minimus muscles from Study I).

4. It was hypothesized that similar to the soleus muscles Pln^{OE} diaphragm strips would exhibit muscle weakness and slower twitch kinetics.

   (The data are inconsistent with the hypothesis. The diaphragm strips from Pln^{OE} mice were not weaker than those from wild-type mice, nor did they have slower rates of relaxation or rates of force development).

Objectives and hypotheses for Thesis Study III

This study sought to determine the role of SLN in the Pln^{OE}-induced CNM. Subsequently, based on the results from these experiments, this study then sought to determine the role of SLN under conditions of mechanical overload, soleus muscle tenotomy, and in the dystrophic *mdx* mouse model. The main objectives for Study III were:

1. To generate a Pln^{OE}/Sln^{KO} mouse by breeding Pln^{OE} mice with Sln^{KO} mice.
2. To characterize SERCA function in the Pln^{OE}/Sln^{KO} mice.
3. To characterize the CNM-like phenotype in the soleus muscles from the Pln^{OE}/Sln^{KO} mice.
4. To characterize *in vitro* soleus muscle force production in Pln^{OE}/Sln^{KO} mice.
5. To characterize the soleus muscle atrophy and proteolytic pathways in the Pln^{OE}/Sln^{KO} mice.
6. To determine the effects of genetic *Sln* deletion on the myofibre growth and remodeling seen during mechanical overload.
7. To determine the effects of genetic *Sln* deletion on the myofibre atrophy and remodeling seen during soleus muscle tenotomy.
8. To generate an mdx/Sln^{KO} mouse by breeding *mdx* mice with Sln^{KO} mice.

9. To determine the effects of genetic *Sln* deletion on myofibre size, remodeling, and muscle pathology in *mdx* mice.

The specific hypotheses (outcomes) for Study II were:

1. It was hypothesized that *Sln* deletion would rescue SERCA function in the Pln^{OE} soleus.

   (The data are inconsistent with the hypothesis. SERCA activity, rates of Ca^{2+} uptake, and SERCA's apparent affinity for Ca^{2+} were similarly reduced in the Pln^{OE}/Sln^{KO} and Pln^{OE}/Sln^{WT} mice).
2. It was hypothesized that *Sln* deletion would mitigate the CNM-like phenotype observed in the Pln^{OE} soleus.

   (The data are inconsistent with the hypothesis. The Pln^{OE}/Sln^{KO} soleus still exhibited greater central nuclei, central aggregation of oxidative activity, and type I fibre predominance and hypotrophy. Additional ultrastructural abnormalities of triad disruption, commonly seen in CNM, were observed in both Pln^{OE}/Sln^{KO} and Pln^{OE}/Sln^{WT} soleus).
3. It was hypothesized that *Sln* deletion would improve force production in the Pln^{OE} soleus.

   (The data are inconsistent with the hypothesis. Force production in the Pln^{OE}/Sln^{KO} soleus was further impaired being significantly reduced at submaximal and maximal frequencies).

4. It was hypothesized that *Sln* deletion would alleviate the soleus muscle atrophy seen in response to *Pln* overexpression partly by attenuating the activities of the major proteolytic enzymes in skeletal muscle.

   (The data are inconsistent with the hypothesis. *Sln* deletion worsened the soleus muscle atrophy in response to *Pln* overexpression and this could not be accounted for by any augmentations in calpain, caspase-3, cathepsin, or 20S proteasome activity. Instead *Sln* deletion caused a failure of type II fibres to hypertrophy, and combined with the failure of type IIA fibres to transition into type I fibres, provided the rationale to perform mechanical overload experiments).

5. Similar to the Pln^{OE} soleus, it was hypothesized that *Sln* deletion during mechanical overload would attenuate the type II fibre hypertrophy and fast-to-slow fibre type transitions.

   (The data are consistent with the hypothesis. For the first time ectopic SLN expression was observed in the overloaded plantaris muscles; and when *Sln* was removed, it led to a failure of type II fibres to hypertrophy and transition towards a slow-oxidative phenotype).

6. Similar to the Pln^{OE} soleus, it was hypothesized that *Sln* deletion during muscle tenotomy would exacerbate the soleus muscle atrophy. In addition, it was hypothesized that *Sln* deletion would accelerate the slow-to-fast fibre type transitions commonly observed with soleus muscle unloading.

   (The data are consistent with the hypothesis. *Sln* deletion exacerbated the soleus muscle atrophy and appeared to have larger percent reductions in myofibre CSA. *Sln* deletion also accelerated the slow-to-fast fibre type transitions).

7. It was hypothesized that *Sln* deletion would reduce myofibre CSA, cause a slow-to-fast fibre type transition, and lower utrophin expression in the soleus and diaphragm muscles from *mdx* mice. It was further hypothesized that *mdx*/*Sln*^{KO} mice would display a worsened dystrophic pathology with greater serum creatine kinase concentration and variability in the minimal Feret's diameter.
   (The data are consistent with the hypothesis. The *mdx*/*Sln*^{KO} mice displayed worsened dystrophic pathology with smaller myofibre sizes, a slow-to-fast fibre type transition, lower utrophin expression, greater serum creatine kinase, and greater variability in the minimal Feret's diameter).

Chapter 2

Thesis Study I

Phospholamban overexpression in mice causes a centronuclear myopathy-like phenotype

Val A. Fajardo[1§], Eric Bombardier[1§], Elliott McMillan[1], Khanh Tran[1], Brennan J. Wadsworth[1], Daniel Gamu[1], Andrew Hopf, Chris Vigna[1], Ian C. Smith[1], Catherine Bellissimo[1], Robin N. Michel[2], Mark A. Tarnopolsky[3,4,5], Joe Quadrilatero[1], A. Russell Tupling[1]*

From the [1]Department of Kinesiology, University of Waterloo, Waterloo, Ontario, Canada, [2]Department of Exercise Science, Concordia University, Montreal, Quebec, Canada, [3]Departement of Kinesiology, [4]Department of Pediatrics, and [5]Department of Medicine, McMaster University, Hamilton, Ontario, Canada.

[§]These authors contributed equally to this work.

Published in *Disease Models and Mechanisms*

Volume 8, Issue 8, Pages 999-1009, August 2015

dmm.biologists.org/content/dmm/8/8/999.full.pdf

First Published May 28, 2015; DOI: 10.1242/dmm.020859

Supplemental Material available at

Disease Models and Mechanisms website

dmm.biologists.org/content/8/8/999.supplemental

2.1 Preface

This Chapter presents Thesis Study I as a 'Full Text' reproduction of the article *Phospholamban overexpression in mice causes a centronuclear myopathy-like phenotype* published in 2015 by Disease Models and Mechanisms as referenced above. Prior to this work, the role of PLN in SERCA regulation and overall muscle health was based on studies

on cardiac tissue (97), with mutations in *PLN* being associated with cardiomyopathy (98). In addition, with the discovery of SLN's role as an uncoupler of SERCA activity and a regulator of muscle-based thermogenesis in skeletal muscle (for review see, (99)), the academic community was seemingly beginning to overlook PLN's role in skeletal muscle health. This work published in Disease Models and Mechanisms showcases the importance of PLN in regulating SERCA and overall muscle health suggesting that increased PLN expression can cause a CNM-like phenotype in mice, and may have a potential role in human CNM.

Articles published in Disease Models and Mechanisms are under the Creative Commons Attribution (CC-BY) license. This license was developed to facilitate open access-namely, free immediate access to, and unrestricted reuse of, original works of all types. This allows for inclusion of any version including final published PDF so long as the source is attributed by citing and linking to the published article on the journal website.

Included in this Chapter are the Overview (Section 2.2), Introduction (Section 2.3), Results (Section 2.4), Discussion (Section 2.5), and Materials and Methods (Section 2.6) of the article, reproduced as published, except in the format of this thesis. Figures (2.1 to 2.5) and Tables (Table 2.1 to 2.2) corresponding to the Results are located in order at the end of Section 2.4. The Supplemental Material for this article, published as an Online Supplement as referenced above, is reproduced in Appendix A as published, except in the format of this thesis. The Supplemental Material includes Supplemental Results comprised of Supplemental Figures A1 – A6 and Tables A1 – A3.

2.2 Overview

Centronuclear myopathy (CNM) is a congenital myopathy that is histopathologically characterized by centrally located nuclei, central aggregation of oxidative activity, and type I

fibre predominance and hypotrophy. Here, we obtained commercially available mice overexpressing phospholamban (*Pln*^{OE}), a well-known inhibitor of sarco(endo)plasmic reticulum Ca^{2+}-ATPases (SERCAs), in their slow-twitch type I skeletal muscle fibres to determine the effects on SERCA function. As expected with a 6-7-fold overexpression of PLN, SERCA dysfunction was evident in *Pln*^{OE} muscles with marked reductions in rates of Ca^{2+} uptake, maximal ATPase activity and the apparent affinity of SERCA for Ca^{2+}. However, our most significant discovery was that the soleus and gluteus minimus muscles from the *Pln*^{OE} mice displayed overt signs of myopathy histopathologically resembling human CNM with centrally located nuclei, central aggregation of oxidative activity, type I fibre predominance and hypotrophy, progressive fibrosis, and muscle weakness, a phenotype that is associated with significant up-regulation of muscle sarcolipin and dynamin 2 content, increased Ca^{2+}-activated proteolysis, oxidative stress, and protein nitrosylation. Moreover, in our assessment of muscle biopsies from three human CNM patients, we found a significant 53% reduction in SERCA activity and trending increases in both total and monomeric PLN content compared to five healthy subjects, thereby justifying future studies with more CNM patients. Altogether our results suggest that the commercially available *Pln*^{OE} mouse represents a novel mouse model phenotypically resembling human CNM and may be used to test potential mechanisms and therapeutic strategies. To date there is no cure for CNM and our results suggest that targeting SERCA function, which has already been shown to be an effective therapeutic target for murine muscular dystrophy and human cardiomyopathy, may represent a novel therapeutic strategy to combat CNM.

2.3 Introduction

The sarco(endo)plasmic reticulum Ca^{2+}-ATPase (SERCA) pumps catalyze the active transport of Ca^{2+} into the sarcoplasmic reticulum (SR) and play a crucial role in muscle relaxation and the maintenance of resting intracellular Ca^{2+} $[Ca^{2+}]_i$, which ranges from 30 to 100 nM in skeletal muscle (1, 8). Phospholamban (PLN) is a small, 52-residue, SR protein capable of physically interacting with and inhibiting SERCA activity by reducing its apparent affinity for Ca^{2+} (31). Mouse (41) and rabbit (95) models overexpressing PLN in slow-twitch (type I) muscle fibres (Pln^{OE}) have been generated by attaching a *Pln* transgene to the β myosin heavy chain (β-MHC) promoter, which preferentially directs high levels of type I skeletal-muscle-specific transgene expression (100-102). In the Pln^{OE} rabbit, obvious signs of muscular dystrophy, including central nucleation, severe muscle wasting, fibrosis, fatty infiltration and muscle weakness, were observed in soleus muscles, which are rich in type I fibres (95). In contrast, Pln^{OE} mice exhibited soleus muscle atrophy but no other signs of myopathy were visualized under the light microscope (41).

We purchased these commercially available Pln^{OE} mice and their wild-type (WT) littermates (000067-MU, FVB/N background, Mutant Mouse Regional Resource Centre, Columbia, MO) to assess SERCA function because the effect of PLN overexpression on SERCA activity and Ca^{2+} transport in skeletal muscle remains uncharacterized. Unlike the study by Song et al., (4), we discovered that the postural soleus and gluteus minimus muscles from Pln^{OE} mice exhibited overt signs of myopathy. Collectively, our data suggest that the Pln^{OE} mouse is a novel myopathy model resembling human centronuclear myopathy (CNM) with additional dystrophic features and potential core-like lesions.

2.4 Results

SERCA function is impaired in Pln^{OE} muscle

Pln^{OE} mice were generated in order to examine the functional importance of PLN in skeletal muscle; however, in the only study published using these mice (41), no measurements of SERCA function were reported because of technical limitations. In order to better define the functional role of PLN in skeletal muscle we assessed SERCA function in these mice focusing our analyses on the postural muscles, soleus and gluteus minimus, since these muscles normally contain approximately 55-65% and 27% type I fibre proportions, respectively. However, these type I fibre levels increase in response to PLN overexpression (discussed below). Western blotting of whole homogenates demonstrated clear overexpression of PLN in these muscles since only 2.5 μg of total protein were loaded for Pln^{OE} mice compared to the 25 μg required for WT mice (Figure 2.1A and supplementary material Figure A3A). Specifically, in the Pln^{OE} soleus relative to WT (n = 7-9 per genotype), monomeric and pentameric PLN levels, normalized to actin, were 6.3-fold (P = 0.00001) and 80-fold (P = 0.0007) higher, respectively. In the Pln^{OE} gluteus minimus muscles relative to WT (n = 5-6 per genotype), monomeric and pentameric PLN levels were 6.7-fold (P = 0.0001) and 23-fold (P = 0.0001) higher, respectively. In addition to the analysis in homogenates, we also performed single-fibre western blot analyses confirming overexpression of PLN specific to type I fibres in this model (supplementary material Figure A1). In contrast, PLN was barely detectable in some WT type I and type IIA fibres (supplementary material Figure A1). This corresponds well with the fact that PLN expression in rodent skeletal muscle is far lower than that in human skeletal muscle where PLN can be found in all type I and type IIA fibres in the vastus lateralis (20).

In agreement with the known effects of PLN overexpression on SERCA function in HEK-293 cells and in transgenic hearts (23, 97), we observed a reduction in SERCA's apparent affinity for Ca^{2+} as indicated by a higher K_{Ca} value and a corresponding rightward shift in the activity-*p*Ca curve in soleus homogenates prepared from Pln^{OE} mice compared with WT (Table 2.1 and Figure 2.1B). Furthermore, maximal rates of SERCA activity (-27%) and rates of Ca^{2+} uptake (-74%) were reduced in the Pln^{OE} soleus compared with WT (Figure 2.1B and C and Table 2.1). The SERCA dysfunction in Pln^{OE} soleus cannot be explained by altered SERCA expression since western blot analysis showed that SERCA1a content is similar in WT and Pln^{OE} muscles (Figure 2.1D), whereas a significant 3-fold increase in SERCA2a expression was observed in the soleus of Pln^{OE} mice (Figure 2.1E). Sarcolipin (SLN), a small SR protein that is structurally and functionally homologous with PLN (32, 33), was also found to be up-regulated by 9-fold in the soleus of Pln^{OE} mice compared with WT (Figure 2.1F). As SLN can inhibit SERCA pumps alone or in combination with PLN (32), these results suggest that SLN may also contribute to the impaired SERCA function we observed in Pln^{OE} muscles. Indeed, forced over-expression of SLN acutely in rat soleus reduces SR Ca^{2+} transport (-31%) and causes severe contractile dysfunction (49).

Soleus muscle atrophy and Ca^{2+}-activated proteolysis in Pln^{OE} mice

Similar to previously described results (41), we also observed atrophy of soleus muscles in Pln^{OE} mice (Figure 2.2A and supplementary material Table A1). Interestingly, when breeding male and female Pln^{OE} mice, soleus muscles weighing $\leq$1 mg were observed, presumably from homozygous Pln^{OE} mice (+/+) because these muscles were no longer seen after breeding male Pln^{OE} mice with female WT mice (Figure 2.2A). Owing to this

limitation of the tissue, we restricted all of our analyses in the present study to heterozygous *Pln*^{OE} mice (+/-). In the study published by Song et al., (2004), a 35-40% reduction in soleus:body weight ratio was observed in *Pln*^{OE} mice at 10-12 weeks of age. In our hands, assessment of soleus:body weight ratio in *Pln*^{OE} mice at 1 month, 4-6 months, and 10-12 months of age indicates a 21%, 43%, and 41% reduction, respectively, when compared to WT mice (supplementary material Table A1). When we include age as a factor, absolute soleus weight and the soleus:body weight ratios were significantly different at 4-6 months and 10-12 months but not at 1 month. To elucidate the mechanisms behind the diminished soleus muscle mass, Song and colleagues reported an approximate 2-fold increase in calpain expression (41). Calpains are a class of proteolytic enzymes that are activated by high levels of $[Ca^{2+}]_i$ (103), and our results show that calpain activity was 1.5-fold higher in soleus from *Pln*^{OE} mice compared with WT (Figure 2.2B), which probably results from reduced SERCA function and greater $[Ca^{2+}]_i$ in *Pln*^{OE} mice. We also observed a significant 1.5- to 2-fold increase in other proteolytic pathways such as caspase-3, cathepsin-B/L activity, and protein ubiquitylation (Figure 2.2C-E), which suggests that the soleus muscle atrophy in *Pln*^{OE} mice is due to a general overall enhancement of proteolytic activity in those muscles.

Central nuclei, progressive fibrosis and oxidative stress in Pln^{OE} mice

As mentioned earlier, previous analyses of *Pln*^{OE} mice revealed no signs of myopathy under the light microscope (41). Consequently, we were surprised that our histological analyses of the soleus muscles from *Pln*^{OE} mice showed obvious signs of pathology that were repeatedly observed (Figure 2.3). In fact, the myopathy was at least partially consistent with the dystrophic-like phenotype observed in *Pln*^{OE} rabbits (95), including greater central nucleation

of fibres, fibre-splitting, atrophy, and progressive fibrosis which became evident at 4-6 months of age (Figure 2.3A to D). Corresponding well with the dystrophic phenotype, we also observed greater whole muscle oxidative stress as indicated by DCF (2', 7;-dichlorofluorescein) fluorescence and protein nitrosylation, effects that may be explained by Ca^{2+} dysregulation (56). Furthermore, we found elevated plasma CK in 4- to 6-month-old Pln^{OE} mice (Figure 2.3E to G); however, the relatively small increase in plasma CK suggests that the dystrophic-like phenotype in Pln^{OE} mice is likely a direct result of impaired SERCA activity and elevated $[Ca^{2+}]_i$ and less likely to be caused by sarcolemmal damage *per se*. A similar finding has been reported in mice overexpressing transient receptor potential canonical 3 which led to greater Ca^{2+} influx, muscular dystrophy, and only slightly elevated plasma CK as a result of a generally intact sarcolemmal membrane (72).

CNM in the Pln^{OE} mouse

Although central nucleation might be an active marker in muscle regeneration and a common feature in muscular dystrophy (104-106), we observed only a small proportion of fibres that were positive for embryonic MHC (supplementary material Figure A2), which is normally expressed transiently during muscle regeneration (107-109). These results, combined with the small elevation in plasma CK, suggest that very little degeneration-regeneration cycling is occurring in Pln^{OE} muscle. Therefore, the Pln^{OE} mouse does not resemble closely dystrophic myopathy; however, central nucleation in the face of low regeneration, progressive fibrosis, and moderate elevations in CK levels is also found in CNM (110). CNM is a congenital myopathy that is diagnosed by the existence of three histopathological features found in muscle biopsies, which include: 1) central nucleation, 2) central

aggregation of oxidative activity, and 3) predominance of type I fibres and hypotrophy (64, 110). Both central aggregation of oxidative activity and type I fibre hypotrophy were evident in soleus sections as early as 1 month of age in Pln^{OE} mice (Figure 2.4A and B and Table 2.2). Type I fibre predominance was established at 4-6 months of age whereas at 1 month, fibres were still transitioning towards the type I fibre distribution since the Pln^{OE} soleus had lower type IIA and greater type I/IIA content compared with WT (Figure 2.4A and Table 2.2). The type I fibre predominance found from 4-6 months is in agreement with previous findings (41), and the increase in the slow-twitch SERCA2a isoform in Pln^{OE} soleus (Figure 2.1E) is also consistent with type I fibre predominance. Taken together, these results indicate that the Pln^{OE} mouse model is a phenocopy of the histological features found in human CNM. Importantly, the soleus muscle was not the only muscle affected by PLN overexpression because the postural gluteus minimus muscle, which normally comprises roughly 27% type I fibres in WT mice, also displayed signs of impaired SERCA function, CNM, and endomysial fibrosis (supplementary material Figure A3, Table A2, and Table A3). Despite a similar level of monomeric PLN overexpression, the relative impairment in SERCA function in the gluteus minimus muscles compared with the Pln^{OE} soleus was lower, with only a 20% reduction in the rates of Ca^{2+} uptake (supplementary material Figure A3C). This may be explained by the fact that the gluteus minimus muscles have a greater number of type II fibres that do not overexpress PLN, which could mask the inhibition of SERCA pumps occurring in the type I fibres. In any event, both the Pln^{OE} soleus and gluteus minimus muscles resembled the histopathological features associated with CNM.

To date, CNMs are known to be genetically heterogeneous (67, 111) and have been attributed to X-linked recessive mutations in the *MTM1* gene encoding myotubularin (112),

autosomal-dominant mutations in the *DNM2* gene encoding dynamin-2 (113) and the *BIN1* gene encoding amphiphysin-2 (114), and autosomal-recessive mutations in *BIN1* (115), *RYR1* encoding the SR ryanodine receptor (116, 117), and *TTN* encoding titin (118). Many different structural abnormalities have been identified that aid in distinguishing between the various human CNMs (64, 67). For example, the autosomal dominant *DNM2*-related CNMs present with radiating SR strands and marked contrast of the diameters between type I and type II fibres (64). In addition to these features, increases in connective tissue and the presence of core formations can also be observed in *DNM2*-related CNMs (67). Since we observed radiating SR strands (Figure 2.4C), type II fibre hypertrophy (Table 2.2 and supplementary material Table A3), progressive fibrosis (Figure 2.3C and D), and potential core-like formations (Figure 2.5) in the Pln^{OE} mice, our results suggest that the CNM phenotype found in these mice resembles autosomal dominant *DNM2*-related CNM. However, because increases in endomysial connective tissue and the presence of core formations may also be observed in *RYR1*-related and *TTN*-related CNM (67, 117), the Pln^{OE} mouse also shares a resemblance to these forms of CNM. We use the term 'potential core-like lesions' since future studies with electron microscopy are required to verify the presence and characterize the structure of cores in the Pln^{OE} mouse.

Muscle function in the Pln^{OE} mouse

General muscle weakness is common in cases of CNM and our analyses of contractile function in isolated intact soleus muscle as well as whole body endurance during treadmill exercise demonstrate that muscle function is impaired in Pln^{OE} mice (supplementary material Figure A4A to E). Specifically, we found that Pln^{OE} mice generate lower normalized force at

both submaximal and maximal stimulation frequencies (30-100 Hz) (supplementary material Figure A4*D*) and reached exhaustion much sooner than WT mice during a treadmill exercise test (supplementary material Figure A4E). In agreement with previous findings (41), we found that normalized twitch force generation of soleus muscle was not different between Pln^{OE} and WT mice, whereas the twitch kinetics were significantly slower in Pln^{OE} compared with WT (supplementary material Figure A4A to C).

PLN and SERCA dysfunction in human CNM

Thus far, it is evident that PLN overexpression in mouse skeletal muscle leads to CNM; however, whether PLN plays a primary pathogenic role in CNM remains unknown. In support of this notion, PLN protein was found to be up-regulated in the tibialis anterior muscles from mice lacking microRNA 133a-1 and 133a-2 where CNM was observed (90). In addition, we obtained muscle biopsies from three patients with CNM and when compared to biopsies from five healthy controls, we found that the maximal rate of SERCA activity was significantly reduced by 53% (supplementary material Figure A5A,) and that monomeric PLN (P = 0.12) and total PLN (P = 0.08) content were greater (supplementary material Figure A5B). Therefore, we provide the first indication of a potential role for SERCA dysfunction and elevated PLN in human CNM; however, caution should be taken when interpreting these results. Recently, we established through single fibre western blotting and immunohistochemical analyses that PLN expression follows SERCA2a and MHC I expression, whereas SLN follows SERCA1a and MHC II expression in healthy human vastus lateralis (20). Since we observed a trend for higher MHC I (supplementary material Figure A5C, P = 0.10) and SERCA2a (Figure A5D, P = 0.10) expression, and significant reductions

in both SERCA1a (supplementary material Figure A5E) and SLN (supplementary material Figure A5F) in CNM muscles compared with healthy controls, it is possible that these differences, including upregulated PLN, are due mostly to the expected type I fibre predominance in CNM patients. Furthermore, in addition to the low sample size used in the present study, the CNM cases obtained were of notable age variability and were genetically unrelated, with one patient harboring a *DNM2* mutation (R369W) and the other two patients remaining genetically unresolved. Importantly, despite these limitations, we were still able to show a 53% reduction in SERCA activity and the expression patterns of the SERCA isoforms, SLN, and PLN are consistent with the expected type I fibre predominance often found in CNM.

Dynamin 2 levels in CNM

As a result of the dominant inheritance of the *DNM2* mutation, one theory is that *DNM2*-related CNM may be caused by a toxic gain-of-function in dynamin 2 (111, 119). In support of this, overexpression of WT dynamin 2 in skeletal muscle results in features associated with CNM (90, 120). In addition, up-regulation of dynamin 2 was observed in skeletal muscles from *mtm1*$^{-/y}$ mice, which accurately models human X-linked myotubular myopathy (XLCNM), and heterozygous knockdown of dynamin 2 in the *mtm1*$^{-/y}$ mouse improves muscle pathology and function (119). We analyzed dynamin 2 protein content in *Pln*^{OE} muscles and found a 5-fold (supplementary material Figure A6A) and 3-fold (supplementary material Figure A6B) higher level in the soleus and gluteus minimus muscles, respectively, compared with WT. Whether dynamin 2 plays a pathological role in the CNM found in the

Pln^{OE} mouse and the exact mechanism leading to its augmented expression requires further investigation.

Elevated levels of dynamin 2 are thought to also play a pathological role in human CNM because results from Laporte's laboratory have shown an approximate 1.5-fold increase in dynamin 2 expression in muscle lysates from three XLCNM patients compared with two healthy controls (90, 119). To confirm whether elevated dynamin 2 contributes to human CNM pathology, we assessed the dynamin 2 protein content in the three CNM muscle biopsies obtained here; however, in contrast to what was previously found in human CNM (90, 119), we found a 35% reduction in dynamin 2 compared to healthy subjects (supplementary material Figure A6C). Notwithstanding the aforementioned sample size and other limitations with our human CNM cases, these findings may suggest that reducing dynamin 2 as a therapeutic strategy may not be appropriate for all forms of human CNM as previously suggested (121) and may be limited to XLCNM.

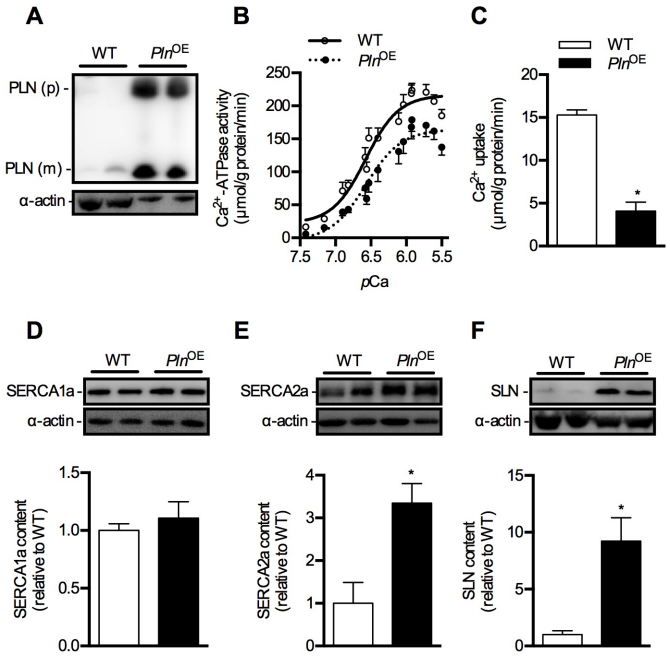

Figure 2.1. SERCA function in soleus muscles in *Pln*^{OE} mice at 4-6 months of age. (**A**) Western blotting for PLN in WT and *Pln*^{OE} mice from soleus muscle homogenates. For WT mice, 25 μg of total protein was loaded whereas only 2.5 μg was required for *Pln*^{OE} mice to detect PLN protein. (**B**) Ca^{2+}-ATPase activity-*p*Ca curves in WT (n = 5) and *Pln*^{OE} mice (n = 6) in the presence of the Ca^{2+} ionophore. (**C**) Ca^{2+} uptake assessed in soleus muscles from WT (n = 4) and *Pln*^{OE} mice (n = 5). Western blotting for SERCA1a (**D**), SERCA2a (**E**), and SLN (**F**) in soleus from WT and *Pln*^{OE} mice (n = 6 per genotype). Actin was used as a loading control and all values are expressed relative to WT. *$P \leq 0.05$ versus WT. All values are presented as mean ± standard error. PLN (p), PLN pentamer; PLN (m), PLN monomer.

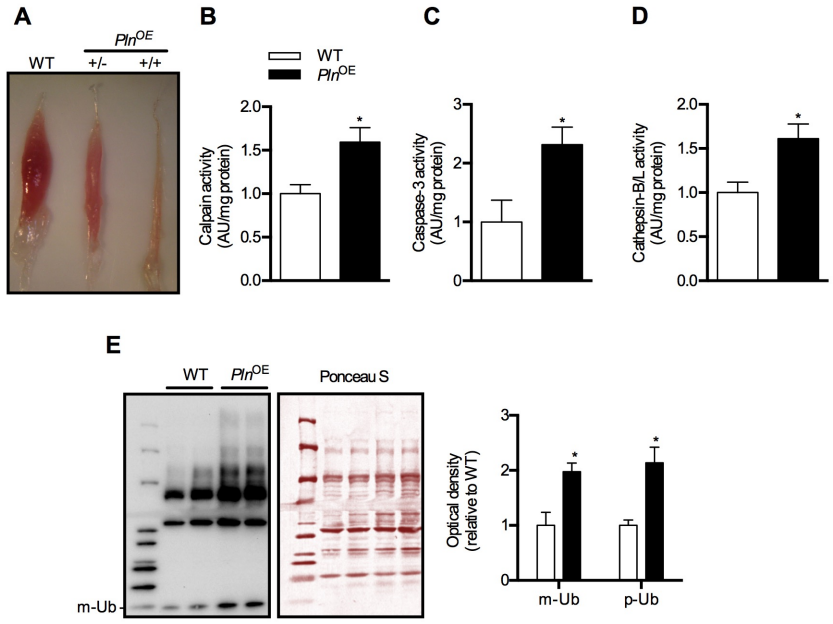

Figure 2.2. Soleus muscles of *Pln*^{OE} mice are atrophied at 4-6 months of age. (**A**) Representative images of soleus muscles extracted from WT and *Pln*^{OE} mice. +/-, heterozygous; +/+, homozygous. (**B**) Calpain activity in soleus homogenates from WT (n = 4) and *Pln*^{OE} mice (n = 5). (**C**) Caspase-3 activity in soleus homogenates from WT (n = 4) and *Pln*^{OE} mice (n = 7). (**D**) Cathepsin-B/L activity in soleus homogenates from WT and *Pln*^{OE} mice (WT n = 4, *Pln*^{OE} n = 6). Calpain activity, caspase-3 activity, and cathepsin-L activity are in arbitrary units normalized to mg protein and are presented relative to WT. (**E**) Total protein extracts from soleus muscles (15 µg) were immunoblotted with anti-ubiquitin (Ub) antibody. Ponceau stain was used as a loading control. The sum of optical densities from detectable ubiquitinated proteins (p-Ub) as well as the optical density of monomeric ubiquitin (m-Ub, 10 kDa) was measured and compared between genotypes (n = 4 per group). Values were normalized to the sum of optical densities of bands visualized through Ponceau stain. *$P \leq 0.05$ versus WT. All values are presented as mean ± standard error.

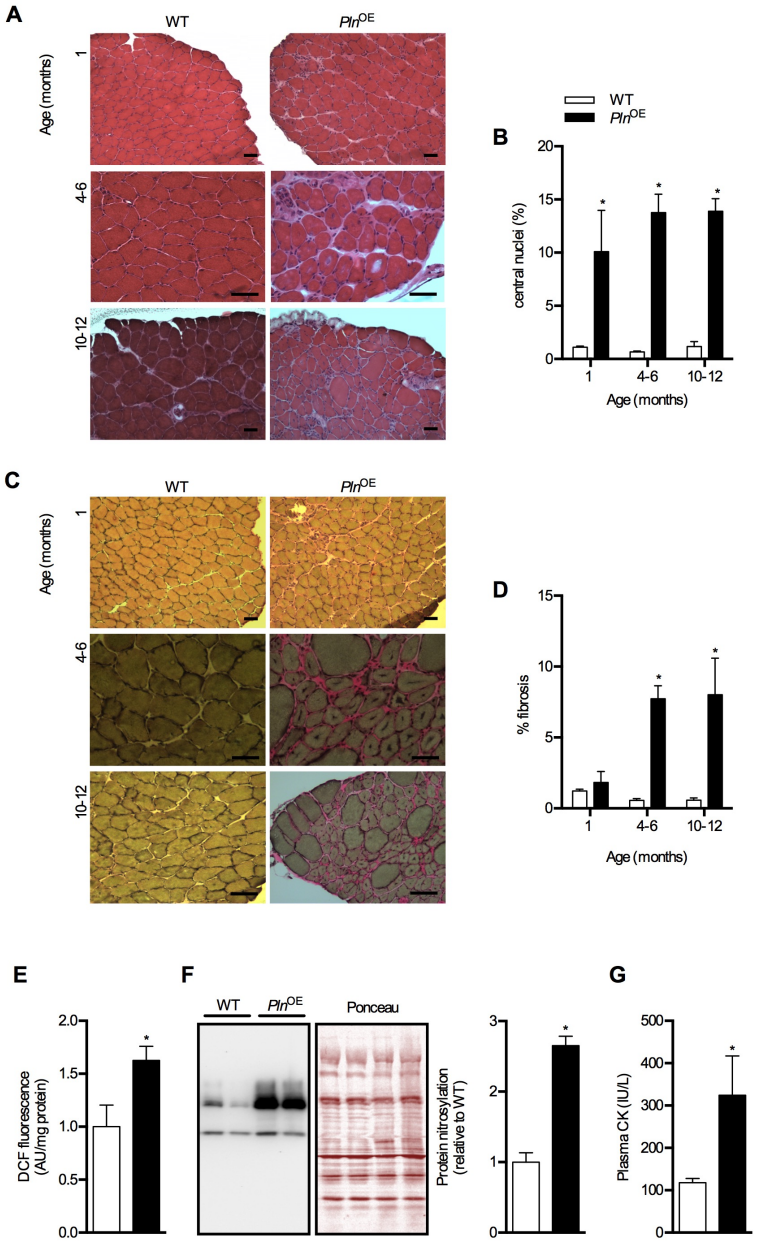

Figure 2.3. Dystrophic features in the soleus muscles from *Pln*^{OE} mice. (**A**) H&E-stained sections of the soleus muscles from WT and *Pln*^{OE} mice at 1 month, 4-6 months, and 10-12 months of age. (**B**) Percent of fibres containing central nuclei in the soleus at 1 month, 4-6 months, and 10-12 months of age (n = 3 per genotype at each age with 300-600 fibres counted per mouse). (**C**) Van Geison stained sections of the soleus muscles from WT and *Pln*^{OE} mice at 1 month, 4-6 months, and 10-12 months of age. (**D**) Quantitation of fibrotic area in the soleus at 1 month, 4-6 months, and 10-12 months of age (n = 3-4 per group at each age). ImageJ software was used to quantify fibrotic area. (**E**) Whole soleus reactive oxygen species generation determined using DCF assay at 4-6 months of age (WT n = 4, *Pln*^{OE} n = 5). (**F**) Total protein extracts from soleus muscles (15 µg) were immunoblotted with anti-nitrotyrosine antibody. The sum of optical densities from detectable nitrosylated proteins (50 – 100 kDa) was measured and compared between genotypes at 4-6 months of age (n = 6 per group). Values were normalized to the sum of optical densities of bands visualized through Ponceau stain. (**G**) Plasma CK levels in WT (n = 5) and *Pln*^{OE} mice (n = 9) at 4-6 months of age. Scale bars in (**A**) and (**C**) are set to 50 µm. *$P \leq 0.05$ versus WT using two-way ANOVA and Tukey's post-hoc analysis for %central nuclei and %fibrosis; Student's t-test for DCF, protein nitrosylation, and plasma CK. All values are presented as mean ± standard error.

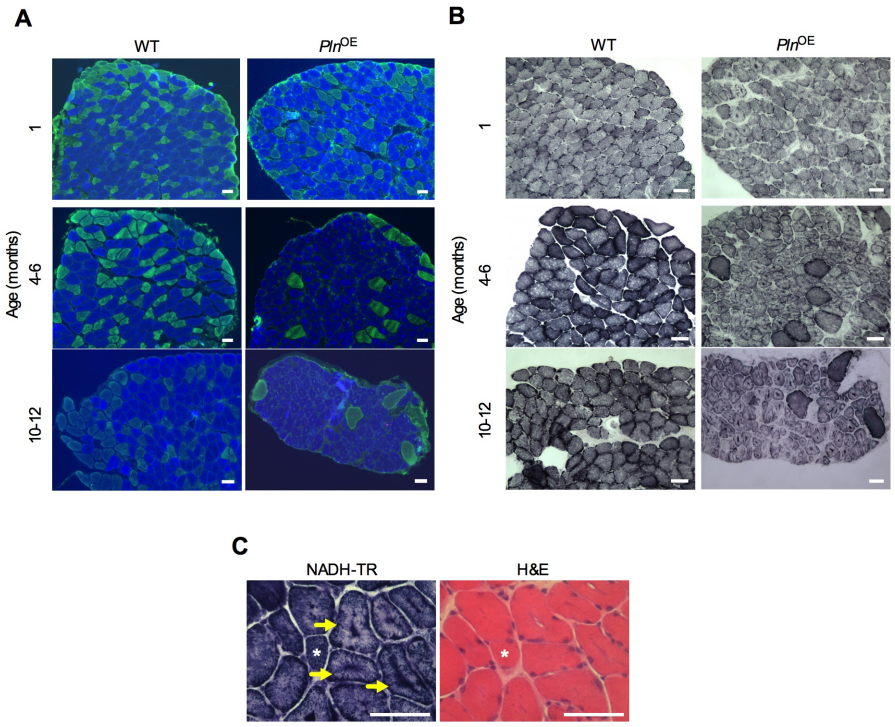

Figure 2.4. Centronuclear myopathy in the soleus muscles from *Pln*^{OE} mice. (**A**) Representative images of soleus muscles showing type I fibre predominance and hypotrophy. MHC immunofluorescence stained sections of the soleus muscles at 1 month, 4-6 months, and 10-12 months of age. Cross sections were stained with MHC antibodies to identify type I (blue), type IIA (green), type IIB (red), and type IIX (unstained) fibres. (**B**) Representative images of soleus muscles showing central accumulation of oxidative activity. SDH stained sections of the soleus muscles display central aggregation of oxidative activity in the *Pln*^{OE} mice at 1 month, 4-6 months, and 10-12 months of age. (**C**) NADH-TR–stained cross sections demonstrating radiating sarcoplasmic reticulum strands in soleus muscles from *Pln*^{OE} mice (arrows). Asterisks represent the same fibre across cryosections. All scale bars are set to 50 μm.

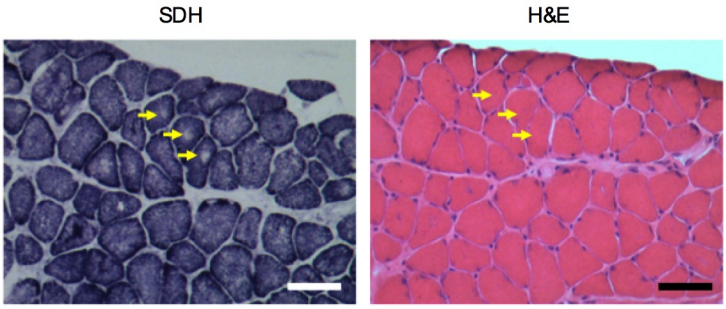

Figure 2.5. Potential core-like lesions in *Pln*^{OE} mouse at 4-6 months of age. SDH stained sections from the soleus muscle show areas devoid of oxidative staining representing potential core-like lesions (yellow arrows). Corresponding H&E stained serial section shows that the lack of oxidative staining with SDH is not due to the presence of a vacuole or an artifact in the muscle fibre.

Table 2.1. SERCA activity in mouse soleus muscles from WT and Pln^{OE} mice at 4-6 months of age.

	V_{max}	K_{Ca}	ΔK_{Ca}
WT	248.4 ± 11.5	6.63 ± 0.05	-
Pln^{OE}	181.6 ± 23.8*	6.47 ± 0.04*	0.16

Values are means ± standard error. Homogenates were isolated from WT (n = 6) and Pln^{OE} (n = 5) mouse soleus muscles and were analyzed for Ca^{2+}-ATPase activity over Ca^{2+} concentrations ranging from *p*Ca 7 to *p*Ca 4.5 to obtain K_{Ca}. K_{Ca} is the Ca^{2+} concentration required to attain the half-maximal Ca^{2+}-ATPase activity rate and is expressed in *p*Ca units. *Significantly different from WT using Student's t-test, $P \leq 0.05$.

Table 2.2. Quantitative analysis of fibre type distribution and cross-sectional area (CSA) in soleus muscles from WT and *Pln*^{OE} mice at 1 month, 4-6 months, and 10-12 months of age.

	1 month	4-6 months	10-12 months
Fibre distribution (%)			
Type I			
WT	56.2 ± 0.8	58.9 ± 6.9	64.1 ± 2.6
Pln^{OE}	60.7 ± 2.5[b]	91.7 ± 2.9*[a]	94.4 ± 1.8*[a]
Type I/IIA			
WT	6.4 ± 1.1[b]	0.5 ± 0.5[a]	0.6 ± 0.3[a]
Pln^{OE}	13.0 ± 1.5*[b]	0.6 ± 0.2[a]	0.7 ± 0.2[a]
Type IIA			
WT	34.0 ± 1.4	35.5 ± 3.1	31.3 ± 1.8
Pln^{OE}	21.9 ± 1.7*[b]	7.7 ± 2.6*[a]	4.9 ± 1.7*[a]
Fibre CSA (μm^2)			
Type I			
WT	1895 ± 158	2051 ± 273	2584 ± 343
Pln^{OE}	1291 ± 93*	871 ± 28*	1190 ± 90*
Type IIA			
WT	1260 ± 89	1915 ± 126	2225 ± 159[a]
Pln^{OE}	1617 ± 103[b]	2922 ± 180*[a]	5342 ± 703*[ab]

Values are means ± standard error (n = 3 per genotype). *Significantly different from WT within the same age; [a]Significantly different from 1 month within the same genotype; [b]Significantly different from 4-6 months within the same genotype; $P \leq 0.05$ using two-way ANOVA including genotype and age as factors and a Tukey's post-hoc test when necessary.

2.5 Discussion

To date, most studies concerning the physiological significance of PLN inhibition of SERCA have focused solely on its role in cardiac muscle health and disease (for review see (97)). To our knowledge, our current study is the first to demonstrate an important role for PLN and SERCA dysfunction in skeletal muscle health and CNM pathology. Specifically, we obtained commercially available Pln^{OE} mice to determine PLN's effect on SERCA function in skeletal muscle and uncovered a mouse model that phenotypically resembles the histopathological features associated with human CNM. In addition, our results with three human CNM patients suggest that SERCA dysfunction, possibly through increased PLN expression, contributes to CNM pathology. Although it is possible that the predominance of type I fibres in human CNM may explain the elevations in PLN expression, it is important to consider our results from the Pln^{OE} mouse, which indicate that overexpression of PLN specifically in type I fibres can cause type I fibre predominance and CNM. Thus, future studies with more CNM patients that are similar in age and genetically related are required to better investigate whether PLN plays a primary pathological role in human CNM.

We cannot fully explain why we repeatedly observed myopathy in the Pln^{OE} mouse while Song et al., did not report such a finding (41). Comparisons are difficult to make since SERCA function was not assessed and histology results were not shown in their study. Strain differences seem unlikely to account for the discrepant results since both transgenic lines were generated on an FVB/N background; however, it is possible that genetic drift and the level of PLN overexpression may be significant factors. Nevertheless, several results are in agreement between the two studies, including type I fibre predominance, atrophy, increased proteolytic markers and slower force kinetics in soleus muscle.

It has been estimated that 25-30% of human CNM cases remain genetically unresolved (64, 111) and our results raise the possibility that mutations in *Pln* leading to increased SERCA inhibition could be involved in those cases. Although *Pln* mutations either resulting in elevated PLN expression (122) or reduced PLN phosphorylation (123, 124) have been causally linked to human cardiomyopathy, it is unknown whether these mutations can affect skeletal muscle health. For example, deletion of arginine 14 (R14del) in the coding region of the *Pln* gene results in increased SERCA inhibition through increased monomeric PLN and reduced PLN phosphorylation at Ser16 by PKA (123). Interestingly, one patient with an R14del mutation in *PLN* developed late-onset mild dilated cardiomyopathy but was initially evaluated in a muscle dystrophy clinic for a 25-year history of slowly progressive muscle weakness (125). Since there were no significant abnormalities in the staining patterns of sarcolemmal proteins, muscular dystrophy was discounted; however, to our knowledge, the existence of CNM was not tested. Recent reports of human cases of CNM coexisting with cardiomyopathy (118, 126, 127) further highlight the importance of assessing the existence of CNM in skeletal muscles from patients with cardiomyopathy arising from *PLN* mutations.

Currently the mechanisms leading to CNM are not completely understood; however several mechanisms have been suggested, including abnormalities of triad structure and function (111, 114, 128-130). As a result of these triad defects, aberrant Ca^{2+} handling and excitation-contraction (EC) coupling are also thought to be important for CNM pathogenesis. Indeed, the identification of mutations in *RYR1* leading to CNM (116, 117) further supports the notion that triad dysfunction, Ca^{2+} dysregulation, and EC coupling are key pathogenic drivers of CNM (111). Since the SERCA pumps regulate SR Ca^{2+} load and, thus,

contractility, the SERCA pumps are also crucial for Ca^{2+} regulation and EC coupling. Thus, our results with the *Pln*^{OE} mice add further support to the hypothesis that defects in triad function, Ca^{2+} handling and EC coupling are important for CNM pathogenesis and extend the hypothesis by adding SERCA dysfunction as a potential pathogenic mechanism. Since abnormalities in triad structure are often found in human and animal CNM, future studies using electron microscopy should examine the triad structure in the *Pln*^{OE} mouse to determine whether structural abnormalities also contribute to the Ca^{2+} dysregulation seen in these mice. Furthermore, although the areas devoid of oxidative staining that cannot be explained by artifacts or the presence of vacuoles may represent core formations in the *Pln*^{OE} mouse, future studies with electron microscopy will confirm and characterize these potential core-like lesions.

One other interesting question raised by our study pertains to the role of SLN in CNM. Similar to PLN, SLN is a SERCA pump inhibitor (28, 32, 33), which suggests that the 7- to 9-fold upregulation in SLN protein found in the *Pln*^{OE} soleus and gluteus minimus muscles may contribute to the SERCA dysfunction, Ca^{2+} dysregulation, and CNM pathology. (33) Interestingly, this response in SLN expression is consistent with other mouse models of myopathy (69, 80, 89-91, 129), but the role of SLN remains unknown. Our finding that SLN content was reduced in human CNM reveals a potential species difference and suggests that this SERCA regulator may have minimal contribution to the SERCA dysfunction and overall CNM pathology. To test whether or not SLN actively contributes to the CNM phenotype found in the *Pln*^{OE} mice, future studies targeting the *Sln* gene are required. Furthermore, a novel micropeptide, myoregulin (MLN), was found to be structurally and functionally homologous with both PLN and SLN (131). When new antibodies targeting MLN protein

expression become available, it will be interesting to determine its response and potential involvement in murine and human CNM and myopathy in general.

In summary, the commercially available *Pln*^{OE} mouse histopathologically resembles human CNM. To date, there is no cure for CNM and many unresolved questions remain, including the mechanisms leading to skeletal muscle defects in patients. Mechanistically, our results from the *Pln*^{OE} mouse are consistent with the hypothesis that triad dysfunction, aberrant Ca^{2+} handling and EC coupling are important for CNM pathogenesis; but whether it is higher cytosolic Ca^{2+} and/or altered Ca^{2+} dynamics that lead to CNM histopathology, and how the muscle translates this dysregulated Ca^{2+} into the CNM phenotype remains unknown and future studies using the *Pln*^{OE} mouse will prove valuable. Furthermore, treatment strategies aimed at improving SERCA function have already shown promise in murine muscular dystrophy (57, 58, 132) and human cardiomyopathy (133-135). Thus, future studies that improve SERCA function through various modes, including adjustment of PLN levels, in the *Pln*^{OE} mouse and other animal models of CNM, could lead to the development of viable therapeutic strategies for CNM patients.

2.6 Materials Methods

***Pln*^{OE} mice**. The *Pln*^{OE} mice were resuscitated from cryopreserved embryos by the mmRRC (000067-MU, FVB/N background) to generate a breeding colony with WT FVB/N mice in our facility. The *Pln* transgene was attached to the β-MHC promoter so that these mice overexpress PLN in their slow-twitch type I skeletal muscle fibres. Animals were housed in an environmentally controlled room with a standard 12:12-hour light-dark cycle and allowed access to food and water *ad libitum*. Experiments were performed on littermate heterozygous

Pln^{OE} and WT males that were between the ages of 1 and 12 months. Reintroduction of homozygous *Pln*^{OE} mice was avoided by breeding heterozygous male *Pln*^{OE} mice with female WT mice. Analysis of 287 newborn mice showed that WT and heterozygous *Pln*^{OE} mice were born at the expected mendelian frequency with a ratio of 137:150. All animal procedures were reviewed and approved by the Animal Care Committee of the University of Waterloo and are consistent with the guidelines established by the Canadian Council on Animal Care.

Human subjects. Five healthy untrained university students were used as healthy controls. All subjects were fully informed of all experimental procedures and all associated risks before written consent was obtained. Written approval for the research was granted by the Human Research Ethics Committee at the University of Waterloo. Three patients with CNM from McMaster University Medical Centre were used in this study. One female (55 years old) patient had CNM due to a missense mutation in dynamin 2 (*DNM2,* 1105C→T, R369W) whereas the other two male CNM patients (17 and 44 year old) remain genetically unresolved. Of the two unresolved cases, one underwent 163-gene next generation sequencing, which included *MTM1, DNM2, RYR1, CACNA1S,* and *TTN*. The other unresolved patient was screened for *MTM1* and *DNM2*; however, he did not return to complete a screen for additional genes. Written approval for the use of material from previously consented and diagnosed patients was granted by the Chair of the Human Research Ethics Committee at McMaster University. All muscle tissue samples (~100 mg) were obtained from the vastus lateralis using the needle biopsy technique under suction (136).

These samples were homogenized and then frozen at -80°C prior to being used for western blotting and SERCA activity assays.

SERCA activity and Ca^{2+} uptake. Ca^{2+}-dependent SERCA activity was assessed in homogenates prepared from mouse (WT and Pln^{OE}) soleus and gluteus minimus muscles and human vastus lateralis muscles over Ca^{2+} concentrations ranging from *p*Ca 7.5 to 4.5 in the presence of the Ca^{2+} ionophore A23187 (Sigma C7522) using a spectrophotometric plate reader assay that has been described previously (137). SERCA activity-*p*Ca curves were generated with GraphPad Prism™ by non-linear regression curve fitting using an equation for a general cooperative model for substrate activation. Ca^{2+} uptake was measured in homogenates in the presence of the precipitating anion, oxalate, using the fluorescent dye Indo-1 and a spectrofluorometer equipped with dual-emission monochromators (138). Rates of Ca^{2+} uptake assessed at a free cytosolic Ca^{2+} concentration of 1500 nM are reported.

Antibodies. Primary antibodies against SERCA2a (2A7-A1), PLN (2D12), and dynamin 2 (PA5-19800) were obtained from Pierce Antibodies. The primary antibody for SERCA1a (A52) was a kind gift from Dr. David MacLennan (University of Toronto) (139). The primary antibody directed against SLN was generated by Lampire Biological Laboratories (20). Anti-ubiquitin (P4D1) and anti-nitrotyrosine (189542) antibodies were obtained from Cell Signaling Technology and Cayman Chemicals, respectively. The primary antibody against α-actin (A4700) was obtained from Sigma Aldrich. The primary antibodies against MHCI (BA-F8), MHCIIa (SC-71), MHCIIb (BF-F3), embryonic MHC (BF-F6) (140, 141) and dystrophin (3B7) (142) were obtained from Developmental Studies Hybridoma Bank.

Secondary antibodies for western blotting, goat anti-mouse IgG (peroxidase conjugated) and goat anti-rabbit IgG (peroxidase conjugated) were obtained from Santa Cruz Biotechnology. Secondary antibodies for immunofluorescence staining, Alexa Fluor 350 anti-mouse IgG_{2b}, Alexa Fluor 488 anti-mouse IgG_1, and Alexa Fluor 555 anti-mouse IgM, were obtained from Molecular Probes.

Western blot analysis. Single fibre Western blots were performed as previously described (20) to determine fibre-type specificity of PLN overexpression. Briefly, single fibres extracted from soleus muscles of WT and *Pln*^{OE} mice were placed into 1x solubilizing buffer. Solubilized proteins were then separated using tricine-based SDS-PAGE (6%-13% layered gel). Separated proteins were then transferred onto 0.2 μm polyvinylidene difluoride (PVDF) membranes. Membranes were then cut at the 75 kDa band (Western C Precision Plus^{TM}, BioRad, CA, USA) and were immunoprobed with PLN (<75 kDa strip) and with MHCI (>75 kDa strip). Following this, membranes were immunoprobed with horseradish peroxidase-conjugated secondary antibodies and antigen-antibody complexes were detected by Luminata Forte^{TM} (Millipore, MA, USA) for PLN, and ECL Western Blot Substrate (BioVision, MA, USA) for MHCI. After detection of MHCI, the membrane was stripped and re-probed with MHCIIa and antigen-antibody complexes were detected using ECL Western Blot Substrate.

Similarly, western blot analysis was performed to determine expression levels of SLN, PLN, SERCA isoforms, and dynamin 2 as well as levels of protein ubiquitylation (Ub) and –nitrosylation (Ny) in mouse (WT and *Pln*^{OE}) and human CNM muscles after homogenates were placed into 1x solubilizing buffer. Solubilized proteins from tissue homogenates, were separated using tricine based SDS-PAGE (13% total acrylamide for PLN and SLN) or a

standard SDS-PAGE (7.5% total acrylamide for SERCA isoforms and dynamin 2 and a 7.5%-15% layered gel for Ub and Ny). Separated proteins were then transferred onto 0.2 μm PVDF membranes (PLN, SERCAs, Ub, Ny) or nitrocellulose membranes (SLN). Membranes were then immunoprobed with their corresponding primary antibodies. Following this, membranes were immunoprobed with horseradish peroxidase-conjugated secondary antibodies and signals were detected by SuperSignal West Femto^{TM} substrate (Pierce, Thermo Fisher Scientific Inc.) for SLN; Luminata Forte^{TM} for SERCA2a, PLN, Ub, Ny, and RyR; and ECL Western Blot Substrate for SERCA1a and dynamin 2. Quantification of optical densities was performed using GeneTools (Syngene, MD, USA) and values were normalized to total protein or α-actin.

Histological, histochemical, and immunofluorescent staining. Soleus and gluteus minimus muscles from WT and *Pln*^{OE} mice were removed and embedded in O.C.T. compound (Tissue-Tek), frozen in liquid nitrogen-cooled isopentane, stored at -80°C, and cut into 10 μm thick cryosections with a cryostat (Thermo Electronic) maintained at -20°C. Histological staining included H&E and Van Gieson and histochemical staining included succinate dehydrogenase (SDH) and NADH-TR activity. Images were acquired with a brightfield Nikon microscope linked to a PixeLink digital camera and quantified with Image-Pro PLUS analysis software and ImageJ software. Immunofluorescence analysis of MHC expression was previously described (20, 96, 143) and performed with primary antibodies against MHCI, MHCIIa, and MHCIIb. Additional immunofluorescence analysis of embryonic MHC expression was conducted with primary antibodies against embryonic MHC along with primary antibodies against dystrophin. Slides were visualized with an Axio Observer Z1

fluorescent microscope equipped with standard red, green, blue filters, an AxioCam HRm camera, and AxioVision software (Carl Ziess). Quantification of fibres and cross-sectional area (CSA) was performed using ImageJ software.

Proteolytic activity and DCF assays. Calpain, caspase-3, and cathepsin-B/L activity were determined in soleus muscle homogenates using the substrates, Suc-LLVY-AMC (Enzo-Life Sciences), Ac-DEVD-AMC (Alexis Biochemicals), and z-FR-AFC (Enzo Life Sciences), respectively (143, 144). These fluorogenic substrates are weakly fluorescent but yield highly fluorescent products following proteolytic cleavage by their respective proteases. Fluorescence was measured using a SPECTRAmax Gemini XS microplate spectrofluorometer (Molecular Devices, Sunnyvale, CA) with excitation and emission wavelengths: 360 nm and 440 nm, respectively for caspase-3; 380 nm and 460 nm, respectively for calpain; 400 nm and 505 nm, respectively for cathepsin. Calpain activity was taken as the difference in fluorescence from homogenate incubated with and without calpain inhibitor. Calpain, caspase-3, and cathepsin activities were normalized to total protein content and expressed as fluorescence intensity in arbitrary units per mg of protein.

Generation of reactive oxygen species in soleus muscle homogenates from WT and Pln^{OE} mice was determined as previously described (143) using 2'7'-dichlorodihydroflurescein-diacetate (DCFH-DA, Invitrogen, Carlsbad, CA) at 37°C. Cellular esterases hydrolyze DCFH-DA to the non-fluorescent DCFH, which can then be oxidized by a variety of ROS to form highly fluorescent DCF. Fluorescence was measured using a SPECTRAmax Gemini XS microplate spectrofluorometer with excitation and emission

wavelengths of 490 nm and 525 nm, respectively. Fluorescence intensity was normalized to total protein content and expressed as arbitrary units per mg of protein.

Plasma CK analysis. WT and *Pln*^{OE} mice were anesthetized using somnotol (0.65 mg/kg body weight) and blood from the left ventricle was drawn into a heparinized syringe. Blood was centrifuged at 5000 *g* for 8 min and the plasma was decanted and stored at -80°C until analysis. CK activity was measured using a kinetic fluorometric assay as previously described (145).

Electrical stimulation and muscle contractility measurements. Experiments were performed on adult (4-6 month) WT and *Pln*^{OE} mice. Mice were killed by cervical dislocation, and the intact soleus muscles were removed and placed into a bath with oxygenated Tyrode solution (95% O_2, 5% CO_2) containing 121 mM $NaCl_2$, 5 mM KCl, 24 mM $NaHCO_3$, 1.8 mM $CaCl_2$, 0.4 mM NaH_2PO_4, 5.5 mM glucose, 0.1 mM EDTA, and 0.5 mM $MgCl_2$, pH 7.3 (146), and was maintained at 25°C. Muscles were situated between flanking platinum electrodes driven by a biphasic stimulator (Model 710B, Aurora Scientific, Inc.) and electrically evoked muscle force was assessed across a range of stimulation frequencies from 1 to 100 Hz. Data were analyzed using Dynamic Muscle Control Data Acquisition software (Aurora Scientific, Inc). Specifically, peak isometric force amplitude (mN) and the maximal rates of force development (+dF/dt) and relaxation (-dF/dt) were determined during a twitch and across the range of stimulation frequencies. Peak isometric force was then normalized to muscle weight (mN/g).

Treadmill exercise. WT and Pln^{OE} mice were assessed for muscle performance by running them to exhaustion on an enclosed motorized treadmill. All animals exercised at a running speed of 8m/min for 10 min followed by 10 min at 16 m/min and then allowed to reach exhaustion at 24 m/min at a 5° incline.

Statistics. All values are presented as means ± standard error. Statistical significance was set to $P \leq 0.05$. Comparisons between WT and Pln^{OE} mice were performed using Students *t*-test; however a two-way repeated measures ANOVA was used for force-frequency analysis, and when age was included as a factor. Post-hoc testing was done using Tukey's HSD. Comparisons between healthy controls and human CNM patients were performed using Students *t*-test.

Chapter 3

Thesis Study II

Diaphragm assessment in mice overexpressing phospholamban in slow-twitch type I muscle fibres

Val Andrew Fajardo[1], Ian Curtis Smith[1], Eric Bombardier[1], Paige J Chambers[1], Joe Quadrilatero[1], A. Russell Tupling[1]

From the [1]Department of Kinesiology, University of Waterloo, Waterloo, Ontario, Canada

Submitted to *Brain and Behavior*

Sept. 11, 2015

Manuscript ID: BRB3-2015-09-0181

3.1 Preface

This Chapter presents Thesis Study II as the manuscript *Diaphragm assessment in mice overexpressing phospholamban in slow-twitch type I muscle fibres* written in journal article style and currently in submission in the open-access journal Brain and Behavior. Since studies on diaphragm and respiratory function in animal models of CNM are limited (147), this Chapter assesses diaphragm structure and function in the Pln^{OE} mice. It was hypothesized that the diaphragm muscles, which normally express 10% type I fibres, would exhibit similar CNM-like features.

In addition, in this Chapter, calcineurin, a serine/threonine Ca^{2+}-dependent phosphatase, was introduced. Calcineurin contains a 60 kDa catalytic subunit and 19 kDa regulatory subunit (148), and upon Ca^{2+}-calmodulin binding to a region in the catalytic subunit, the autoinhibtory domain is ousted from the active cleft thereby increasing

calcineurin's phosphatase activity (149). The focus on calcineurin in this Chapter was based on its effects on stimulating muscle growth and the slow-oxidative fibre type gene program [for review see (150)]. To exert its effects, calcineurin dephosphorylates the family of transcription factors, nuclear factor of activated T-cells (NFATs), thereby allowing for their nuclear translocation and subsequent promotion of genes involved in muscle growth and the oxidative phenotype (150, 151). Of note, calcineurin activation and NFAT nuclear localization have been shown to be responsive only to sustained, low-amplitude Ca^{2+} signals rather than high-amplitude Ca^{2+} transients (152-154). There are five NFAT members in vertebrates, with only NFATc1, NFATc2, NFATc3, and NFATc4 being responsive to calcineurin (150, 155-158). Throughout the literature, NFATc1 has been the predominant indicator of calcineurin activation under states of skeletal muscle remodeling, and this isoform, specifically, has been shown to promote the genes controlling the expression of slows isoform proteins such as myoglobin, troponin I, and MHCI (8, 148, 150, 159-161).

Included in this Chapter are the Overview (Section 3.2), Introduction (Section 3.3), Material and Methods (Section 3.4), Results (Section 3.5), and Discussion (3.6) of the manuscript in the format of this thesis. Figures (Figures 3.1 to 3.3) and Table 3.1 corresponding to the Results are located in order at the end of Section 3.5. The Supplemental Material for this article, submitted as Supporting Information is displayed in Appendix B in the format of this thesis. The Supplemental Material includes Supplemental Results comprised of Supplemental Figures B1 – B3.

3.2 Overview

Aims: Phospholamban (PLN) and sarcolipin (SLN) are small inhibitory proteins that regulate the sarco(endo)plasmic reticulum Ca^{2+}-ATPase (SERCA) pump. Previous work from our

laboratory revealed that in the soleus and gluteus minimus muscles of mice overexpressing PLN (Pln^{OE}), SERCA function was impaired, dynamin 2 (3-5 fold) and SLN (7-9-fold) were upregulated, and features of human centronuclear myopathy (CNM) were observed. Here, we examined the diaphragm muscles of Pln^{OE} mice, as diaphragm function in mouse models of CNM has not been well studied to date. **Methods:** Diaphragm muscles from Pln^{OE} and WT mice were subjected to histological/histochemical/immunofluorescent staining, Ca^{2+}-ATPase and Ca^{2+} uptake assays, Western blotting, and *in vitro* electrical stimulation. **Results:** Our results demonstrate that PLN overexpression reduced SERCA's apparent affinity for Ca^{2+} but did not reduce maximal SERCA activity or rates of Ca^{2+} uptake. SLN was upregulated 2.5-fold whereas no changes in dynamin 2 expression were found. With respect to CNM, we did not observe type I fibre predominance, central nuclei, or central aggregation of oxidative activity in diaphragm, although type I fibre hypotrophy was present. Furthermore, *in vitro* contractility assessment of Pln^{OE} diaphragm strips revealed no reductions in force-generating capacity, maximal rates of relaxation, or maximal rates of force development. **Conclusions:** Therefore, the effects of PLN overexpression on skeletal muscle phenotype differ between diaphragm and the postural limb muscles, soleus and gluteus minimus. Uncovering the mechanisms behind the apparent resistance to CNM in Pln^{OE} diaphragm may aid in the development of novel therapeutic strategies.

3.3 Introduction

Centronuclear myopathies (CNM) are a group of congenital myopathies that, along with general muscle weakness, display increased proportion of fibres containing central nuclei, type I fibre predominance and hypotrophy, and central aggregation of oxidative

activity upon muscle biopsy (62, 64). Phospholamban (PLN) is a small (52 amino acid) protein that physically interacts with and inhibits the sarco(endo)plasmic reticulum Ca^{2+}-ATPase (SERCA) pump (31). Recently, we found that the soleus and gluteus minimus muscles from mice overexpressing PLN (Pln^{OE}) in their slow-twitch type I skeletal muscle fibres had impaired SERCA function and displayed the histopathological features associated with human CNM (162). Based on the appearance of radiating sarcoplasmic strands, type II fibre hypertrophy, and endomysial fibrosis, the CNM observed in the Pln^{OE} mice resembles human autosomal dominant CNM and, to an extent, *RYR1*-related and *TTN*-related CNM (67).

A recently published review highlighted that although diaphragm and ventilatory function have been examined in several murine models of myopathy including Pompe disease and Duchenne muscular dystrophy, among other neuromuscular diseases, similar reports are not available for animal models of CNM (147). Murine diaphragm normally consists of around 10% type I fibres (163, 164); therefore, in the present study we investigated the hypothesis that the diaphragm from Pln^{OE} mice would display impaired SERCA function, muscle weakness, and the appearance of the histopathological features associated with human CNM.

3.4 Materials and Methods

Animals and tissue collection

A total of 15 wild-type (WT; 30.9 ± 1.2 g) and 16 Pln^{OE} (30.7 ± 0.9 g) 4-6 month old mice were used in the study. Animals were housed in an environmentally controlled room with a standard 12:12-hour light-dark cycle and allowed access to food and water *ad libitum*.

Mice were sacrificed by cervical dislocation and diaphragm, soleus, and gluteus minimius muscles were extracted. We restricted analyses to the costal regions of the diaphragm muscles. Diaphragm strips were either used for the assessment of SERCA function, contractility, or histological/histochemical/immunofluorescence staining. Nuclear and cytosolic fractions from the diaphragm, soleus, and gluteus minmus muscles were extracted as previously described (143). All animal procedures were reviewed and approved by the Animal Care Committee of the University of Waterloo and are consistent with the guidelines established by the Canadian Council on Animal Care.

SERCA activity and Ca^{2+} uptake.

Ca^{2+}-dependent SERCA activity was assessed in homogenates prepared from mouse (WT and Pln^{OE}) diaphragm muscles over Ca^{2+} concentrations ranging from *p*Ca 7.0 to 4.8 in the presence of the Ca^{2+} ionophore A23187 (Sigma C7522) using a spectrophotometric plate reader assay that has been described previously (137). SERCA activity-*p*Ca curves were generated with GraphPad Prism™ by non-linear regression curve fitting using an equation for a general cooperative model for substrate activation. Ca^{2+} uptake was measured in muscle homogenates in the presence of the precipitating anion, oxalate, using the fluorescent dye Indo-1 and a spectrofluorometer equipped with a monochromator to control the excitation wavelength (355 nm) and two photomultiplier tubes to detect emitted light (405 and 485 nm) (138). Rates of Ca^{2+} uptake were assessed at a free Ca^{2+} concentration of 1.0μM.

Antibodies

Primary antibodies against SERCA2a (2A7-A1), PLN (2D12), NFATc1 (7A6) and dynamin 2 (PA5-19800) were obtained from Pierce Antibodies. The primary antibody for calcineurin was obtained from Milliopore (07-1491). The primary antibody for SERCA1a

(A52) was a kind gift from Dr. David MacLennan (University of Toronto) (139). The primary antibody directed against sarcolipin (SLN) was generated by Lampire Biological Laboratories (20). The primary antibody against α-actin (A4700) was obtained from Sigma Aldrich. The primary antibodies against MHCI (BA-F8), MHCIIa (SC-71), and MHCIIb (BF-F3) were obtained from Developmental Studies Hybridoma Bank. Primary antibodies for histone H2B and CuZnSOD were obtained from Upstate Cell Signaling Solutions and Stressgen Bioreagents, respectively. Secondary antibodies for Western blotting, goat anti-mouse IgG (peroxidase conjugated) and goat anti-rabbit IgG (peroxidase conjugated) were obtained from Santa Cruz Biotechnology. Secondary antibodies for immunofluorescence staining, Alexa Fluor 350 anti-mouse IgG_{2b}, Alexa Fluor 488 anti-mouse IgG_1, and Alexa Fluor 555 anti-mouse IgM, were obtained from Molecular Probes.

Western blot analysis

Western blot analysis was performed to determine expression levels of SERCAs, SLN, PLN, and dynamin 2 in the diaphragm muscles from WT and Pln^{OE} mice as previously described (162). In addition, calcineurin expression and NFAT nuclear localization in soleus, gluteus minimus, and diaphragm muscles were assessed. Electrophoretically separated proteins were transferred onto 0.2 μm polyvinylidene difluoride (PVDF) membranes (PLN, SERCAs, dynamin 2, NFATc, calcineurin) or nitrocellulose membranes (SLN). Membranes were then immunoprobed with their corresponding primary antibodies and thereafter, were immunoprobed with horseradish peroxidase-conjugated secondary antibodies. Antigen-antibody complexes were detected by SuperSignal West Femto™ substrate (Pierce, Thermo Fisher Scientific Inc.) for SLN; Luminata Forte™ (Millipore, MA, USA) for PLN and SERCA2a; and ECL Western Blot Substrate (BioVision, MA, USA) for SERCA1a, NFAT,

calcineurin, and dynamin 2. Quantitation of optical densities was performed using GeneTools (Syngene, MD, USA) and were normalized to total protein or α-actin.

Histological, histochemical, and Immunofluorescence staining

Diaphragm muscles from WT and Pln^{OE} mice were removed and embedded in O.C.T. compound (Tissue-Tek), frozen in liquid nitrogen-cooled isopentane, stored at -80°C, and cut into 10 μm thick cryosections with a cryostat (Thermo Electronic) maintained at -20°C. Haematoxylin and eosin (H&E) staining along with stains for succinate dehydrogenase (SDH) activity were performed. Images were acquired with a brightfield Nikon microscope linked to a PixeLink digital camera and quantified with Image-Pro PLUS analysis software and ImageJ software. Immunofluorescence analysis of MHC expression was previously described (20, 96, 143) and performed with primary antibodies against MHCI, MHCIIa, and MHCIIb. Slides were visualized with an Axio Observer Z1 fluorescent microscope equipped with standard red/green/blue filters, an AxioCam HRm camera, and AxioVision software (Carl Ziess). Quantification of fibres and cross-sectional area (CSA) was performed using ImageJ software.

In vitro diaphragm contractile assessment

Diaphragm strips were isolated and immediately placed into a bath of oxygenated Tyrode's solution (95% O_2, 5% CO_2) containing 121 mM $NaCl_2$, 5 mM KCl, 24 mM $NaHCO_3$, 1.8 mM $CaCl_2$, 0.4 mM NaH_2PO_4, 5.5 mM glucose, 0.1 mM EDTA, and 0.5 mM $MgCl_2$, *p*H 7.3 (3) and were maintained at 25°C. Muscle strips were situated between flanking platinum electrodes driven by a biphasic simulator (Model 710B, Aurora Scientific, Inc.) and electrically evoked muscle force was assessed across a range of stimulation frequencies from 1 to 100 Hz at optimum length for force production. Data were analyzed using Dynamic

Muscle Control Data Acquisition software (Aurora Scientific, Inc). Specifically, peak isometric force amplitude (mN) and the maximal rates of force development (+dF/dt) and relaxation (-dF/dt) were determined across the range of stimulation frequencies. Peak isometric force was then normalized to the calculated CSA of the muscle strip (m / l*d) where m is the muscle mass, l is the length, and d is mammalian skeletal muscle density (1.06 mg/mm^3) (165). A fatigue protocol (70 Hz for 350 ms every 2 seconds for 5 min) was performed to determine the number of contractions required to reduce force to 60% of the force of the initial 70 Hz contraction.

Statistics

All values are presented as means ± standard error. Statistical significance was set to $P \leq 0.05$. Most comparisons between WT and Pln^{OE} mice were performed using unpaired Students t-tests; however a two-way repeated measures ANOVA was used for force-frequency analysis of peak isometric force.

3.5 Results

SERCA function and expression of Ca^{2+} handling proteins

Phospholamban overexpression was evident in the diaphragm homogenates from Pln^{OE} mice as only 2.5 μg of total protein was required to detect PLN compared to the 25 μg required in the WT diaphragm (Figure 3.1A). PLN overexpression in diaphragm muscles led to a rightward shift in the activity-pCa curves (Figure 3.1B) and a significant increase in K_{Ca} compared to WT (Table 3.1, $P = 0.02$). However, maximal SERCA activity was not significantly different between genotypes (Table 3.1, $P = 0.45$). We did observe lower rates of Ca^{2+} uptake in the Pln^{OE} diaphragm homogenates compared to WT (Figure 3.1C),

however this only approached statistical significance ($P = 0.08$). Western blot analysis revealed no differences in the expression of SERCA1a (Figure 3.1D) or SERCA2a (Figure 3.1E) between WT and Pln^{OE} mice. SLN expression was found to be upregulated nearly 2.5-fold in the diaphragm homogenates from Pln^{OE} mice compared to WT (Figure 3.1F, $P < 0.001$).

Assessment of CNM features in diaphragm muscles from Pln^{OE} mice

H&E and SDH staining of diaphragm cryosections revealed no elevations in the percentage of fibres showing central nuclei (WT, 1.2 ± 0.2% vs. Pln^{OE}, 1.2 ± 0.3%, $P = 0.86$) or evidence of central aggregation of oxidative activity in the Pln^{OE} diaphragm (Figure 3.2A and B). A significant reduction in the percentage of type I fibres was found (Figure 3.2C and D, $P < 0.001$) and although individually the type II fibres (IIA, IIX, IIB) were not different between genotypes, there was a significant increase in the collective percentage of all type II fibres in the Pln^{OE} diaphragm (WT, 86.5 ± 0.7 % vs. Pln^{OE}, 95.0 ± 1.8%, $P < 0.001$). Furthermore, we observed a significant reduction ($P < 0.001$) in type I fibre CSA and a significant increase in type IIA ($P = 0.01$), type IIX ($P < 0.001$), and type IIB ($P < 0.001$) CSA in the Pln^{OE} diaphragm (Figure 3.2E). Western blotting for dynamin 2 expression in diaphragm revealed no significant differences between WT and Pln^{OE} mice (Figure 3.2F, $P = 0.87$).

Diaphragm contractility

Representative twitch and tetanic (100 Hz) force tracings illustrate no significant differences in absolute force production between WT and Pln^{OE} diaphragm strips (Figure 3.3A and B). In addition, twitch kinetics were unaltered with no differences in maximal rates of relaxation (-dF/dt: WT, 0.35 ± 0.017 vs. Pln^{OE}, 0.35 ± 0.04, mN/ms, $P = 0.89$) or maximal

rates of force development (+dF/dt: WT, 5.04 ± 0.51 vs. Pln^{OE}, 5.87 ± 0.68 mN/mm^2/ms, P = 0.34). Interestingly, across submaximal and maximal frequencies, Pln^{OE} diaphragm strips generated more specific force compared to WT but the difference was not significant (Figure 3.3C, P = 0.15). Finally, in response to a fatiguing stimulation protocol, Pln^{OE} diaphragms required on average 100 ± 8 contractions to reach 60% maximum isometric force at 70 Hz compared to 132 ± 19 in the WT diaphragm; however, this difference was not statistically significant (Figure 3.3D, P = 0.16).

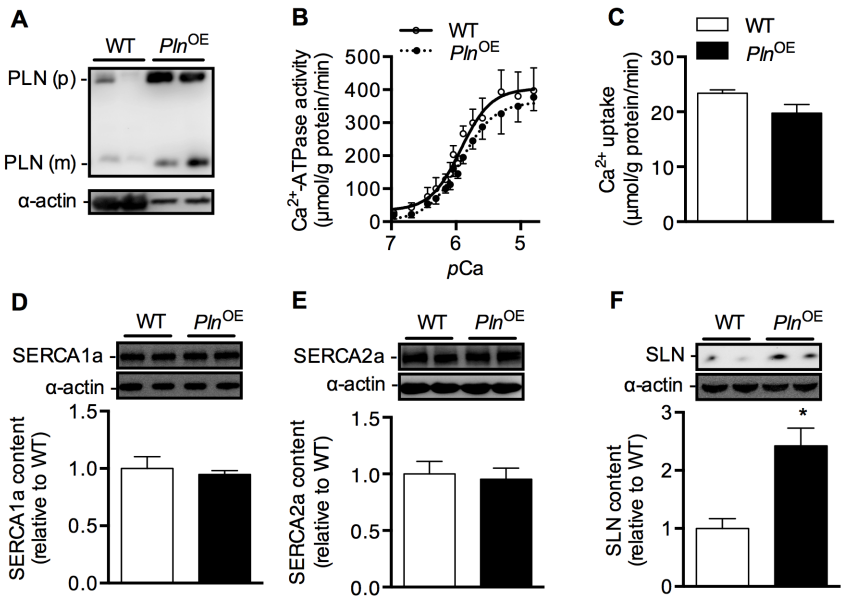

Figure 3.1. SERCA function in diaphragm muscles in *Pln*^{OE} mice at 4-6 months of age. **A:** Western blotting for PLN in WT and *Pln*^{OE} mice from diaphragm muscle homogenates. For WT mice, 25 μg of total protein was loaded whereas only 2.5 μg was required for *Pln*^{OE} mice to detect PLN protein. **B:** Ca^{2+}-ATPase activity-*p*Ca curves in WT (n = 6) and *Pln*^{OE} mice (n = 6) in the presence of the Ca^{2+} ionophore. **C:** Ca^{2+} uptake assessed in diaphragm muscles from WT (n = 4) and *Pln*^{OE} mice (n = 5). Western blotting for SERCA1a (**D**), SERCA2a (**E**), and SLN (**F**) in soleus from WT and *Pln*^{OE} mice (n = 4-5 per genotype). Total protein loaded was 1 μg, 4 μg, and 25 μg for SERCA1a, SERCA2a, and SLN, respectively. Actin was used as a loading control and all values are expressed relative to WT. *$P \leq 0.05$ versus WT using Student's t-test. All values are presented as mean ± standard error.

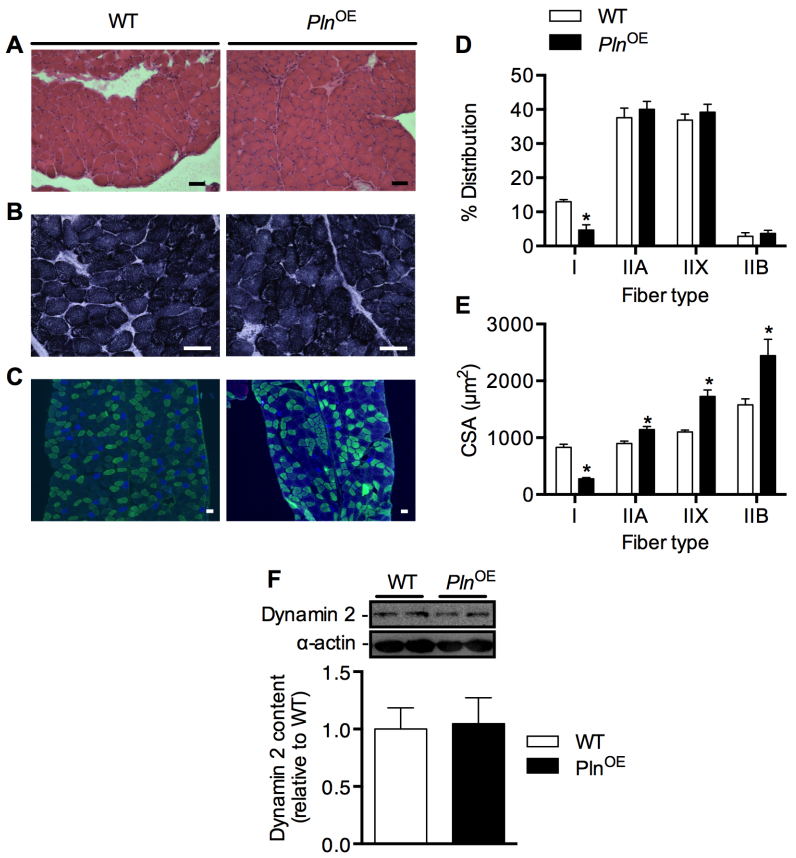

Figure 3.2. Diaphragm muscles from *Pln*^{OE} mice do not display CNM. Representative diaphragm cryosections from *Pln*^{OE} and WT mice after H&E staining (**A**), SDH staining (**B**), immunofluorescence staining for fibre type analysis (**C**). Cross sections were stained with MHC antibodies to identify type I (blue), type IIA (green), type IIB (red), and type IIX (unstained). **D:** Quantitative analysis of fibre type distribution in diaphragm muscles from WT and *Pln*^{OE} mice at 4-6 months of age. **E**: Quantitative analysis of fibre type cross-sectional area (CSA) in diaphragm muscles from WT and *Pln*^{OE} mice at 4-6 months of age. **F:** Dynamin 2 expression in diaphragm homogenates from WT and *Pln*^{OE} mice (n = 6 per genotype). Total protein loaded for dynamin 2 was 7.5 µg. *$P \leq 0.05$ versus WT using Student's t-test. All values are presented as mean ± standard error. Scale bars in **A-C** are set to 50 µm.

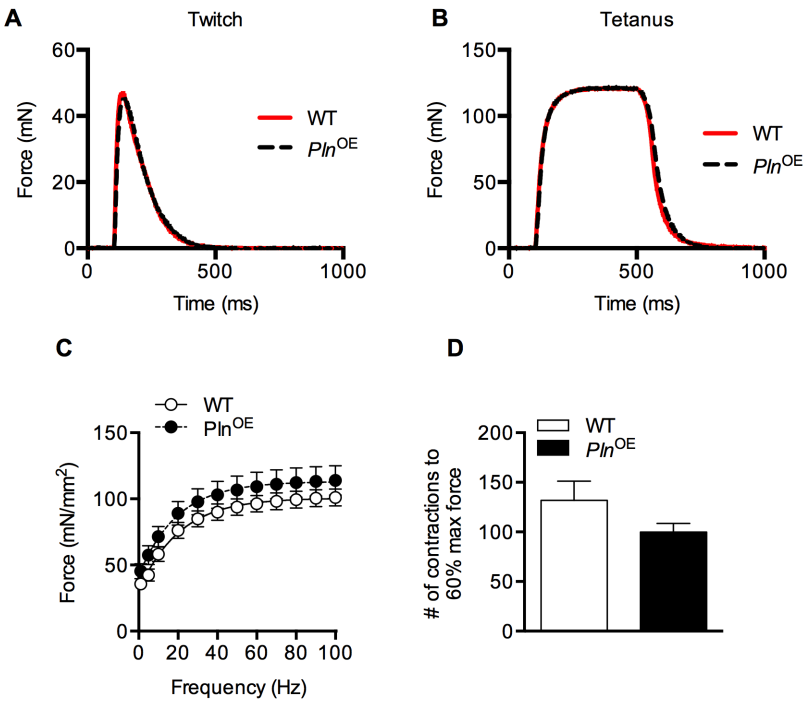

Figure 3.3. Diaphragm contractility in *Pln*^{OE} and WT mice at 4-6 months of age (n = 6 per genotype). **A:** Representative twitch (**A**) and tetanic (**B**) force tracings from WT and *Pln*^{OE} diaphragm strips. **C:** Force-frequency curve analysis in diaphragm strips from WT and *Pln*^{OE} mice. **D:** Number of contractions to reduce force to 60% of initial isometric force when isolated diaphragm strips underwent a fatiguing stimulation protocol (70 Hz for 350 ms every 2 seconds for 5 min).

Table 3.1. SERCA activity in mouse diaphragm muscles from WT and Pln^{OE} mice at 4-6 months of age.

Genotype	V_{max}	K_{Ca}	ΔK_{Ca}
WT	409.1 ± 29.8	5.98 ± 0.02	-
Pln^{OE}	382.1 ± 17.3	5.90 ± 0.02*	0.08

Values are means ± standard error. Homogenates were isolated from WT (n = 6) and Pln^{OE} (n = 5) mouse diaphragm muscles and were analyzed for Ca^{2+}-ATPase activity over Ca^{2+} concentrations ranging from *p*Ca 7 to *p*Ca 4.8 to obtain K_{Ca}. K_{Ca} is the Ca^{2+} concentration required to attain the half-maximal Ca^{2+}-ATPase activity rate and is expressed in *p*Ca units (negative logarithm of $[Ca^{2+}]$). *Significantly different from WT using Student's t-test, $P \leq 0.05$.

3.6 Discussion

Studies examining diaphragm function in animal models of CNM are limited as recently highlighted in a review by Smith, Goddard, and Childers (147). However, in a study published in the same year, Cowling and colleagues showed histopathological abnormalities with more atrophic fibres containing mislocalized nuclei in the diaphragm muscles from *mtm1*$^{-/y}$ mice (119), a mouse model which accurately recapitulates human X-linked myotubular myopathy (166). Correspondingly, *mtm1*$^{-/y}$ mice have a very short lifespan (6-14 weeks) (166) which is consistent with the severe respiratory complications often leading to early death reported in human cases of myotubular myopathy (110). We have recently reported that the *Pln*^{OE} mouse histopathologically resembles human autosomal dominant CNM (162), which, in contrast to myotubular myopathy, is generally less severe, and patients often have a normal lifespan with very few respiratory complications (64, 110, 113). Here, we have shown that the *Pln*^{OE} diaphragm exhibits type I fibre hypotrophy but does not display type I fibre predominance, increased central nuclei, central aggregation of oxidative activity or muscle weakness. In agreement with the differences in disease severity found in the diaphragm between mouse models, the *Pln*^{OE} mice live much longer than *mtm1*$^{-/y}$ mice, albeit, shorter than their WT littermates (Supplementary Figure B1).

Previous studies have shown that elevated dynamin 2 in skeletal muscle can lead to features of CNM (90, 120) while reducing its expression can improve muscle function and alleviate murine CNM pathology (119). Since, dynamin 2 is upregulated 3-5 fold in the *Pln*^{OE} soleus and gluteus minimus (162) but not diaphragm (Figure 3.2F), it is possible that differences in dynamin 2 expression could explain the lack of CNM phenotype in the *Pln*^{OE} diaphragm. How PLN overexpression and impaired SERCA function leads to increased

dynamin 2 in the affected muscles is unclear. Furthermore, although dynamin 2 has been implicated in the pathology of murine CNM, its role in human CNM is less established since we have recently observed a 35% reduction in its expression in muscle biopsies from CNM patients (162) while others have seen a 2-fold increase in patients with myotubular myopathy (119).

Our findings of minimal histopathological defects within the Pln^{OE} diaphragm despite PLN overexpression may argue against a potential role of elevated PLN in CNM pathology. An important difference between diaphragm and the postural limb muscles in the Pln^{OE} model is that SERCA function was not impaired in the diaphragm to the extent we observed in the soleus and gluteus minimus muscles (162). Although we did observe a reduction in SERCA's apparent affinity for Ca^{2+} as indicated by a rightward shift in the activity-*p*Ca curves and a significantly higher K_{Ca}, maximal SERCA activity was not reduced in the Pln^{OE} diaphragm compared to WT. Furthermore, rates of Ca^{2+} uptake were only trending to be lower in the Pln^{OE} diaphragm compared to WT (-15%), whereas Ca^{2+} uptake measured at the same *p*Ca was significantly reduced in the Pln^{OE} soleus (-75%) and gluteus minimus muscles (-25%) (Supplementary Figure B2). Combined with the unaltered maximal rates of relaxation in the Pln^{OE} diaphragm strips, collectively, these results suggest that the relatively modest impairment in SERCA function in the Pln^{OE} diaphragm may explain the lack of CNM histopathology in that muscle.

Differences in the severity of SERCA dysfunction across skeletal muscles in the Pln^{OE} mouse may also be due to differences in SLN expression. SLN is a well-known structural and functional homolog of PLN (20, 26, 28, 167) and, together, they have been shown to form a superinhibitory ternary complex with SERCA that not only reduces

SERCA's affinity for Ca^{2+}, but also the maximal rates of SERCA activity (28) and Ca^{2+} uptake (33). Interestingly, compared to the soleus and gluteus minimus, where SLN protein was upregulated 9-fold and 7-fold, respectively (162), SLN in the diaphragm was only elevated 2.5-fold. Upregulated SLN protein and/or mRNA is becoming widely known as a common feature in many myopathies (69, 89-91) and findings in the mdx mouse and mdx-utrophin double knockout model suggest that its expression may be directly proportional to disease severity (80). Similarly, SLN may follow disease severity in the Pln^{OE} mouse since the myopathy in the diaphragm, where only abnormalities in fibre CSA were evident, is far less severe than that found in the Pln^{OE} soleus and gluteus minimus, where all histopathological signs of CNM with additional endomysial fibrosis and core-like aspects were evident (162). However, the role that SLN plays in the Pln^{OE} mouse model of CNM or any other animal model of myopathy remains unknown.

Another potential explanation for the differences in SERCA function across the skeletal muscles may be that the healthy murine diaphragm comprises only 10% type I fibres and the Pln^{OE} diaphragm only consists of 4% type I fibres, which overexpress PLN, compared to the 99% and 50% previously found in the Pln^{OE} soleus and gluteus minimus muscles, respectively (162). In this model, it is possible that there may be a threshold percentage of type 1 fibres required to see impairments in SERCA and the concomitant muscle pathology. We suspect that in compensation for the type I fibre hypotrophy, the type II fibres of the postural soleus and gluteus minimus muscles exhibit greater load-bearing activity thereby leading to the sustained elevations of $[Ca^{2+}]_i$ required for calcineurin activation. Calcineurin signaling is known to promote both the slow-oxidative fibre phenotype (152, 154, 168) and myofibre hypertrophy (155, 169). Similar to a previous study

where calcineurin expression was found to be higher in the *Pln*^{OE} soleus compared with WT (41), our findings indicate greater calcineurin expression and NFAT nuclear content in the soleus and gluteus minimus muscles, but not in the *Pln*^{OE} diaphragm (Supplementary Figure B3). Moreover, calsarcin-2, an endogenous calcineurin inhibitor, is known to be highly expressed in diaphragm muscles (170). Thus, the inability to promote calcineurin-signaling may help to explain both the lower percent of type I fibres and the apparent increased susceptibility to muscle fatigue in the *Pln*^{OE} diaphragm compared with WT. Of note, respiratory muscles do not undergo transformation, particularly with respect to MHC isoform, due to training and inactivity in the same way as limb muscle fibres (171), which suggests that the reduced type I and increased type II fibre population represents a selective loss or underdevelopment of type I fibres due to PLN overexpression rather than a shift from slow-to-fast. Finally, type II fibre hypertrophy without calcineurin activation in the *Pln*^{OE} diaphragm may be explained by other Ca^{2+}-dependent systems, like calmodulin-dependent kinase II which is also important for adaptive muscle growth (172). Overall, the decreased percentage of type I fibres along with an increase in type II fibre CSA could be viewed as an adaptive response that helps maintain or even enhance force production and limit the CNM phenotype in the *Pln*^{OE} diaphragm (Figure 3.3C). This innate response may represent a novel therapeutic strategy combatting CNM and other congenital myopathies such as central cores since these are all type I fibre-related myopathies (62).

In summary, our results indicate that the *Pln*^{OE} diaphragm, compared with soleus and gluteus minimus, is generally more resistant to the CNM phenotype. Although the bases for these muscle differences are unclear, understanding the underlying mechanisms may lead to the generation of novel therapeutic strategies. Our findings here point to differences in SLN

expression and type I fibre distribution as potential contributing factors, and future studies will determine their impact.

Chapter 4

Thesis Study III

Sarcolipin is vital for muscle growth and remodeling and counters disease pathology

Val A. Fajardo, Dan Gamu, Bradley A. Rietze, Catherine Bellissimo, Andrew Mitchell, Darin Bloemberg, Paige J. Chambers, Frenk Kwon, Eric Bombardier, Joe Quadrilatero, A. Russell Tupling*

Department of Kinesiology, University of Waterloo, 200 University Ave., Waterloo, ON, N2L 3G1 Canada

Submitted to *Nature Medicine*

Nov. 3, 2015

Manuscript ID: NMED-L78623

4.1 Preface

Prior to this study, the question asking why SLN is upregulated across many conditions of muscle disease and damage had long remained unanswered. Several results within the literature and from this thesis led to the initial hypothesis that removing this upregulation of SLN may actually be beneficial for muscle function and integrity. First, SLN is a well-known inhibitor of the SERCA pump (28, 32, 33) and improving SERCA function in muscular dystrophy either through overexpression (58, 82, 83) or increased protection from cytotoxic damage via greater heat shock protein 72 interactions (57) has shown to increase muscle force producing capabilities and mitigate the dystrophic pathology by normalizing Ca^{2+} regulation in the muscle. Second, the increase in SLN content seems to progress with disease severity as shown in *mdx* and *mdx*/*Utr*$^{-/-}$ mice (88), and in the *Pln*^{OE} mice as highlighted in Thesis Study II. Third, acute overexpression of SLN in rat soleus muscle was

shown to cause drastic impairments in force production (49). Thus, with Ca^{2+} dysregulation being a main pathological defect in many myopathies, it is easy to speculate that removing SLN and improving SERCA's ability to regulate $[Ca^{2+}]_i$ could benefit muscle function and structure.

Importantly, while $[Ca^{2+}]_i$ overload may be a pathogenic factor, other Ca^{2+}-dependent processes are required in diseased states to elicit necessary adaptive responses. One, in particular, is calcineurin signaling, which was introduced in Thesis Study II. In muscular dystrophy, calcineurin activation is required to promote the slow-oxidative fibre phenotype (154, 155, 173), which is considered a viable therapeutic strategy (174-177). In fact, calcineurin activation has been shown to alleviate *mdx* pathology by promoting the expression of the dystrophin homolog utrophin and by enhancing the muscle's regenerative capacity (175, 178-180). Conversely, in a previous study, it was shown that inhibiting calcineurin activation worsens the dystrophic pathology in *mdx* mice (177). In addition, calcineurin activation can increase the expression of PGC-1α (181), which has also been shown to effectively combat muscular dystrophy and muscle atrophy (174, 182). Aside from diseased states, pharmacological inhibition of calcineurin results in a failure of myofibres to hypertrophy in response to mechanical overload stimulus (155) or insulin-like growth factor treatment (156, 169), and also prevents myoblast differentiation during muscle development (183). Altogether, these findings demonstrate the importance of Ca^{2+} signaling through calcineurin in promoting overall muscle health and countering disease pathology. Interestingly, SLN has been shown to stimulate calcineurin signaling to enhance oxidative capacity and combat obesity (184).

This Chapter adds further support of calcineurin's role in muscle health and SLN's role in stimulating calcineurin by using the Pln^{OE} mouse, two additional models of myopathy (tenotomy and *mdx*), and one model of muscle growth and remodeling (mechanical overload). Chapter 4 presents Thesis Study III as the manuscript *Sarcolipin is vital for muscle growth and remodeling and countering disease pathology* written in journal article style and currently in submission in Journal of Biological Chemistry. Included in this Chapter are the Overview (Section 4.2), Introduction (Section 4.3), Materials and Methods (Section 4.4), and the Results and Discussion (Section 4.5) of the manuscript in the format of this thesis. Figures 4.1 to 4.8 and Tables 4.1 and 4.2 are located in order at the end of Section 4.5.

4.2 Overview

Sarcolipin (SLN) is an important metabolic regulator in muscle that is recruited after high-fat feeding to uncouple the sarco(endo)plasmic reticulum Ca^{2+}-ATPase (SERCA) pump, increase energy expenditure, and combat obesity. Similar to high-fat feeding, SLN expression in skeletal muscle is also highly upregulated across various myopathic states, however to date, the physiological significance of this response remains unknown. Here, we used three different mouse models of disease/damage (centronuclear myopathy, tenotomy, and muscular dystrophy), and one mouse model of compensatory hypertrophy (mechanical overload), and found that, in the absence of *Sln*, myofibers were consistently smaller, had a faster fiber phenotype, and, in the case of muscular dystrophy, exhibited greater muscle degeneration. Thus, SLN upregulation in muscle not only combats obesity, but also muscle disease, and is an adaptive response that is necessary for muscle growth and remodelling and may provide a novel therapeutic strategy to counter a number of neuromuscular disorders.

4.3 Introduction

Sarcolipin (SLN) is a small regulator of the sarco(endo)plasmic reticulum Ca^{2+}-ATPase (SERCA) pump that has garnered a tremendous amount of attention in the field of muscle physiology and metabolism for its role in countering obesity (99). Specifically, we and others have found that under conditions of high-fat feeding, SLN expression in skeletal muscles increases 3-5-fold (2, 44) and combats obesity by uncoupling SERCA-mediated Ca^{2+} transport from ATP hydrolysis (3). As a result, scientists are now beginning to examine the role of SLN in human obesity (185). In addition to high-fat feeding, SLN expression is highly upregulated across a variety of muscle diseases and conditions (69, 87-89, 91-93, 186), however the physiological significance of this change in SLN expression has yet to be determined. Thus, the objective of this study was to determine the role of SLN in muscle disease and damage.

4.4 Materials and Methods

Mice. The Pln^{OE} and Sln^{KO} mice have been described previously(21, 187) and the *mdx* mice were purchased from The Jackson Laboratory (001801, Maine, USA). C57BL/6J Pln^{WT}/Sln^{WT}, Pln^{OE}/Sln^{WT}, Pln^{OE}/Sln^{KO} mice were generated by backcrossing heterozygous male FVB/N Pln^{OE} animals with either C57BL6/J Sln^{KO} or Sln^{WT} littermate females for 6 generations. As a result, all *Pln* overexpressing mice were heterozygous, and the Pln^{WT}/Sln^{WT} and Pln^{OE}/Sln^{WT} littermate mice were cousins to the Pln^{OE}/Sln^{KO} mice. To generate the mdx/Sln^{KO} and *mdx* colonies, homozygous *mdx* females ($X^{mdx}X^{mdx}$) were crossed with homozygous Sln^{KO} males ($Sln^{-/-}$). The resulting F1 progeny were hemizygous *mdx* males ($X^{mdx}Y$) and heterozygous mdx females ($X^{mdx}X$) that were all heterozygous for *Sln*

deletion ($Sln^{-/+}$). After crossing the hemizgous *mdx* females with heterozygous *mdx* males from F1, we selected the founders for the two separate lines used in this study. First, the *mdx*/Sln^{KO} colony was produced by breeding F2 hemizygous *mdx* females with F2 dystrophin-positive males, and both sires and dams were homozygous negative for *Sln* ($Sln^{-/-}$). Second, the *mdx*/Sln^{WT} (*mdx*) colony was produced by breeding F2 hemizygous *mdx* females with F2 dystrophin-positive males, and both sires and dams were homozygous positive for *Sln* ($Sln^{+/+}$). As a result, the *mdx* and *mdx*/Sln^{KO} mice were cousins at best and were on a C57BL6/J:C57BL/10 background. All animals used in the study were adult mice ranging from 3-6 months of age. Animals were housed in an environmentally controlled room with a standard 12:12-hour light-dark cycle and allowed access to food and water *ad libitum*. All animal procedures were reviewed and approved by the Animal Care Committee of the University of Waterloo and are consistent with the guidelines established by the Canadian Council on Animal Care.

Simultaneous plantaris mechanical overload and soleus muscle tenotomy. To mechanically overload the plantaris muscles, WT and Sln^{KO} mice (3-4 months) were first anaesthetized with 2% isofluorane in a precision vaporizer. Next, the soleus and gastrocnemius tendons were transected as previously described(188) and mice were left for two weeks in individually housed cages to adapt. Subsequently, the mice were killed by cervical dislocation and the plantaris (sham and overload) and soleus (sham and tenotomized) muscles were isolated and either homogenized in homogenizing buffer (250 mM sucrose, 5 mM HEPES, 0.2 mM PMSF, 0.2% [w/v] NaN_3) or embedded in O.C.T. compound (Tissue-Tek) frozen in liquid nitrogen-cooled isopentane then stored at -80°C until further analysis.

Cardiotoxin injury. Acute myotoxic injury was applied to anaesthetized (2% isofluorane in a precision vaporizer) WT and *Sln*^{KO} mice (3-4 months) by injecting 10 μM cardiotoxin (Sigma-Aldrich) dissolved in sterile saline into the tibialis anterior (TA) muscles. At days 7, 14, or 21 post-injection, animals were killed by cervical dislocation and their TA muscles were extracted and either homogenized or embedded in O.C.T. compound frozen in liquid nitrogen-cooled isopentane then stored at -80°C until further analysis.

SERCA function. Ca^{2+}-dependent SERCA activity was assessed in soleus homogenates over Ca^{2+} concentrations ranging from *p*Ca 7.2 to 5.4 in the presence of the Ca^{2+} ionophore A23187 (Sigma C7522) using a spectrophotometric plate reader assay as previously described(137). Maximal SERCA activity was taken from the raw data and SERCA activity-*p*Ca curves were generated with GraphPad Prism™ by non-linear regression curve fitting using an equation for a general cooperative model for substrate activation. Ca^{2+} uptake was measured at a free [Ca^{2+}] of 1500 nM in soleus homogenates in the presence of precipitating anion, oxalate, using the fluorescent dye Indo-1 and a spectrofluorometer equipped with dual-emission monochromators(138).

Daily food intake and activity. Daily food consumption (g/day) and cage activity were measured using a comprehensive laboratory animal monitoring system (CLAMS; Oxymax series; Columbus Instruments, Columbus, OH, USA) as previously described(2). This system is equipped with a feed scale for monitoring mass of food consumed, as well as *X*- and *Z*-axes infrared photocell detectors that allow for monitoring ambulatory activity (when 2

adjacent *x*-axis beams were broken in succession) and total cage activity. Mice were placed in the CLAMS for a 3-day period for 3 separate trials and had free access to food and water.

Antibodies. Primary antibodies against PLN (2D12), phosphorylated-NFAT (PA5-38301), and total NFAT (MA3-024) were obtained from Pierce Antibodies. The primary antibody directed against SLN was generated by Lampire Biological Laboratories(20). The utrophin (610896) antibody was purchased from BD Biosciences. LC3B (2775) and p62 (GP62-C) antibodies were obtained from Cell Signaling Technology and Progen Biotechnik, respectively. The primary antibody against actin (A2066) was obtained from Sigma Aldrich. The primary antibodies against MHCI (BA-F8), MHCIIa (SC-71), and MHCIIb (BF-F3) were obtained from Developmental Studies Hybridoma Bank. Secondary antibodies for western blotting, goat anti-mouse IgG (peroxidase conjugated) and goat anti-rabbit IgG (peroxidase conjugated) were obtained from Santa Cruz Biotechnology. Secondary antibodies for immunofluorescence staining, Alexa Fluor 350 anti-mouse IgG_{2b}, Alexa Fluor 488 anti-mouse IgG_1, and Alexa Fluor 555 anti-mouse IgM, were obtained from Molecular Probes.

Western blotting. Western blotting was performed to determine expression levels of SLN, PLN, phosphorylated-NFAT, total NFAT, utrophin, LC3, and p62. Solubilized proteins from tissue homogenates, were separated using tricine based SDS-PAGE (13% total acrylamide for PLN and SLN) or standard SDS-PAGE (6% total acrylamide for utrophin; 7.5% total acrylamide for phosphorylated-NFAT, total NFAT; 12% total acrylamide for p62 and LC3). Separated proteins were then transferred onto 0.2 μm PVDF membranes for all analyses

except for SLN, which utilized nitrocellulose membranes. Membranes were then immunoprobed with their corresponding primary antibodies and subsequently immunoprobed with horseradish peroxidase-conjugated secondary antibodies. Antigen-antibody complexes were detected by SuperSignal West Femto™ substrate (Pierce, Thermo Fisher Scientific Inc.) for SLN, utrophin, and phosphorylated NFAT; Luminata Forte™ for and PLN; and ECL Western Blot Substrate for total NFAT, LC3 and p62. Quantification of optical densities was performed using GeneTools (Syngene, MD, USA) and values were normalized to total protein after ponceau staining or actin.

Histological, histochemical, and immunofluorescent staining. Soleus, plantaris, and diaphragm muscles embedded in O.C.T. compound were cut into 10 μm thick cryosections with a cryostat (Thermo Electronic) maintained at -20°C. Histological staining included H&E and Van Gieson and histochemical staining included succinate dehydrogenase (SDH) activity. Images were acquired with a brightfield Nikon microscope linked to a PixeLink digital camera and quantified with ImageJ software. Immunofluorescence analysis of MHC expression was previously described(96) and performed with primary antibodies against MHCI, MHCIIa, and MHCIIb. Slides were visualized with an Axio Observer Z1 fluorescent microscope equipped with standard red, green, blue filters, an AxioCam HRm camera, and AxioVision software (Carl Ziess). Quantification of fiber distribution and cross-sectional area (CSA) was performed using imageJ software. The minimal Feret's diameter, which is the minimum distance of parallel tangents at opposing borders of the muscle fiber(189), was quantified using H&E-stained sections with imageJ software.

Proteolytic activity. Caspase-3 and cathepsin-B/L activity were determined in soleus muscle homogenates using the substrates Ac-DEVD-AMC (Alexis Biochemicals) and z-FR-AFC (Enzo Life Sciences), respectively, whereas calpain and 20S proteasome activity were determined using Suc-LLVY-AMC (Enzo-Life Sciences)(187). These fluorogenic substrates are weakly fluorescent but yield highly fluorescent products following proteolytic cleavage by their respective proteases. Fluorescence was measured using a SPECTRAmax Gemini XS microplate spectrofluorometer (Molecular Devices, Sunnyvale, CA) with excitation and emission wavelengths of 360 nm and 440 nm (caspase-3), 380 nm and 460 nm (calpain and 20S proteasome), or 400 nm and 505 nm (cathepsin), respectively. To distinguish between calpain and 20S proteasome activity, the specific inhibitors Z-Leu-Leu-CHO (calpain; Enzo-Life Sciences) and epoxomicin (20S proteasome; Cayman Chemical) were incubated and the difference in fluorescence from homogenates incubated with and without the respective inhibitors was measured. All proteolytic activities were normalized to total protein content and expressed as fluorescence intensity in arbitrary units per mg of protein.

Serum creatine kinase analysis. *mdx* and *mdx*/*Sln*^{KO} mice were anesthetized using somnotol (0.65 mg/kg body weight) and blood from the left ventricle was drawn into a syringe. Blood was centrifuged at 5,000 *g* for 8 min and the serum was decanted and stored at -80°C until analysis. CK activity was measured using a kinetic fluorometric assay as previously described (145).

Electrical stimulation and muscle contractility measurements. *Pln*^{WT}/*Sln*^{WT}, *Pln*^{OE}/*Sln*^{WT}, and *Pln*^{OE}/*Sln*^{KO} mice were killed by cervical dislocation, and the intact soleus muscles were

removed and placed into a bath with oxygenated Tyrode solution (95% O_2, 5% CO_2) containing 121 mM $NaCl_2$, 5 mM KCl, 24 mM $NaHCO_3$, 1.8 mM $CaCl_2$, 0.4 mM NaH_2PO_4, 5.5 mM glucose, 0.1 mM EDTA, and 0.5 mM $MgCl_2$, pH 7.3(146), and was maintained at 25°C. Muscles were situated between two platinum electrodes and force was electrically evoked and assessed across a range of stimulation frequencies from 1 to 100 Hz using a biphasic stimulator (Model 710B, Aurora Scientific, Inc.). Peak isometric force amplitude (mN) was analyzed using Dynamic Muscle Control Data Acquisition software (Aurora Scientific, Inc) and then normalized to muscle weight (mN/g).

Electron Microscopy. To examine the triad structures in the soleus muscles of Pln^{WT}/Sln^{WT}, Pln^{OE}/Sln^{WT}, and Pln^{OE}/Sln^{KO} mice we performed transmission electron microscopy (TEM). Briefly, muscle samples (1 cubic mm each) were fixed immediately, in 2.5% glutaraldehyde (EM grade) in 0.2M phosphate buffer (pH 7.4) overnight at 4°C. Subsequently, samples were postfixed in 1% osmium tetraoxide in the same buffer, dehydrated in a graded acetone series, and embedded in an epon-aldarite resin. Semithin sections (0.74 μm) were stained with toluidine blue and placed on a hot plate for 30 seconds to determine orientation of samples. Ultrathin longitudinal sections (90 nm) were cut on a Leica Reichart Ultracut E microtome, double contrasted with uranyl acetate (50% in methanol) and lead citrate (0.4% w/v in boiled H_2O), and viewed in a CM 10 Philips TEM. Sarcoplasmic reticulum areas were quantified using imageJ.

Statistics. All values are presented as means ± standard error (SEM). Statistical significance was set to $P \leq 0.05$. Comparisons between Pln^{WT}/Sln^{WT}, Pln^{OE}/Sln^{WT}, and Pln^{OE}/Sln^{KO} mice

were performed using a one-way ANOVA with a Tukey's post-hoc test; however a two-way repeated ANOVA with a Tukey's post-hoc test was used for force-frequency analysis. For mechanical overload and tenotomy experiments, we examined the effects of overload and tenotomy (vs. sham) separately in WT mice and Sln^{KO} mice. These planned comparisons on stratified datasets were executed using a two-way repeated measures ANOVA for myofiber CSA, a non-parametric two-sample Kolmogorov-Smirnov test for fiber CSA frequency distribution, and paired t-tests (one-tailed) for fiber type distribution and p-NFAT/NFAT. Comparisons between *mdx* and *mdx*/Sln^{KO} mice were performed using either a Student's t-test or two-way ANOVA. Finally, comparisons between cardiotoxin-injured WT and Sln^{KO} mice at days 7, 14, and 21 were performed using a Student's t-test at each day. Any significant differences in standard deviations amongst our datasets were adjusted for using Welch's corrections.

4.5 Results and Discussion

Phospholamban (PLN) is a well-known inhibitor of SERCA pumps and its overexpression in mouse slow-twitch type I skeletal muscle fibers (Pln^{OE}) causes impaired SERCA function, soleus muscle atrophy, centronuclear myopathy (CNM)-like phenotype, and a 7-9-fold upregulation of SLN protein (187). To examine the role of SLN in muscle myopathy, we first crossed Pln^{OE} mice with Sln^{KO} mice. Since forced over-expression of SLN in skeletal muscle represses SR Ca^{2+} uptake and impairs contractile function (49), we hypothesized that removing *Sln* would improve SERCA function (26) and alleviate the muscle weakness and myopathy observed in the Pln^{OE} mice. Contrary to our hypothesis, and despite 8-fold higher SLN in Pln^{OE}/Sln^{WT} compared with Pln^{WT}/Sln^{WT} mice ($P = 0.005$, Fig.

4.1A), rates of Ca^{2+} uptake (-18-20%) and SERCA's apparent affinity for Ca^{2+} (K_{Ca}) were similarly reduced in the Pln^{OE}/Sln^{WT} and Pln^{OE}/Sln^{KO} mice compared with Pln^{WT}/Sln^{WT} mice, and there were no differences in maximal SERCA activity (V_{max}) (Fig. 4.1B-C and Table 4.1).

Corresponding with the lack of improvement in SERCA function, *Sln* deletion did not mitigate CNM pathology since the three typical hallmarks (central nuclei, type I fiber predominance and hypotrophy, and central aggregation of oxidative activity) (64) and additional ultrastructural/histopathological features of triad disruption (111, 128), endomysial fibrosis and core-like aspects (187) were found to a similar degree and, perhaps, even greater in Pln^{OE}/Sln^{KO} mice compared with Pln^{OE}/Sln^{WT} (Fig. 4.1D-L). Indeed, we found evidence that *Sln* deletion worsened the Pln^{OE}-induced myopathy by exacerbating soleus muscle atrophy and weakness, revealed by significant reductions in the soleus:body weight ratio and mass-specific force at submaximal and maximal frequencies (50-100 Hz) (Fig. 4.2). The soleus muscle atrophy in Pln^{OE}/Sln^{KO} mice could not be explained by differences in body weight, daily ambulation, daily food intake (Table 4.2), or increases in either proteolytic enzyme activities or autophagic signaling compared with Pln^{OE}/Sln^{WT} (Fig. 4.3).

In response to the type I fiber hypotrophy induced by *Pln* overexpression, the type II fibers of the soleus muscles experience greater and longer load-bearing activities causing them to hypertrophy and undergo a fast-to-slow fiber type transition (Ref (187) and Fig. 1G and H). Strikingly, the type II fibers from the Pln^{OE}/Sln^{KO} soleus failed to hypertrophy (Fig. 4.1H), therefore accounting, at least in part, for the exacerbated soleus muscle atrophy and weakness. In addition, the fast-to-slow fiber type conversion in the Pln^{OE}/Sln^{KO} soleus was less prominent as the percent of type IIA fibers remained high (~36%) and was not different from the Pln^{WT}/Sln^{WT} soleus (Fig. 4.1G). Similar to that with *Pln* overexpression, the type II

fibers from mechanically overloaded plantaris muscles also display myofiber hypertrophy and a fast-to-slow fiber type shift as a result of synergist ablation of soleus and gastrocnemius muscles (155). Therefore, we questioned whether *Sln* deletion would also impair the muscle growth and remodelling in this model. To this end, we mechanically overloaded plantaris muscles for 2 weeks by performing soleus and gastrocnemius tenotomy (surgical transection of the tendon) (188), which in the WT mice induced ectopic expression of SLN (Fig. 4.4A). Interestingly, we detected a significant main effect of surgery in the WT mice indicating myofiber hypertrophy ranging from +22% to +48% (Fig. 4.4B); however, there were no significant differences in myofiber CSA between sham and overloaded muscles in Sln^{KO} mice (Fig. 4B). Furthermore, fiber size distribution indicates that the overloaded Sln^{KO} plantaris is characterized by an increase in smaller fibers (<2,400 μm^2) and a reduction in larger fibers (>3,600 μm^2) compared with WT (Fig. 4.4C). With respect to the expected fast-to-slow fiber type transition, we found a significant increase in type I and IIA fiber percentage in the WT mice, but not in Sln^{KO} mice (Fig. 4.4D). Thus, the plantaris myofibers from Sln^{KO} mice failed to hypertrophy and transition towards a slow-oxidative fiber phenotype after overload stimulus similar to that seen in Pln^{OE}/Sln^{KO} mice.

To explain the attenuation in both type II fiber hypertrophy and fiber type conversions in the absence of *Sln*, we focused on calcineurin, the Ca^{2+}-calmodulin dependent serine/threonine phosphatase known to regulate these cellular adaptations (154, 155, 169) and, perhaps more importantly, shown to be responsive to SLN (184). Specifically, in a previous study using *Sln* overexpressing mice, calcineurin phosphatase activity was increased 25% and led to a significant dephosphorylation of the calcineurin substrate NFAT in skeletal muscle (184). Here, in response to mechanical overload, we found a significant decrease in

phosphorylation of NFAT (-61%) in WT mice, which was blunted in Sln^{KO} mice (-22%) (Fig. 4.5A). Similarly, we found that Pln^{OE}/Sln^{KO} soleus had more phosphorylated NFAT compared with Pln^{OE}/Sln^{WT} (Fig. 4.5B), which altogether suggests lowered calcineurin signaling in these muscles that lack SLN. These results are in agreement with previous findings (184) and show that SLN upregulation may trigger calcineurin-mediated muscle growth and remodelling that, in the case of Pln^{OE} mice, combats muscle atrophy and weakness.

To further characterize SLN's role in muscle myopathy, we also examined the tenotomized soleus, which is a model of hindlimb unloading, that unlike mechanical overload, causes muscle degeneration and a slow-to-fast fiber type shift (190, 191). Here, we show that tenotomy increased SLN in soleus muscles 14-fold ($P = 0.004$, Fig. 4.6A), and, similar to Pln^{OE}/Sln^{KO} mice, led to a more severe soleus muscle atrophy in the absence of *Sln* (Fig. 4.6B). As expected, a significant main effect of tenotomy in WT mice was detected indicating a 29% to 38% reduction in average myofiber CSA (Fig. 4.6C). Interestingly, Sln^{KO} mice also exhibited significant myofiber atrophy, although with a slightly higher percent reduction (33% to 42%) in average myofiber CSA (Fig. 4.6C). Moreover, the Sln^{KO} tenotomized soleus is characterized by an increase in small myofibers with a CSA <1,500 μm^2 and a decrease in large myofibers (>2,250 μm^2) (Fig. 4.6D). With respect to the expected slow-to-fast fiber type transition, WT tenotomized soleus muscles exhibited a partial slow-to-fast fiber type transition with a significant decrease and trending increase in type IIA and type IIX fiber percent, respectively (Fig. 4.6E). Strikingly, the Sln^{KO} tenotomized soleus displayed an accelerated slow-to-fast fiber type transition with a significant decrease and increase in type I and type IIX fiber percent, respectively (Fig. 4.6E).

The percent of type IIA fibers from tenotomized Sln^{KO} soleus muscles also exhibited a trending decrease compared with sham. Calcineurin normally stabilizes/counteracts the effects of reduced mechanical loading (192), and consistent with SLN's putative role in stimulating calcineurin (184), we found a significant decrease in phosphorylation of NFAT in WT (-57%), which was blunted in Sln^{KO} mice (-32%) (Fig. 4.6F). Thus, combined with the experiments with mechanical overload and Pln^{OE} mice, these results suggest that SLN recruitment is required to potentiate muscle growth and slow muscle atrophy, possibly by amplifying calcineurin activation.

Lastly, we examined the dystrophic *mdx* mouse model, where SLN upregulation in a variety of muscle types has been observed (88), by generating *mdx*/Sln^{KO} mice (Fig. 4.7A). Consistent with the results throughout this study, our findings with *mdx*/Sln^{KO} mice show reduced myofiber area with significant main effects of *Sln* deletion in the soleus and diaphragm muscles (Fig. 4.7B). Furthermore, *Sln* deletion caused a slow-to-fast fiber type transition in soleus and diaphragm muscles relative to *mdx* (Fig. 4.7C), which may be maladaptive since promoting a slow-oxidative fiber phenotype is considered an attractive therapeutic strategy to increase expression of the dystrophin homolog, utrophin, that provides compensatory membrane stability (175). Calcineurin controls utrophin expression (176, 177), and lower utrophin levels in the *mdx*/Sln^{KO} muscles (Fig. 4.7D) further supports SLN's putative role in calcineurin activation and accounts for the enhanced myofiber breakdown revealed with higher serum CK (Fig. 4.7E). In addition, *mdx*/Sln^{KO} mice had greater heterogeneity in myofiber size, indicated by the minimal Feret's diameter coefficient of variation (Fig. 4.7F and G) which is a sensitive and reliable measure of muscular dystrophy (189). The combined effects of greater muscle breakdown, lowered myofiber CSA, and

impaired muscle regeneration revealed with lower central nuclei (Fig. 4.7H) as a result of *Sln* deletion, likely accounts for the greater variation in the minimal Feret's diameter, and demonstrates clearly that *Sln* deletion worsens *mdx* pathology. Furthermore, the impaired regenerative capacity was supported with cardiotoxin experiments, whereby in response to acute muscle injury, the TA muscles from Sln^{KO} mice exhibited a delay in muscle regeneration (Fig. 4.8). Specifically we found ectopic expression of SLN by day 21 post-injury, and removal of this adaptive response led to a failed clearing of central nuclei and smaller CSAs of regenerating fibers at that time point. In the context of muscular dystrophy, where constant degeneration and regeneration cycling occurs, these results suggest that in the absence of SLN, this balance may shift toward greater muscle degeneration, which could also account for the greater serum CK and variability in the minimal Feret's diameter observed in *mdx*/Sln^{KO} mice (Fig. 4.7E and G).

In summary, our study has addressed the long-unanswered question pertaining to SLN's upregulation across many skeletal muscle diseases. Here, we have demonstrated a novel role for SLN in countering disease by regulating muscle growth and remodelling, and future studies should determine whether increasing SLN in diseased or damaged states represents a viable therapeutic strategy. Indeed, high-fat feeding upregulates SLN (2, 44) and has been shown to benefit muscle structure and function in *mdx* mice (193). Furthermore, our results provide another way in which SLN can offset obesity since promoting skeletal muscle growth can reduce/attenuate adiposity and improve glucose metabolism (194-196). Thus, in conclusion, our results demonstrate further the importance of SLN in overall muscle health, and we propose that increasing SLN in muscle not only counters obesity, but also muscle disease, and could potentially prevent the muscle wasting that occurs during aging

and cachexia (197, 198). We anticipate that future studies examining the underlying mechanisms responsible for SLN's effects on muscle growth and remodelling will lead to the generation of novel therapeutic strategies.

TABLE 4.1. **SERCA activity in mouse soleus muscles from Pln^{WT}/Sln^{WT}, Pln^{OE}/Sln^{WT}, and Pln^{OE}/Sln^{KO} mice.**

	Pln^{WT}/Sln^{WT}	Pln^{OE}/Sln^{WT}	Pln^{OE}/Sln^{KO}
SERCA activity			
V_{max}	390.1 ± 8.9	392.7 ± 21.5	379.9 ± 12.2
K_{Ca}	6.34 ± 0.02	6.27 ± 0.01*	6.24 ± 0.02*
ΔK_{Ca}	-	0.07	0.10

Soleus muscle homogenates were isolated from Pln^{WT}/Sln^{WT} (n = 7), Pln^{OE}/Sln^{WT} (n = 6), and Pln^{OE}/Sln^{KO} mice (n = 6) and were analyzed for Ca^{2+}-ATPase activity over Ca^{2+} concentrations ranging from *p*Ca 7.2 to *p*Ca 5.4 to obtain K_{Ca}. K_{Ca} is the Ca^{2+} concentration required to attain the half-maximal Ca^{2+}-ATPase activity rate and is expressed in *p*Ca units. *Significantly different from Pln^{WT}/Sln^{WT} using a one-way ANOVA with a Tukey's post hoc test, $P \leq 0.05$. Values are means ± SEM.

TABLE 4.2. **Body weight, daily activity and daily food intake measures from Pln^{WT}/Sln^{WT}, Pln^{OE}/Sln^{WT}, and Pln^{OE}/Sln^{KO} mice.**

Parameter	Pln^{WT}/Sln^{WT}	Pln^{OE}/Sln^{WT}	Pln^{OE}/Sln^{KO}
Body weight	35.9 ± 0.8	37.5 ± 0.8	36.0 ± 1.1
Food intake (g/d)	4.9 ± 0.5	5.2 ± 0.3	4.7 ± 0.4
Total activity (counts/d)	15,354 ± 1,073	11,070 ± 1,690	12,072 ± 1,468
Ambulatory activity (counts/d)	5,435 ± 680	3,665 ± 681	3,950 ± 641

Values are means ± SEM (n = 18-23, for the average body weight of Pln^{WT}/Sln^{WT}, Pln^{OE}/Sln^{WT}, and Pln^{OE}/Sln^{KO} mice; n = 6 per genotype for daily food consumption, ambulation, and total activity). Ambulatory activity counts were when the mouse crossed 2 adjacent x-axis infrared beams in succession. One-way ANOVA revealed no significant effect of genotype for body weight ($P = 0.37$), food intake ($P = 0.48$), total activity ($P = 0.12$), or dual beam activity ($P = 0.17$).

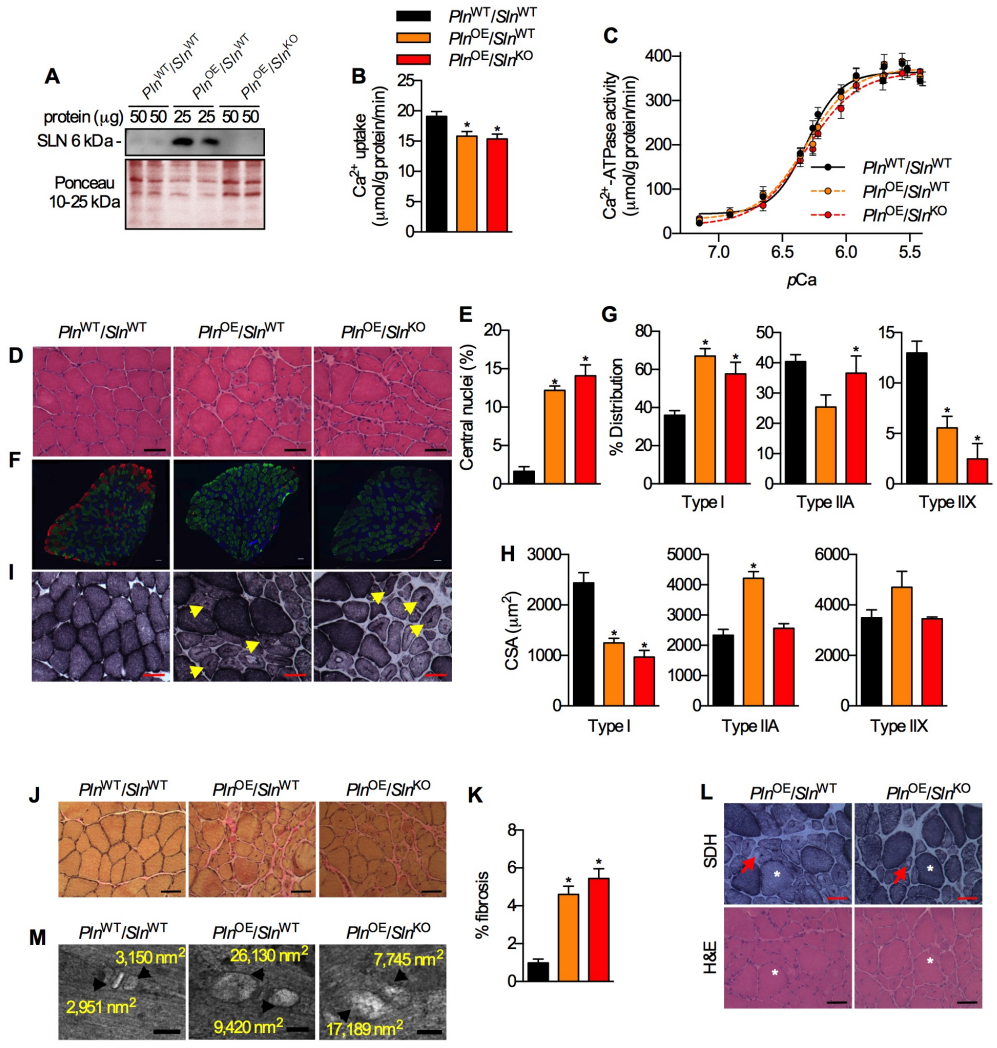

Figure 4.1. *Sln* deletion does not rescue SERCA function or the CNM-like phenotype in Pln^{OE} mice. (**A**) Representative Western blot image of SLN in soleus muscles across genotypes. Ponceau was used as a loading control. Rates of Ca^{2+} uptake (**B**) and SERCA activity-*p*Ca curves (**C**) measured from soleus homogenates (n = 6-7). Representative H&E-stained sections (**D**) revealing greater central nuclei (**E**) in Pln^{OE}/Sln^{KO} and Pln^{OE}/Sln^{WT} soleus. Representative immunofluorescent fiber-type staining (**F**) showing type I fiber predominance (**G**) and hypotrophy (**H**) in Pln^{OE}/Sln^{WT} and Pln^{OE}/Sln^{KO} mice. Type I (blue), -IIA (green), -IIB (red), and -IIX (unstained); type IIB fibers were only found in WT (5.9 ± 1.6%). Representative SDH-stained sections (**I**) illustrating central aggregation of oxidative activity (yellow arrowheads) in Pln^{OE}/Sln^{KO} and Pln^{OE}/Sln^{WT} soleus. (**J**) Representative Van Gieson-stained soleus sections displaying enhanced endomysial fibrosis quantified (**K**) using imageJ software. (**L**) Representative SDH-stained and H&E-stained sections displaying core-like aspects in Pln^{OE}/Sln^{WT} and Pln^{OE}/Sln^{KO} soleus muscles that cannot be explained by the presence of an artifact or vacuole. Arrows point to the core-like aspect and asterisks depict the same fiber within serial sections. (**M**) Transmission electron micrographs illustrating triad disruptions with swollen sarcoplasmic reticulum in both Pln^{OE}/Sln^{WT} and Pln^{OE}/Sln^{KO} soleus muscles. Arrowheads point to the swollen sarcoplasmic reticulum with corresponding area. For (**B**, **E**, **G**, **H**, and **K**), * significantly different from Pln^{WT}/Sln^{WT} using a one-way ANOVA with a Tukey's post-hoc test, $P \leq 0.05$. All values are means ± SEM. CSA, cross-secitonal area. All scale bars are set to 50 μm except for (**M**) where scale bars are set to 100 nm.

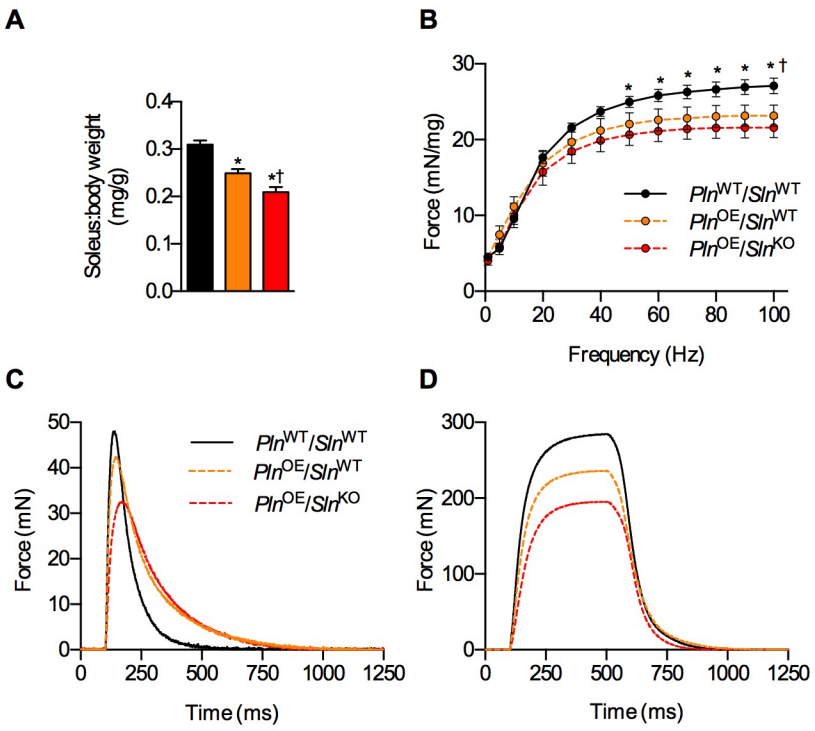

Figure 4.2. *Sln* deletion worsens muscle atrophy and weakness in Pln^{OE} mice. (**A**) Soleus:body weight (mg/g) ratio (n = 18-22). (**B**) Force-frequency curve analysis in isolated soleus muscles (n = 6-7). Representative twitch (**C**) and tetanic (**D**, 100 Hz) force tracings from Pln^{WT}/Sln^{WT}, Pln^{OE}/Sln^{WT}, Pln^{OE}/Sln^{KO} soleus muscles. For (**A**), * significantly different from Pln^{WT}/Sln^{WT}, and †significantly different from Pln^{OE}/Sln^{WT} using a one-way ANOVA with a Tukey's post-hoc test, $P \leq 0.05$. For (**B**), *Pln^{WT}/Sln^{WT} vs. Pln^{OE}/Sln^{KO}, $P \leq 0.05$; $^{\dagger}Pln^{WT}/Sln^{WT}$ vs Pln^{OE}/Sln^{WT}, $P \leq 0.05$ with a two-way repeated measures ANOVA and a Tukey's post-hoc test. All values are means ± SEM.

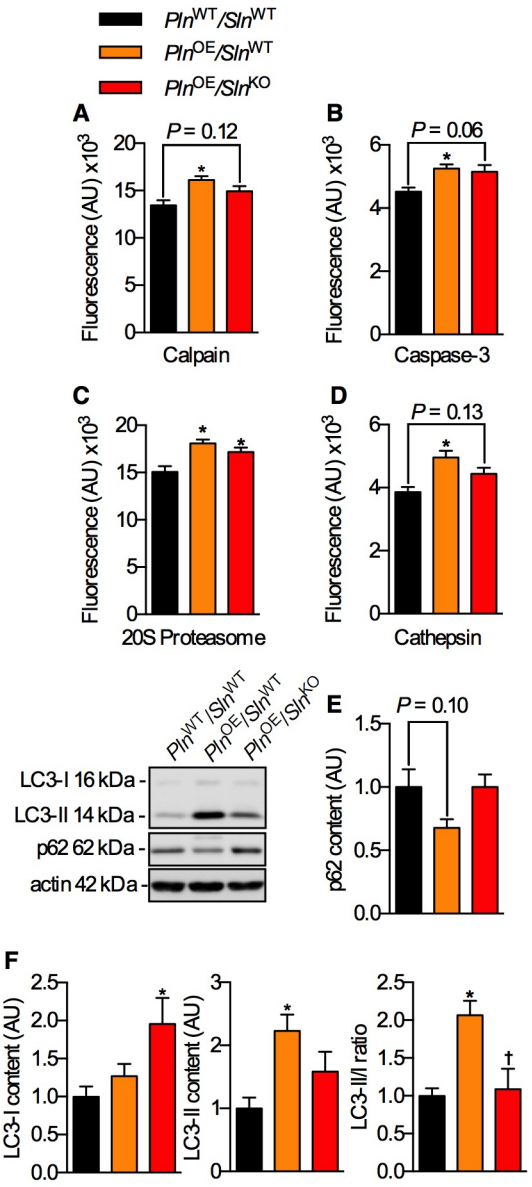

Figure 4.3 *Sln* deletion does not augment proteolytic activity and autophagic signaling in response to *Pln* overexpression. Calpain (**A**), caspase-3 (**B**), and 20S proteasome activity assays (**C**). Enhanced autophagy revealed by increased cathepsin activity (**D**), decreased p62 levels (**E**) and increased LC3-II/I content (**F**) in Pln^{OE}/Sln^{WT} mice is attenuated in Pln^{OE}/Sln^{KO} mice. *Significantly different from Pln^{WT}/Sln^{WT}, †significantly different from Pln^{OE}/Sln^{WT} using a one-way ANOVA and a Tukey's post-hoc test, $P \leq 0.05$. For proteolytic measures, n = 6-7; for p62, LC3-I and –II content, n = 11-12 and optical densities were normalized to actin. All values are means ± SEM.

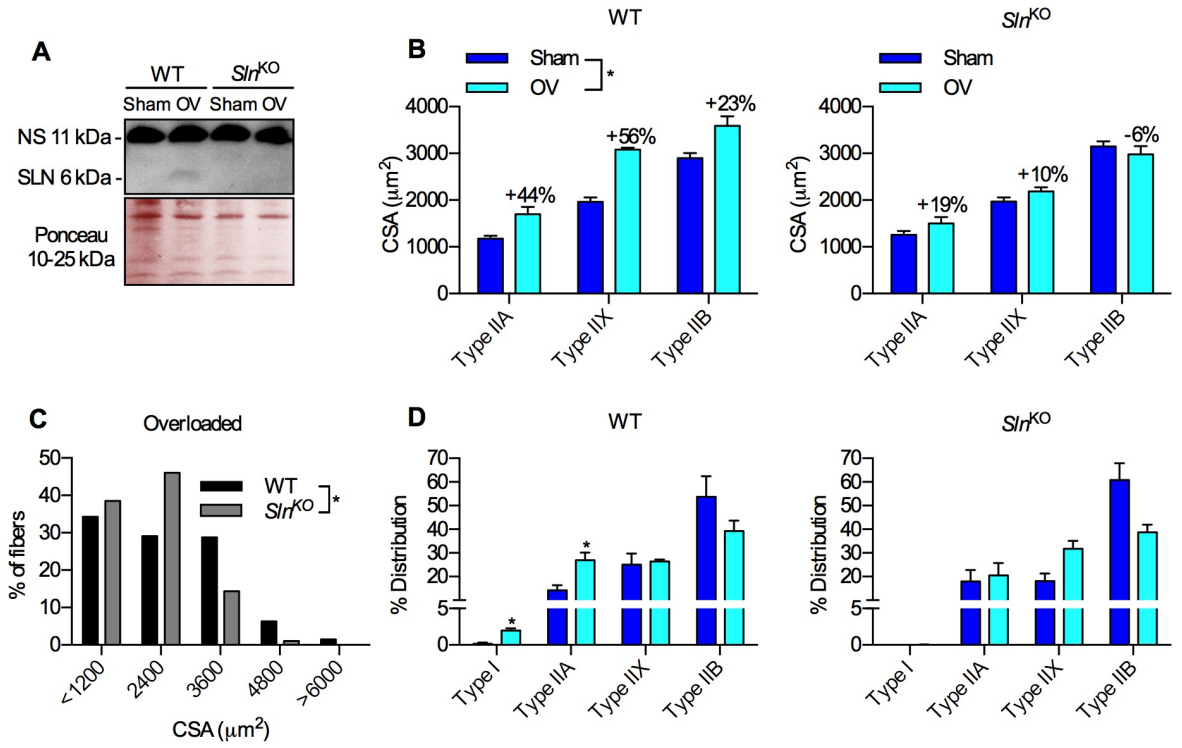

Figure 4.4 *Sln* deletion blunts myofiber hypertrophy and fast-to-slow fiber type transitions during mechanical overload of the plantaris muscles. (**A**) Western blot image illustrating ectopic expression of SLN in the overloaded (OV) plantaris. NS, non-specific bands were included to show that protein was loaded in all lanes and ponceau stain demonstrates equal loading (75 µg of plantaris homogenate protein loaded). (**B**) Fiber type cross-sectional area (CSA) and fiber size frequency histograms (**C**) quantified using imageJ after performing immunofluorescent staining (n = 3-4 per group). (**D**) Fiber type changes in response to mechanical overload in WT and Sln^{KO} mice. For (**B**), *denotes a main effect of mechanical overload using a two-way repeated measures ANOVA, $P < 0.05$; for (**D**), *significantly different from sham using a paired t-test (one tailed) within a genotype, $P \leq 0.05$. All values are means ± SEM except for (**C**) where a two-sample Kolmogorov-Smirnov test was used to compare frequency distributions (WT n = 271 fibres from 3 animals, Sln^{KO} n = 278 fibres from 4 animals). CSA, cross-secitonal area.

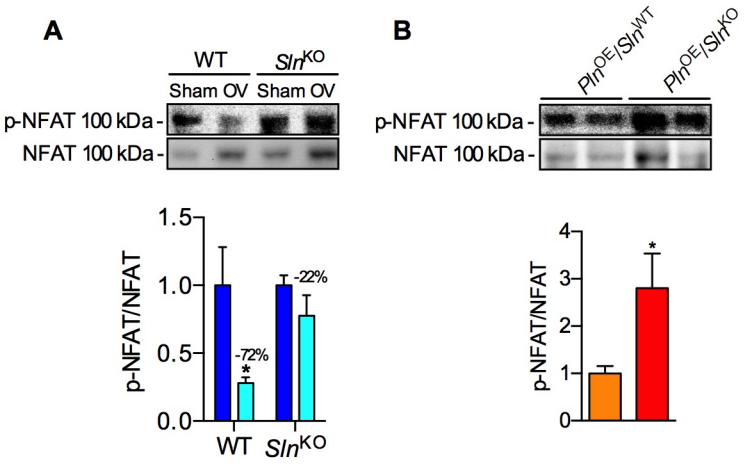

Figure 4.5. Phosphorylated NFAT as a marker of calcineurin signaling in mechanical overload experiments and in the Pln^{OE}/Sln^{WT} and Pln^{OE}/Sln^{KO} soleus muscles. (**A**) Phosphorylation status of NFAT in the sham and OV plantaris muscles from WT and Sln^{KO} mice (7.5 μg of plantaris homogenate protein was loaded, n = 4-6 per group, expressed relative to sham). (**B**) Phosphorylation status of NFAT in soleus muscles from Pln^{OE}/Sln^{WT} and Pln^{OE}/Sln^{KO} mice (n = 7–11 per group, expressed relative to Pln^{OE}/Sln^{WT}). For (**A**), *significantly different from sham using a paired t-test (one tailed) within a genotype, $P \leq 0.05$; for (**B**), *significantly different from Pln^{OE}/Sln^{WT} using a Student's t-test, $P \leq 0.05$. All values are means ± SEM.

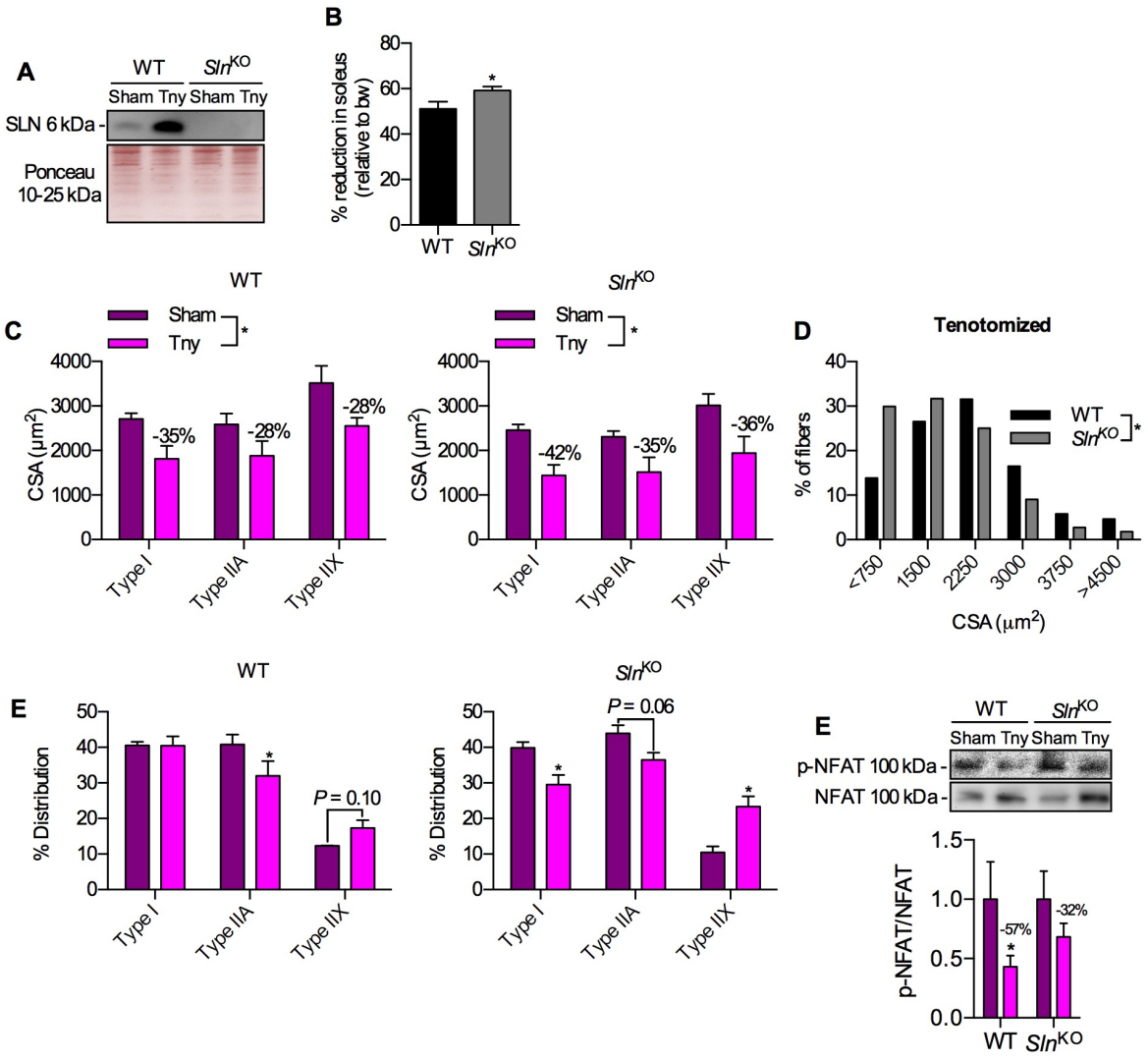

Figure 4.6. *Sln* deletion exacerbates soleus muscle atrophy and slow-to-fast fiber type conversions in response to tenotomy. (**A**) Western blot image depicting SLN content in WT sham and tenotomized (Tny) soleus muscles (n = 5). 25 μg of soleus homogenate protein was loaded for each lane and equal loading was ensured with ponceau stain. (**B**) Percent reduction in soleus muscle mass after Tny expressed relative to body weight (bw). (**C**) Fiber type cross-sectional area (CSA) and fiber size frequency histograms (**D**) quantified using imageJ after performing immunofluorescent staining (n = 3-4 per group). (**E**) Fiber type changes in response to tenotomy in WT and Sln^{KO} mice. (**F**) Calcineurin activation as measured through the phosphorylation status of NFAT in the sham and Tny soleus muscles from WT and Sln^{KO} mice (7.5 μg of soleus homogenate protein was loaded, n = 5-6 per group, expressed relative to sham. For (**B**)**,** *significantly different from WT using a Student's t-test, $P \leq 0.05$; for (**C**), *denotes a significant main effect of tenotomy using a two-way repeated measures ANOVA, $P \leq 0.05$; for (**E** and **F**), *significantly different from sham using a paired t-test (one tailed) within a genotype, $P \leq 0.05$. All values are means ± SEM except for (**D**) where a two-sample Kolmogorov-Smirnov test was used to compare frequency distributions (WT n = 260 fibres from 3 animals, Sln^{KO} n = 331 fibres from 4 animals).

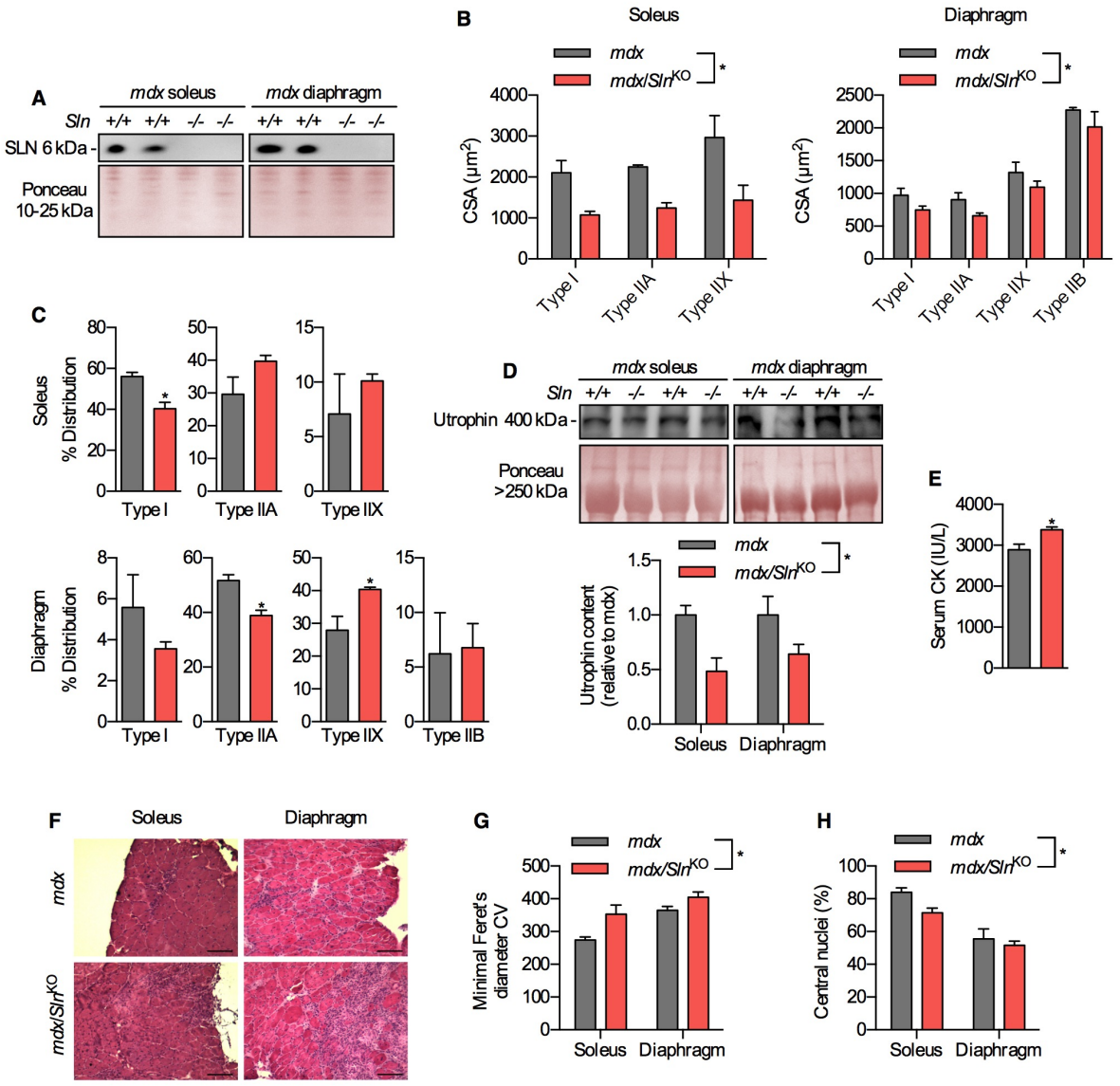

Figure 4.7. *Sln* deletion (-/-) promotes a slow-to-fast fiber type shift, reduces utrophin expression, and worsens dystrophic pathology in *mdx* mice. (**A**) Representative Western blot image of SLN in *mdx* soleus and diaphragm muscles. Equal loading was ensured with ponceau stain (12.5 µg of homogenate protein). (**B**) Fiber type cross-sectional area (CSA) and distribution (**C**) in soleus and diaphragm muscles from *mdx* and *mdx*/*Sln*^{KO} mice quantified using imageJ after immunofluorescent staining (n = 3-4 per genotype). (**D**) Western blot quantification of utrophin in soleus and diaphragm muscles from *mdx* and *mdx*/*Sln*^{KO} mice (n = 3-4 per genotype, 30 µg of homogenate protein). Equal loading was ensured with ponceau stain. (**E**) Serum creatine kinase (CK) levels in *mdx* and *mdx*/*Sln*^{KO} mice (n = 3-4 per genotype). (**F**) Representative H&E-stained sections of soleus and diaphragm muscles illustrating worsened pathology and greater fiber heterogeneity in the *mdx*/*Sln*^{KO} mice. (**G**) Minimal Feret's diameter coefficient of variation (CV) calculated from H&E-stained sections. CV = (standard deviation /mean of the minimal Feret's diameter) x 1000; n = 3-4 per genotype; 50 fibers analyzed per section. (**H**) Impaired regenerative capacity in *mdx*/*Sln*^{KO} mice revealed by lower central nuclei (%) upon H&E staining (n = 3-4 per genotype). For (**B**, **D**, **G** and **H**), *denotes a significant main effect of *Sln* deletion using a two-way ANOVA, $P \leq 0.05$; for (**C** and **E**), *significantly different from *mdx* using Student's t-test, $P \leq 0.05$. All scale bars are set to 100 µm. All values are means ± SEM.

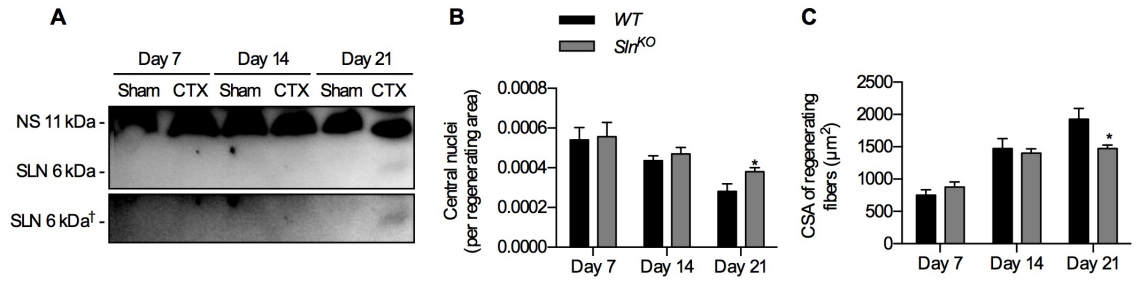

Figure 4.8. *Sln*^{KO} mice exhibit delayed muscle regeneration after acute cardiotoxin injury. (**A**) Ectopic expression of SLN in tibialis anterior muscles only by day 21 post-injury suggests a role for SLN in the later stages of muscle regeneration. †The inset below clearly reveals SLN expression by day 21 after adjusting for brightness and contrast; NS, non-specific bands were included to show that protein was loaded in all lanes (75 μg of TA homogenate protein loaded). (**B**) Fibers with central nuclei, normalized to area of regeneration, remain elevated in *Sln*^{KO} mice at day 21 post-injury, and the average cross-sectional area (CSA, **C**) of regenerating fibers at day 21 post-injury is smaller in *Sln*^{KO} mice indicating a delay in the later stages of muscle regeneration. *Significantly different from WT, using a Student's t-test at each day, $P \leq 0.05$. All values are means ± SEM.

Chapter 5

Summary, Perspectives, and Future Directions

5.1 Summary

This thesis began with two main objectives: 1) characterize and diagnose the myopathy observed in the *Pln*^{OE} mouse and 2) determine the role for SLN upregulation. Initially, it was hypothesized that PLN overexpression would lead to a dystrophic myopathy (Chapter 2); however, the myopathy found in the *Pln*^{OE} soleus and gluteus minimus muscles more closely resembled CNM. This finding led to the study described in Chapter 3, which focused on the diaphragm muscles as studies assessing diaphragm and respiratory function in animal models of CNM, at the time, were limited (147). In this chapter, it was hypothesized that the diaphragm muscles would also display muscle weakness and exhibit a CNM-like phenotype; however the *Pln*^{OE} diaphragm did not exhibit CNM and showed no impairments in force production. The relatively small impairments in SERCA function and SLN upregulation (2.5-fold) in the *Pln*^{OE} diaphragm muscles, amongst other findings from current literature, led to the hypothesis that *Sln* deletion would improve SERCA function and alleviate the CNM phenotype observed in the *Pln*^{OE} soleus muscles (Chapter 4). In contrast, genetic deletion of *Sln* worsened the *Pln*^{OE}-induced myopathy and had similar effects on two other models of damage/disease (tenotomy and *mdx*). Experiments with mechanical overload surgery, and results for NFAT phosphorylation and utrophin expression suggest that sarcolipin counters disease pathology by activating calcineurin. In conclusion, the studies presented in this thesis provide a better understanding of the role of PLN and SLN in skeletal muscle disease and are summarized below in table format with respect to their key findings, conclusions, and novel/important contributions.

Table 5.1.1. Summary of Chapter 2 - Thesis Study I: *Phospholamban overexpression in mice causes a centronuclear myopathy-like phenotype.*

Key findings	▪ Type I fibre-specific PLN overexpression reduces maximal SERCA activity, rates of Ca^{2+} uptake, and SERCA's apparent affinity for Ca^{2+} assessed in soleus and gluteus minimus muscle homogenates. ▪ SLN was upregulated 7- and 9-fold, respectively in soleus and gluteus minimus muscles from Pln^{OE} mice. ▪ Soleus muscles from Pln^{OE} mice exhibited progressive muscle atrophy and displayed severe muscle weakness *in vitro* by 4-6 months of age. ▪ Unlike the original report by Song et al., (2004), the soleus and gluteus minimus muscles exhibited signs of myopathy that phenotypically recapitulated human CNM (central nuclei, type I fibre predominance and hypotrophy, and central aggregation of oxidative activity) with additional endomysial fibrosis and core-like lesions. ▪ The CNM phenotype in Pln^{OE} mice resembles the autosomal dominant form of CNM as well as *RYR*-related and *TTN*-related CNM. ▪ Analyses of three muscle biopsies from genetically unrelated CNM patients show significant reductions in maximal SERCA activity and a trending increase in PLN expression compared with healthy controls. ▪ Consistent with other mouse models of CNM, increased levels of dynamin-2 were observed in the Pln^{OE} soleus and gluteus minimus muscles; however, a significant reduction in dynamin-2 from muscle biopsies from CNM patients compared with healthy controls was detected.
Conclusion	▪ PLN overexpression in mice can lead to a CNM phenotype, and the trending increase in PLN expression in human CNM, suggests that PLN may play a pathological role in this disease.
Novel/important contributions	▪ The physiological role of PLN in cardiac muscle is well known with a variety of genetic mutations leading to cardiomyopathy; however the role of PLN in skeletal muscle disease remained largely overlooked. This study, for the first time, demonstrates the importance of PLN in murine and human CNM pathology. ▪ 20-30% of CNM cases remain genetically unresolved and scientists may now view *PLN* as a novel gene candidate. ▪ To date, there is no cure for CNM and it is possible that targeting PLN may represent a viable therapeutic strategy. ▪ The Pln^{OE} mouse is a commercially available animal model that faithfully captures all CNM histopathological features and can be used to study the underlying mechanisms leading to these lesions as well as testing novel therapeutic strategies.

Table 5.1.2. Summary of Chapter 3 - Thesis Study II: *Diaphragm assessment in mice overexpressing phospholamban in slow-twitch type I muscle fibres*.

Key findings	▪ SERCA's apparent affinity for Ca^{2+} was lower in Pln^{OE} diaphragm compared with WT; however, neither maximal SERCA activity nor rates of Ca^{2+} uptake were significantly different. ▪ SLN expression was upregulated; but only 2.5 fold. ▪ Isolated diaphragm strips from Pln^{OE} mice did not display muscle weakness or slowing in twitch kinetics. ▪ Unlike the Pln^{OE} soleus and gluteus minimus muscles, the diaphragm muscles did not display all histopathological features associated with CNM and only exhibited type I fibre hypotrophy. ▪ Consistent with the lack in CNM phenotype, levels of dynamin 2 were unaltered between Pln^{OE} and WT diaphragm muscles. ▪ There was a greater proportion of the type II fibres that also exhibited significant myofibre hypertrophy in the Pln^{OE} diaphragm.
Conclusion	▪ Diaphragm muscles from Pln^{OE} mice conferred resistance to Pln^{OE}-induced CNM and were not weaker than their WT littermates.
Novel/important contributions	▪ This study demonstrates that the diaphragm muscles from Pln^{OE} mice do not display CNM, which is consistent with the very little respiratory complications found in patients with autosomal dominant CNM. ▪ Understanding the underlying mechanisms that allow the diaphragm to resist the Pln^{OE}-induced CNM may lead to the development of novel therapeutic strategies. This study highlights two possibilities: • SLN expression appeared to follow disease severity in Pln^{OE} mice; therefore SLN's role in myopathy should be investigated in the future. • Type I fibres are those primarily affected in the congenital myopathies (CNM and CCD), therefore reducing their proportions in skeletal muscles, similar to that seen in the Pln^{OE} diaphragm muscles, may represent a viable therapeutic strategy.

Table 5.1.3. Summary of Chapter 4 - Thesis Study III: *Sarcolipin is vital for muscle growth and remodeling and counters disease pathology.*

Key findings	▪ Pln^{OE}/Sln^{KO} soleus muscles did not show improved SERCA function or mitigation of the CNM phenotype. ▪ Pln^{OE}/Sln^{KO} soleus muscles had pronounced force reduction and exacerbated muscle atrophy, which could not be explained by differences in body weight, food intake, daily activity, or muscle proteolysis. ▪ Pln^{OE}/Sln^{KO} soleus muscles did not display any compensatory type II fibre hypertrophy and showed a delayed transition toward a type I fibre population. ▪ The failure to hypertrophy and transition toward a type I fibre population upon greater load bearing stimulus, was repeated in the mechanically overloaded Sln^{KO} plantaris muscles, and could be explained by attenuated calcineurin signaling. ▪ Soleus muscle atrophy and slow-to-fast fibre type transitions typically observed after tenotomy were accelerated in Sln^{KO} mice and can be explained by attenuated calcineurin signaling. ▪ Muscles from *mdx*/Sln^{KO} mice had smaller myofibre size, a slow-to-fast fibre type transition, greater degeneration as revealed by serum creatine kinase concentrations, and greater variability in myofibre size indicated by a larger minimal Feret's diameter CV. ▪ Lowered utrophin expression in muscles from *mdx*/Sln^{KO} mice suggest that calcineurin signaling is impaired. ▪ The larger variability in minimal Feret's diameter in the *mdx*/Sln^{KO} mice likely represents a combined effect of enhanced muscle degeneration, reduced myofibre size, and impaired muscle regeneration as shown with central nuclei counts in the *mdx*/Sln^{KO} muscles and in acute cardiotoxin injury experiments in Sln^{KO} mice.
Conclusion	▪ SLN plays a vital role in countering muscle disease by promoting muscle growth and remodeling by stimulating calcineurin signaling.
Novel/important contributions	▪ This study answered a question that has remained elusive for many years: what is the role of SLN upregulation in skeletal muscle disease? The results from this study are the first to show the importance of SLN in mediating an adaptive response necessary in combatting a widespread of muscle diseases/conditions. ▪ The role of SLN in stimulating muscle growth shown in this study could account, in part, for the increased adiposity and impaired glucose metabolism seen in high-fat fed Sln^{KO} mice. ▪ The role of SLN in stimulating muscle growth shown in this study may also lead to novel therapeutic regiments against muscle wasting in aging and cachexia.

5.2 Perspectives and future directions

PLN and CNM: mechanistic insight

The results from this thesis clearly demonstrate that PLN overexpression causes a CNM-like phenotype in mice; however the exact mechanisms leading to greater central nuclei, type I fibre predominance and hypotrophy, and central aggregation of oxidative activity in the muscles from Pln^{OE} mice and in all other forms/models of CNM remain unknown. However, recently, there is gaining interest with triad structural anomalies being thought to have a key role in the pathogenesis of CNM (111, 128, 129, 199, 200), which is supported by the presence of swollen SR membranes in Pln^{OE} mice (Figure C2). Dynamin 2 is a GTPase critical for both membrane fission and tubulation with the speed of GTPase activity dictating either membrane fission (fast GTP hydrolysis) or membrane tubulation (slow GTP hydrolysis) (201). In CNM, it is posed that speeding up dynamin 2's GTPase activity either through *Dnm2* mutations or increased expression of dynamin 2 can cause triad abnormalities (SR and t-tubule swelling/vacuolization) (90, 130, 200, 202, 203). Therefore, it is possible that the increase in dynamin 2 in the Pln^{OE} soleus and gluteus minimus muscles could contribute to the defects in triad structure and CNM pathology in these mice. Although the exact mechanisms linking PLN overexpression to dynamin 2 upregulation is unknown, SABiosciences mining tool for discovering relevant transcription factors regulating murine *Dnm2* suggests that sterol regulatory binding protein 1 (SREBP-1) may be involved (Figure 5.2.1). Interestingly, SREBP-1 can be activated by calpains and could therefore provide a link for PLN overexpression and dynamin 2 upregulation; however future studies are required to substantiate this speculation (204).

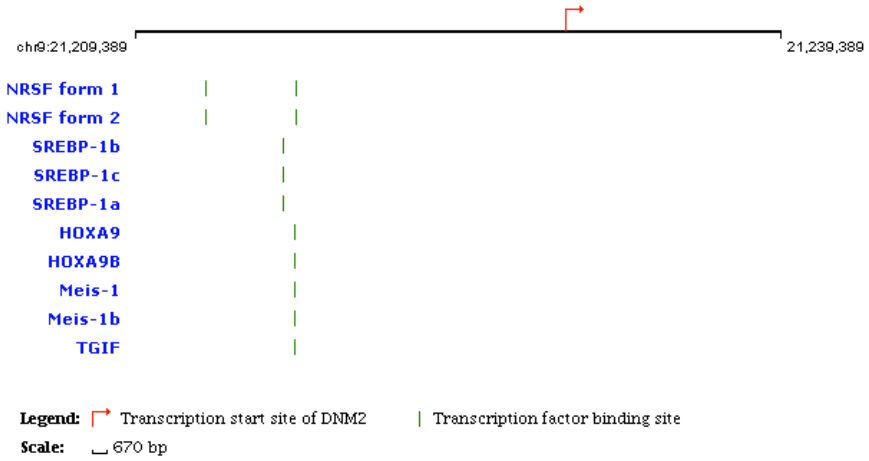

Figure 5.2.1. Transcription factors predicted to regulate murine *Dnm2* expression using SABiosciences' Text Mining Application and the UCSC Genome Browser. http://www.sabiosciences.com/chipqpcrsearch.php?species_id=1&factor=Over+200+TF&gene=DNM2&nfactor=n&ninfo=n&ngene=n&B2=Search

Of note, while dynamin 2 may have a role in Pln^{OE}-induced CNM and other mouse models (90, 203), its role in human CNM is still in question given the results from Chapter 2 (Figure A6). Specifically, a significant reduction in dynamin 2 expression in muscle biopsies from CNM patients was observed despite having a trending increase in PLN content (Figure A5). Although purely speculative, increased PLN expression could also lead to triad defects by altering levels of phosphoinositide-3 phosphate (PIP3), since the kinase responsible for its synthesis, phosphoinositide-3 kinase (PI3K), can be activated by Ca^{2+} (205). In myotubular myopathy, the most severe form of CNM, mutations in *MTM1* lead to reduced myotubularin protein, which is a 3-phosphoinositide phosphatase. Moreover, it is thought that the concomitant rise in PIP3 levels results in defective membrane trafficking, triad structural defects, muscle weakness, and CNM (199, 200). Thus, it is possible that PLN overexpression and SERCA dysfunction may enhance the activity of PI3K and cause a CNM phenotype by raising PIP3 levels much like that seen in animal models ($mtm1^{-/y}$) and human

patients with this X-linked form of CNM. Furthermore, it is possible that PLN could contribute to the dysregulated PIP3 levels found in patients and animal models of myotubular myopathy, and this should be investigated with future studies.

Finally, it has also been proposed that impaired autophagy can be a pathogenic mechanism leading to CNM (67, 206, 207); but exactly how this occurs is still unknown. Interestingly, in a recent study, it was shown that autophagy specifically targets PLN for degradation (208), therefore raising the possibility that impairments in autophagy can cause CNM, at least partly, through elevated PLN protein. Impaired autophagy does not seem to be a causal factor in the Pln^{OE}-induced CNM since autophagic signaling appeared elevated with PLN overexpression (Figure C4); nevertheless, it would be interesting to determine whether enhancing autophagy either genetically, pharmacologically (ie. metformin), or through other means (caloric restriction) could rescue the CNM phenotype found in Pln^{OE} mice by targeting PLN for degradation.

MEF2 and SLN expression: a positive feedback mechanism

To date, the factors controlling *Sln* expression remain largely undetermined and only one study provides a potential candidate (209). In this study by Zhao and colleagues (2002), the *Sln* noncoding region was found to have a highly conserved binding sequence for the myocyte enhancer factor 2 (MEF2) transcription factor. In support of a role for MEF2 in the control of *Sln* expression, both *Mef2* and *Sln* are greatly expressed in the atria compared to the ventricles in mouse (209). In skeletal muscle, protein levels of MEF2 are similar in slow and fast mouse muscles, however its primary inhibitors, histone deacetylase (HDAC) -4, -5, and -7 are expressed in far lower quantities in mouse soleus compared to EDL (210).

Correspondingly, tests from our laboratory have only detected SLN in mouse soleus, gluteus minimus, diaphragm and atrial muscles (Figures 2.1, A3, and 3.1, and reference (20)), and to date, we have not detected SLN in mouse WT chow-fed EDL muscles.

Interestingly, calcineurin also stimulates the activity of MEF2 by enhancing its DNA binding through dephosphorylation of MEF2, and it's the synergist action between MEF2 and NFAT that is thought to control muscle growth and remodeling (154, 211-214). Therefore, if MEF2 controls *Sln* expression, then SLN's regulation of calcineurin signaling, as shown in Chapter 4, points to the existence of a positive feedback mechanism where calcineurin signaling increases SLN expression to further amplify calcineurin activity (Figure 5.2.2). In addition to calcineurin, members of the CAMK family (I, II and IV) also stimulate MEF2 transcriptional activity by phosphorylating HDACs leading to their extrusion from the nucleus (214, 215). Therefore, CAMKs may also stimulate SLN expression, and similar to calcineurin, SLN may further amplify CAMKs signaling through its action on the SERCA pump. Future studies should investigate the role of MEF2 in regulating *Sln* expression and to determine the feasibility of this positive feedback mechanism, and could benefit from the use of *Mef2* knockout mice (216).

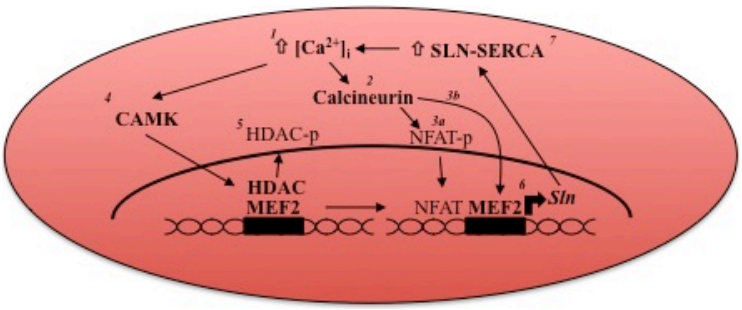

Figure 5.2.2. Speculated positive feedback mechanism for Ca^{2+}-dependent *Sln* expression. (1) Rise in $[Ca^{2+}]_i$ activates calcineurin (2) and mediates dephosphorylation of NFAT (3a) for nuclear localization, and MEF2 (3b) to enhance DNA binding. (4) Members of the CAMK family (I, II, and IV) are also activated and phosphorylates HDAC (5) resulting in nuclear extrusion and stimulating MEF2 activity. (6) Synergist action of MEF2 and NFAT promotes *Sln* transcription and SLN protein interacts with SERCA and inhibits its function (7) contributing to the rise in $[Ca^{2+}]_i$.

If correct, the Ca^{2+}-dependent *Sln* expression system proposed in Figure 5.2.2 could explain why our laboratory has only detected SLN in the soleus, gluteus minimus, diaphragm, and atrial muscles of mice, as these muscles exhibit the tonic activity patterns and, thus the sustained elevations in $[Ca^{2+}]_i$ required for calcineurin signaling (8, 152, 154, 160, 168). Indeed, a previous study has shown that soleus muscles fibres contain a high amount of nuclear NFATc1 (66%) compared with TA muscles (14%) in the basal state suggestive of greater calcineurin signaling (161). Moreover, Tothova et al. (2006) showed that TA muscles subjected to electrical stimulation mimicking slow-motor unit activity patterns (20 Hz for 10 s, every 30 s, for 60 min) exhibited calcineurin-dependent NFATc1 nuclear shuttling, which could not be observed with a faster, less frequent stimulation pattern (100 Hz for 0.6 s, every 60 s, for 60 min). Thus, calcineurin-NFAT signaling is dependent on nerve activation and favours repetitive low-frequency long duration activity patterns, and therefore could explain why SLN was only found in the overloaded plantaris muscles and not sham, since soleus and gastrocnemius tenotomy cause plantaris muscles to take on a postural

role with a tonic activity pattern (Figure 4.2). The fact that *Sln* deletion prevented the overload-induced myofibre growth and fast-to-slow fibre type transition indicates that SLN plays a critical role in maintaining $[Ca^{2+}]_i$ required for calcineurin and potentially CAMK signaling, and provides evidence for this positive feedback loop.

The Ca^{2+}-dependent *Sln* expression pathway acting through MEF2 shown in Figure 5.2.2 could also explain why SLN is commonly upregulated in muscle disease, since Ca^{2+} dysregulation and impaired SERCA function are often found (reviewed in Chapter 1). In addition, inflammation may also stimulate *Sln* expression, as pro-inflammatory cytokines can augment the activity of the mitogen activated protein kinase p38α (217), which can then increase MEF2's transcriptional activity by enhancing its DNA binding capacity (218). Thus, both elevated $[Ca^{2+}]_i$ and inflammation in diseased states may enhance SLN expression through MEF2 and warrants further investigation, especially if increasing SLN content represents a viable therapeutic strategy.

The proposed Ca^{2+}-dependent *Sln* expression pathway and positive feedback loop also highlights an important experimental limitation in this thesis - the lack of $[Ca^{2+}]_i$ measures. These types of experiments could provide strong evidence for SLN's role in sustaining the $[Ca^{2+}]_i$ required for calcineurin signaling seen in Pln^{OE} mice, mechanical overload, soleus tenotomy and *mdx* mice (Thesis Study III). In addition, the fact that SERCA function was not improved in Pln^{OE}/Sln^{KO} mice (Figure 4.1b and c) may suggest that SLN could not have enhanced calcineurin signaling by sustaining the elevations in $[Ca^{2+}]_i$. Alternatively, this can be explained by the sheer overexpression of PLN occurring in the type I fibres, thereby masking any improvement in SERCA function expected in the type II fibres that eventually led to their failure to hypertrophy and transition towards a slow-oxidative

phenotype. Thus, $[Ca^{2+}]_i$ measures or assessment of SERCA function at the single fibre level would prove useful in determining how SLN activates calcineurin and could possibly explain the discrepant results found in the Pln^{OE}/Sln^{KO} mice.

SLN and regulation of muscle mass

It is well understood that SLN expression is greater in skeletal muscles from larger mammals compared to smaller ones (22, 24). Results from our laboratory support this notion since SLN can easily be found in single fibres (20) and in as much as 2 μg of human vastus lateralis homogenate (Figure A5). In contrast, in WT mice, SLN cannot be detected in single fibres, and 25 μg of homogenate protein are typically required for detection in soleus muscles. Furthermore, in rat soleus muscles, where myofibres are ~3-4x larger than those from mice (96), SLN can be detected in single fibres (Figure 5.2.3) and with only 20 μg of homogenate protein (219). To date, the reason for this pattern of expression across mammalian species is unknown; however, the findings presented in Chapter 4 of this thesis indicating a role for SLN in regulating muscle mass poses an interesting question: can differences in SLN expression contribute to differences in muscle size across species? Even within species it would also be interesting to determine if changes in SLN expression could contribute to various conditions of muscle wasting such as aging and cachexia. With respect to aging, previous studies have shown an inability of plantaris muscles from aged mice to hypertrophy in response to mechanical overload (220, 221). Therefore, future studies could determine: 1) whether reductions in SLN content in aged skeletal muscles could account for the age-related muscle loss, and 2) whether a failure to recruit SLN during mechanical overload can account for the aged plantaris' inability to adapt to the overload stimulus (220, 221).

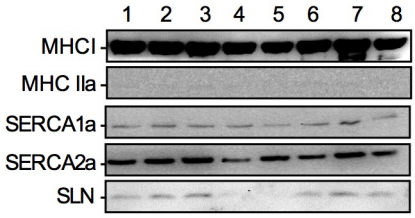

Figure 5.2.3. Single fibre Western blot image demonstrating SLN expression from rat soleus muscles. All fibres were type I fibres that were positive for myosin heavy chain I, and both SERCA1a and SERCA2a were detected in every single fibre.

Importantly, this thesis did not examine the exact mechanisms leading to calcineurin-mediated myofibre hypertrophy. However, it is known that existing myofibres can grow in size through fusion with additional myoblasts (222, 223). Indeed, satellite cells are critical in skeletal muscle growth induced by growth hormones (214) and during mechanical overload (224, 225). Interestingly, NFATc2, another calcineurin-responsive NFAT isoform (150), has been implicated in skeletal muscle growth through its stimulatory action on myoblast to myotube/myofibre fusion (223, 226). In fact, it has been previously shown that myotubes deficient in NFATc2 fail to hypertrophy upon treatment with growth hormone (227). Moreover, regenerating myofibres from *Nfatc2*-null mice were significantly smaller than their WT counterparts, specifically during the later stages of muscle regeneration (226). Of interest, this finding is similar to the cardiotoxin injury experiments reported in Study III, whereby Sln^{KO} mice exhibited a failure to hypertrophy at 21 days post-cardiotoxin injury (Figure C4). Although the exact mechanism leading to NFATc2-induced muscle growth and myoblast fusion is unknown, it is thought that NFATc2 controls the expression of various cell-cell interaction factors and/or proteins secreted for recruitment of myoblasts (226). Nevertheless, SLN's role in activating calcineurin shown here (Study III) and by Maurya et

al., (2015) suggests that SLN may activate NFATc2, and future studies could determine whether SLN is involved in muscle growth via effects on myoblast fusion. In addition, during mechanical overload, calcineurin has been shown to repress the expression of myostatin (151), a potent negative regulator of skeletal muscle growth (228). Therefore, one additional way in which SLN could induce muscle growth is by potentially attenuating the expression of myostatin and this should be examined with future studies.

PLN and SLN divergence: additional support

The results from this thesis provide additional insight into the divergence between PLN and SLN. Specifically, the findings show that PLN overexpression can cause CNM, muscle atrophy, and weakness, whereas an increase in SLN expression is required to maintain muscle mass, stimulate muscle growth/remodeling, and counter disease pathology. Recent findings from M. Periasamy's laboratory support the beneficial effects of increased SLN expression, as *Sln* overexpressing (Sln^{OE}) mice exhibited enhanced contractility and reduced susceptibility to fatigue (229). Interestingly, the enhanced contractility in the face of SLN overexpression is inconsistent with a previous study in which forced overexpression of SLN drastically impaired contractility (49). This discrepancy may be explained by experimental design whereby the findings from Tupling et al. (2002) represent the acute effects of SLN overexpression, and those from Sopariwala et al. (2015) represent the effects of chronic SLN overexpression where certain cellular adaptations can thrive. For example, the results from this thesis indicating SLN's role in myofibre size suggest that perhaps an increase in myofibre CSA in Sln^{OE} mice could explain the enhanced contractility; however this was not measured (229). Moreover, SLN's activation of calcineurin signaling shown in

study III and in *Sln*^{OE} mice (184) can enhance oxidative capacity and increase fatigue resistance. Thus, it is clear that increasing SLN over a long period can provide multiple benefits in muscle metabolism, structure, and function, which again are in contrast to PLN, where its overexpression causes detrimental effects such as weakness and atrophy. Future studies should investigate the reasons why PLN and SLN have distinct effects on muscle structure and function.

The notion that PLN and SLN may have different roles in muscle physiology and cellular signaling in response to certain stressors is difficult to comprehend given that both of these proteins are viewed as inhibitors of the SERCA pump. However, it is interesting to note the differences in the pattern of expression in response to these various stressors. With respect to mechanical overload experiments, the plantaris muscles already expressed PLN in the sham condition, and were not different from the overloaded condition (Figure 5.2.4). Furthermore, PLN expression in soleus muscles was found to be significantly reduced in *mdx* muscles compared with WT, as well in response to high fat feeding (Figure 5.2.5), whereas, PLN content was significantly elevated in the tenotomized soleus (Figure 5.2.6). Altogether, these data suggest that, unlike SLN which is consistently upregulated across these models, PLN's response is variable, and this may precede their different roles in muscle physiology.

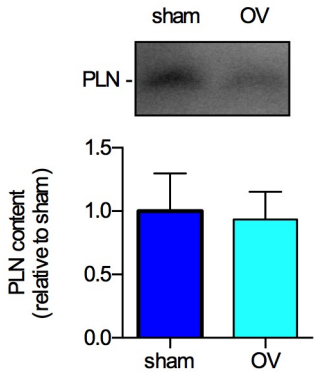

Figure 5.2.4. PLN expression is unaltered in plantaris muscles in response to mechanical overload (OV). Ponceau was used as a loading control and all data are expressed relative to sham (n = 6 per genotype).

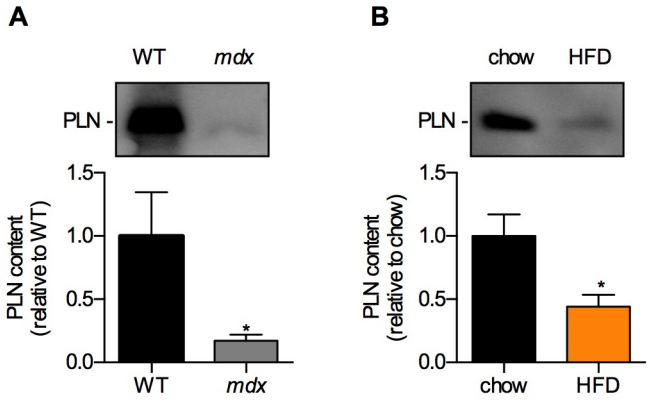

Figure 5.2.5. PLN expression is reduced in soleus muscles from *mdx* mice (A) and mice fed a high-fat diet (HFD) (B). Ponceau was used as a loading control and all data are expressed relative to WT or chow. n = 5 per genotype for (A) and 8 per dietary group for (B). *Significantly different from WT (A) or chow (B) using a Student's t-test, $P \leq 0.05$. For (B), mice were fed a high-fat diet (42% kcal) for 8 weeks.

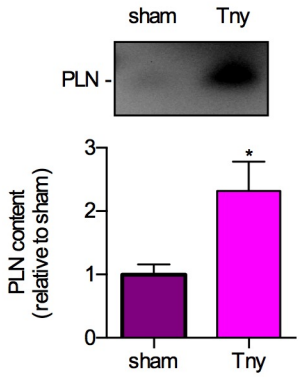

Figure 5.2.6. PLN expression is upregulated in soleus muscles in response to tenotomy (Tny). Ponceau was used as a loading control and all data are expressed relative to sham (n = 6 per genotype). * Significantly different from sham using a paired (two-tailed) t-test, $P \leq 0.05$.

Nonetheless, the question of whether SERCA inhibition induced by PLN can promote muscle growth and remodeling and calcineurin activation similar to SLN irrespective of the differences in their protein expression remains. Although, it would be possible for PLN to stimulate calcineurin signaling likely through SERCA inhibition, differences in its regulation of SERCA may suggest that its capacity to enhance $[Ca^{2+}]_i$ suitable for calcineurin activation may be lower than SLN. In particular, PLN is thought to dissociate from SERCA upon Ca^{2+} binding and may only bind to SERCA in its E2 Ca^{2+} unbound state, whereas SLN can bind to SERCA throughout its catalytic cycle despite the presence of Ca^{2+} (30). This would suggest that while PLN can prevent Ca^{2+} from binding to SERCA and thus elevate the $[Ca^{2+}]_i$ required for calcineurin activation, perhaps the concomitant rise in $[Ca^{2+}]_i$ within that specific microdomain may also cause an appreciable dissociation of PLN from SERCA. Therefore, PLN may not amplify calcineurin as well as SLN that is able to maintain its physical interaction with SERCA.

In the context of the *Pln*^{OE} model, the sheer overexpression of PLN may be able to circumvent the competitive displacement that occurs with Ca^{2+} and may allow for the

calcineurin signaling that presumably leads to the type I fibre predominance. Nevertheless, the fast-to-slow fibre type shift was blunted when *Sln* was genetically removed from the Pln^{OE} mice thereby highlighting the importance of SLN upregulation. In addition, although PLN was upregulated in soleus tenotomy and could also potentially circumvent the competitive displacement that occurs with Ca^{2+} and allow for greater calcineurin signaling in that particular model, it is important to note the consistent association between muscle atrophy and PLN expression. In the Pln^{OE} soleus and tenotomized soleus muscles from this thesis, and in the denervated EDL and soleus muscles from a recent study (manuscript currently in submission in collaboration with Dr. Jerome Frennette; see reference (230)), PLN expression was significantly upregulated. Thus, future experiments in Pln^{KO} mice using soleus tenotomy or sciatic nerve denervation should be done to determine whether the upregulation in PLN causes muscle atrophy similar to that seen in the Pln^{OE} mice. Lastly, the fact that PLN was not upregulated (ie. unaltered or reduced) in the mechanical overload and *mdx* mouse models, may mean that PLN would likely have a smaller role in amplifying calcineurin signaling compared with SLN that was found to upregulated and can remain bound to SERCA during conditions of elevated $[Ca^{2+}]_i$.

Future experiments using primary cell cultures from both Sln^{KO} and Pln^{KO} myofibres may directly assess whether PLN and SLN stimulates calcineurin signaling and to what extent. For example, primary myoblasts/myotubes from Pln^{KO} and Sln^{KO} muscles could be treated with ionomycin, a Ca^{2+} mobilizing agent often used in these types of experiments, to determine whether NFAT nuclear localization occurs differently in the absence of PLN or SLN compared with WT (226, 231). Alternatively, stimulating muscles with a repetitive tonic low frequency pattern (20 Hz, for 10 s every 30 seconds) causes rapid NFATc1 nuclear

localization in adult TA muscles (161), and could potentially be used in the investigation of whether or not PLN and SLN directly activates calcineurin and NFAT localization. However, since SLN was only found in the overloaded TA muscle (Figure 4.4), experiments on the overloaded condition would be most appropriate.

Current ongoing experiments within our laboratory will also provide further indication of whether or not PLN and SLN have similar roles in muscle physiology and calcineurin signaling. With respect to muscle metabolism and obesity, it is now thought that SLN's activation of calcineurin, and thus, oxidative capacity, plays a vital role in combatting the effects of high-fat feeding (184, 232). Preliminary data from our laboratory suggests that the Pln^{KO} mice respond differently to a high-fat diet compared with Sln^{KO} mice and may ultimately suggest that PLN may not have a role in stimulating calcineurin. With respect to *mdx*, we have generated the *mdx*/Pln^{KO} mice in similar fashion to the *mdx*/Sln^{KO} mice, and future experiments on muscle fibre type, size, and integrity will provide further indication of whether PLN can stimulate calcineurin signaling, given calcineurin's importance in dictating fibre type specialization, size, and muscle regeneration (150, 151, 178-180, 226, 233, 234).

If PLN does not stimulate calcineurin at least to the capacity of which SLN can, then although purely speculative, the data presented in this thesis and found within the current literature may suggest that PLN in skeletal muscle offers dynamic control of Ca^{2+} handling, similar to that in cardiac tissue, whereas SLN in skeletal muscle may be utilized and recruited more for cellular signaling processes. Essentially, SLN's ability to inhibit SERCA in the face of greater $[Ca^{2+}]_i$ may make SLN more suitable for cellular signaling and mediating necessary adaptations, and may explain why it is consistently elevated across many skeletal muscle diseases and also during muscle growth and development (24). Future experiments

with other models of skeletal muscle disease, damage and aging, will provide further evidence for the role of SLN in countering pathology. In contrast, the dissociation of PLN from SERCA under conditions of elevated $[Ca^{2+}]_i$ may allow for greater SERCA mediated Ca^{2+} uptake and may elicit similar chronotropic and inotropic effects normally found in cardiac muscle (97). Perhaps it is of no coincidence that PLN is found primarily in type I fibres (20) that have greater β-adrenergic receptors compared with type II (235), as this would also provide further dynamic control of Ca^{2+} handling and muscle contractility via PLN phosphorylation. In the context of disease, it is possible that PLN overexpression and the potential concomitant loss in this dynamic control of Ca^{2+}, as result of a failure of Ca^{2+} to displace PLN from SERCA, may also have a role in CNM pathology and muscle atrophy. Indeed, there are loss-of-function *PLN* mutations that do not inhibit SERCA, yet cause cardiomyopathy, as a result of a failure to phosphorylate normal PLN molecules and to promote the dynamic control of Ca^{2+} (98). Future experiments, knocking in these various loss-of-function *Pln* mutants in the skeletal muscles of mice to determine whether they also cause atrophy and CNM muscle pathology would be of interest, as it would provide further insight on PLN's role in muscle pathology and could potentially explain the divergence between PLN and SLN reported in this thesis.

Appendices

Appendix A

Supplementary Material for Thesis Study I in Chapter 2

Supplementary Results

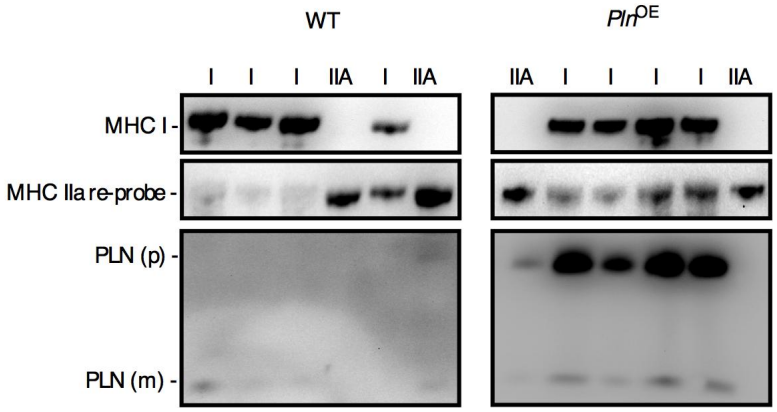

Figure A1. PLN is overexpressed in type I fibres from soleus muscles. PLN expression in single fibres from WT mice was modestly detected in some type I and type IIA fibres and is clearly overexpressed in type I fibres from *Pln*^{OE} mice. MHCI was used to identify type I fibres. After detection of MHCI, membranes were stripped and re-probed with MHCIIa to identify type IIA fibres. Residual signals from MHCI were still present after the stripping and re-probing protocol. PLN (p), PLN pentamer; PLN (m), PLN monomer.

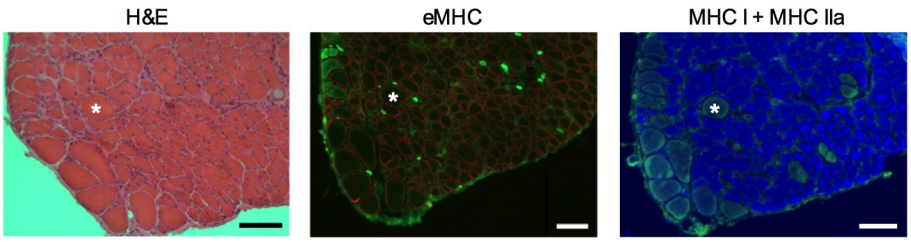

Figure A2. Embryonic MHC in soleus muscles of Pln^{OE} mice**.** Centrally-located nuclei depicted through H&E staining cannot be fully explained by muscle regeneration as myosin heavy chain immunofluorescent stained sections of the soleus muscles show only minimal fibres positive for embryonic myosin heavy chain (eMHC, green). Cross sections were stained with dystrophin (red) to mark the sarcolemmal membrane of the fibre. Fibre-type analysis indicates that centrally-located nuclei are predominantly found in type I fibres (MHC I, blue) but can also be seen in some type IIA fibres (MHC IIa, green). Scale bars are set to 100 μm**.** White asterisks represent the same fibre in serial cross-sections.

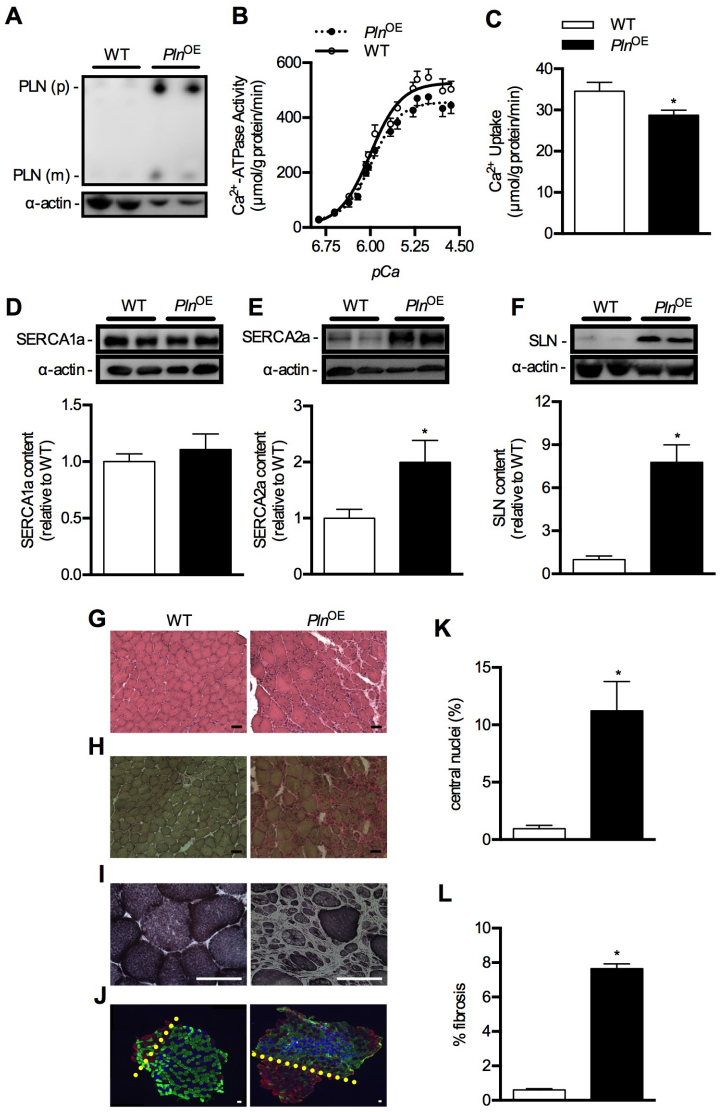

Figure A3. Impaired SERCA function and CNM in gluteus minimus muscles from *Pln*^{OE} mice. (**A**) Western blotting for PLN in WT and *Pln*^{OE} mice from gluteus minimus homogenates. For WT mice, 25 µg of total protein was loaded whereas only 2.5 µg was required for *Pln*^{OE} mice to detect PLN protein. (**B**) Ca^{2+}-ATPase activity-*p*Ca curves in WT (n = 7) and *Pln*^{OE} mice (n = 6) in the presence of the Ca^{2+} ionophore . (**C**) Ca^{2+} uptake assessed in soleus and gluteus minimus muscles from WT (n = 6) and *Pln*^{OE} mice (n = 6). Western blotting for SERCA1a (**D**), SERCA2a (**E**), and sarcolipin (SLN; **F**) in soleus from WT and *Pln*^{OE} mice (n = 6 per genotype). Actin was used as a loading control and all values are expressed relative to WT. Representative gluteus minimus cross sections after H&E (**G**), Van Gieson (**H**), SDH (**I**), and immunofluorescent (**J**) staining. Cross sections were stained with MHC antibodies to identify type I (blue), type IIA (green), type IIB (red), and type IIX (unstained). Yellow dashed lines in (**J**) indicate the area that likely represents the gluteus medius and not the gluteus minimus. (**K**) Percent of fibres containing central nuclei in the gluteus minimus at 4-6 months (n = 4 per genotype at each age with 300-600 fibres counted per mouse). (**L**) Quantitation of fibrotic area in the soleus at 4-6 months of age (n = 4 per genotype). ImageJ software was used to quantify fibrotic area. *Significantly different from WT using Student's t-test, $P \leq 0.05$. All values are presented as mean ± standard error. Scale bars in ***(G)- (J)*** are set to 50 µm.

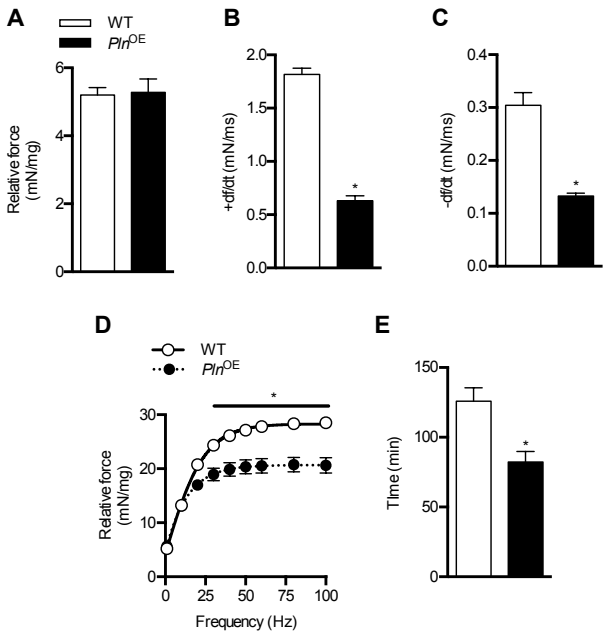

Figure A4. Muscle function in Pln^{OE} mice. (**A**) Soleus isometric twitch force normalized to mass in 4-6 month old mice (WT n = 17, Pln^{OE} = 6). (**B**) Maximum rates of isometric twitch force development in soleus muscles from 4-6 month old mice (WT n = 17, Pln^{OE} = 6). (**C**) Maximum rates of isometric twitch force relaxation in soleus muscles from 4-6 month old mice (WT n = 17, Pln^{OE} = 6). (**D**) Force-frequency analysis in soleus muscles from 4-6 month old mice (WT n = 17, Pln^{OE} = 6). (**E**) Treadmill exercise performance of 4-6 month old mice measured as time (min) to exhaustion. * Significantly different from WT, $P \leq 0.05$. All values are presented as mean ± standard error.

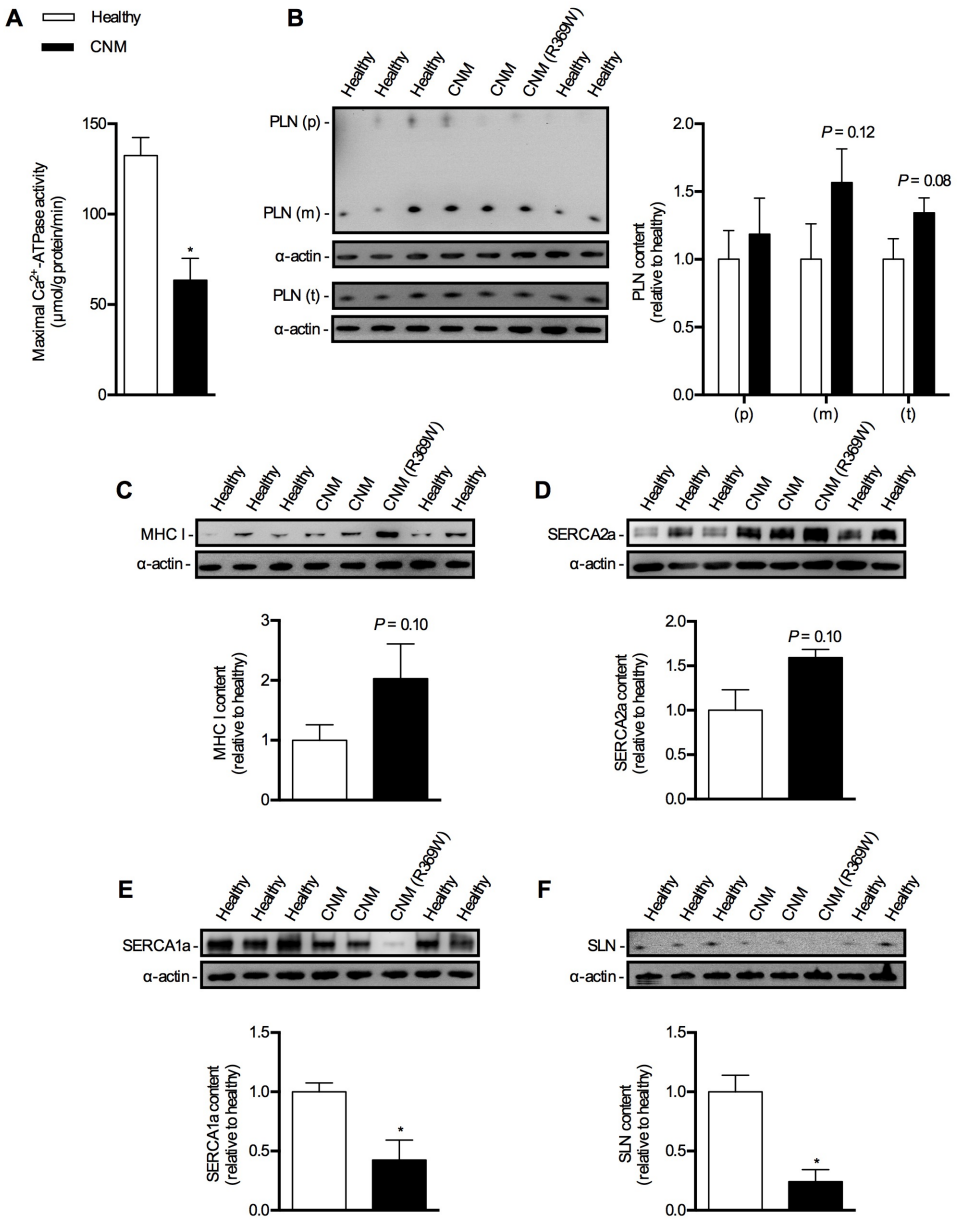

Figure A5. Ca^{2+}-ATPase activity and protein expression in muscle biopsies from three patients with centronuclear myopathy (CNM). (**A**) Maximal rates of SERCA ATPase activity in biopsies from patients with CNM and healthy controls. Western blotting for PLN (**B**), MHC I (**C**), SERCA2a (**D**), SERCA1a (**E**), and SLN (**F**) in biopsies from patients with CNM and healthy controls. Actin was used as a loading control. *Significantly different from healthy using Student's t-test, $P \leq 0.05$. All values are presented as mean ± standard error. PLN (m), monomeric PLN; PLN (p) pentameric PLN; PLN (t), total boiled PLN. For PLN, MHCI, and SERCA2a 1 µg of total protein was loaded. For SERCA1a 0.5 µg of total protein was loaded. For SLN 2 µg of total protein was loaded. CNM (R369W), *DNM2*-CNM patient.

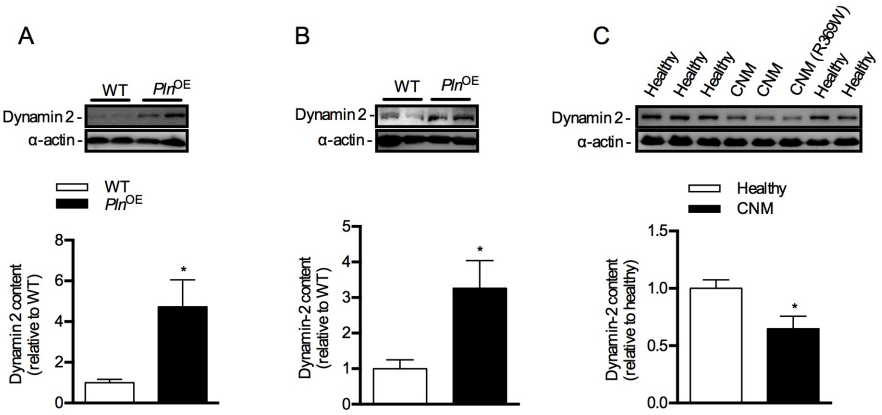

Figure A6. Dynamin 2 protein content in the *Pln*^{OE} soleus (**A**) and *Pln*^{OE} gluteus minimus (**B**) muscles, and in muscle biopsies from three CNM patients compared to five healthy controls (**C**). For mouse soleus and gluteus minimus muscles, 7.5 µg of total protein were loaded, and 2 µg were loaded for human vastus lateralis. Actin was used as a loading control. *Significantly different from WT or healthy, using Student's t-test, $P \leq 0.05$. All values are presented as mean ± standard error. CNM (R369W), *DNM2*-CNM patient.

Table A1. Body weight, soleus weight, and soleus:body weight ratios in WT and Pln^{OE} mice at 1 month, 4-6 months, and 10-12 months of age.

	1 month	4-6 months	10-12 months
Body weight			
WT	22.9 ± 0.7	30.8 ± 0.8	33.1 ± 1.1
Pln^{OE}	22.4 ± 0.5	29.2 ± 0.5	33.7 ± 0.5
Soleus weight			
WT	4.5 ± 0.4	6.5 ± 0.4	5.8 ± 0.4
Pln^{OE}	3.3 ± 0.3	3.6 ± 0.3*	4.0 ± 0.1*
Soleus:body weight			
WT	0.19 ± 0.01	0.21 ± 0.01	0.17 ± 0.01
Pln^{OE}	0.15 ± 0.01	0.12 ± 0.01*	0.10 ± 0.01*

Values are means ± standard error. 1 month (WT, $n = 8$; Pln^{OE}, $n = 8$); 4-6 months (WT, $n = 15$; Pln^{OE}, $n = 15$); 10-12 months (WT, $n = 8$; Pln^{OE}, $n = 6$). *Significantly different from WT within the same age group, $P \leq 0.05$ using two-way ANOVA including genotype and age as factors and a Tukey's post-hoc test when necessary.

Table A2. SERCA activity in gluteus minimus muscles from WT and Pln^{OE} mice at 4-6 months of age.

Genotype	V_{max}	K_{Ca}	ΔpCa_{50}
WT	558.5 ± 29.1	5.99 ± 0.02	-
Pln^{OE}	477.1 ± 24.5*	5.96 ± 0.01	0.03

Values are means ± standard error. Homogenates were isolated from WT and Pln^{OE} mouse gluteus minimus muscles and were analyzed for Ca^{2+}-ATPase activity over Ca^{2+} concentrations ranging from *p*Ca 7 to *p*Ca 4.5 to obtain K_{Ca}. K_{Ca} is the Ca^{2+} concentration required to attain the half-maximal Ca^{2+}-ATPase activity rate and is expressed in *p*Ca units. *Significantly different from WT using Student's t-test, $P < 0.05$. A trend was observed for the K_{Ca} in the gluteus minimus muscles from WT and Pln^{OE} mice ($P = 0.10$).

Table A3. Quantitative analysis of fibre type distribution and cross-sectional area (CSA) in gluteus minimus muscles from WT and *Pln*^{OE} mice at 4-6 months of age.

	Fibre distribution (%)	Fibre CSA (μm^2)
Type I		
WT	26.9 ± 0.5	2713 ± 102
Pln^{OE}	47.7 ± 2.4*	1009 ± 180*
Type IIA		
WT	50.4 ± 1.7	2177 ± 110
Pln^{OE}	31.9 ± 2.9*	3026 ± 461
Type IIX		
WT	10.2 ± 1.0	2401 ± 118
Pln^{OE}	8.7 ± 0.7	3913 ± 406*
Type IIB		
WT	7.2 ± 0.7	4388 ± 189
Pln^{OE}	9.4 ± 0.3	5465 ± 267*

Values are means ± standard error (n = 5-6 per genotype). *Significantly different from WT within the same age; $P \leq 0.05$ using Student's t-test.

Appendix B

Supplementary Material for Thesis Study II in Chapter 3

Supplementary Results

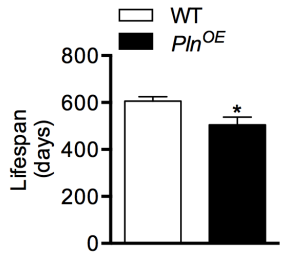

Figure B1. Lifespan of Pln^{OE} (n = 23) and WT (n = 17) mice. *Significantly different from WT, using Student's t-test, $P \leq 0.05$.

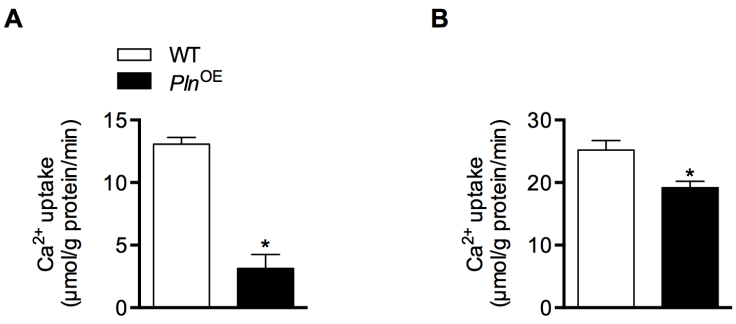

Figure B2. Ca^{2+} uptake assays in the soleus (**A**) and gluteus minimus (**B**) muscles from *Pln*^{OE} and WT mice. Ca^{2+} uptake assays were assessed at a *p*Ca of 6.0. *Significantly different from WT, using Student's t-test, $P \leq 0.05$. WT, soleus n = 4, gluteus minimus n =6; *Pln*^{OE}, soleus n = 4, gluteus minimus n = 6.

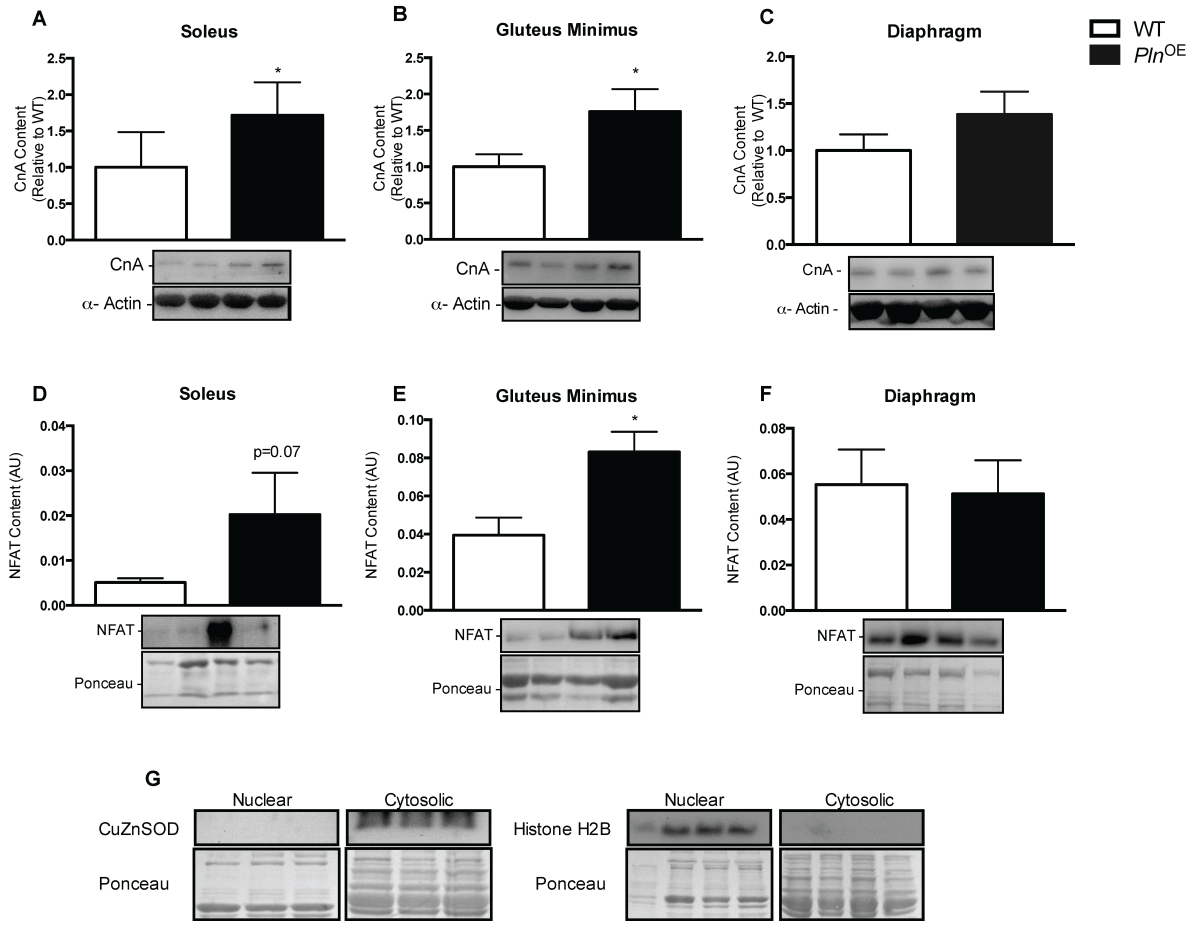

Figure B3. Calcineurin (CnA) and nuclear factor of activated T-cell (NFAT) nuclear content in soleus (**A**, **D**), gluteus minimus (**B**, **E**) and diaphragm (**C**, **F**) muscles from Pln^{OE} and WT mice. (**G**) Nuclear cell fraction purity demonstrated through Western blots from tibialis anterior muscles using Histone H2B and CuZnSOD as nuclear and cytosolic markers, respectively. Two tailed Student's t-tests were used to assess statistical significance for CnA expression across skeletal muscles (n = 6 per genotype). Based on those results, one tail Student's t-tests were used for NFAT content analysis (n = 4 per genotype). $*P \leq 0.05$.

Appendix C

Note on on total fibre count

The total fibre count is a useful measure in determining whether changes in muscle mass is due to hyper- or hypoplasia. In addition, changes in the fibre type distribution in the absence of changes in total fibre count, may also suggest that a 'true' shift in fibre type is more likely occuring. In the Pln^{OE} mouse model reported in Study I of this thesis, there was a significant main effect of age ($P = 0.05$) and genotype ($P = 0.03$) when assessing the total fibre count Figure C1. The main effect of age suggests that as animals aged there was a reduction in total fibre count, which corresponds well with sarcopenia that occurs with aging. The main effect of genotype suggests that there were an increase number of fibres in the Pln^{OE} mice, which is inconsistent with the muscle atrophy that occurs in the soleus muscles of these fibres. This could potentially be explained by the splitting of the type I fibres into smaller caliber myofibres as a result of the selective PLN overexpression and may also contribute to the greater proportion of type I fibres found in these muscles.

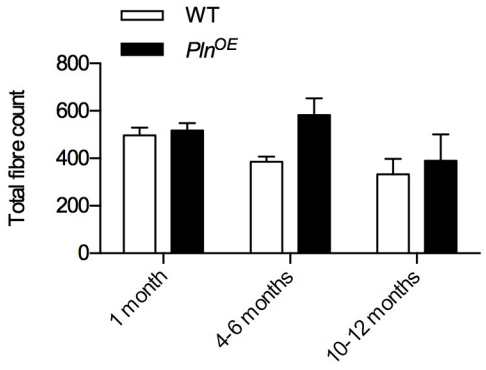

Figure C1. Total fibre count in Pln^{OE} and WT soleus muscles at 1 month, 4-6 months, and 10-12 months of age. Two-way ANOVA detected a significant main effect of age and genotype, but no interaction, $P \leq 0.05$.

In the diaphragm muscles assessed in Study II of this thesis, there was a trending decrease in the total fibre counts found in response to Pln^{OE} ($P = 0.06$) which may correspond well with the selective loss of type I fibres and thus increase in type II fibre proportion (Figure C2). However, caution should be taken when interpreting total fibre counts from the diaphragm, as the total number would be highly dependent on the size of the diaphragm strip extracted for fibre type analyses.

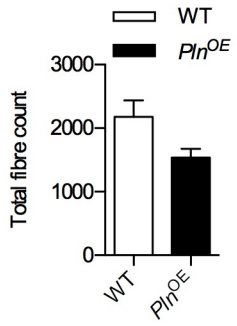

Figure C2. Total fibre count in Pln^{OE} and WT diaphragm strips 4-6 months of age. Student's t-test detected a trend, $P = 0.06$.

The total fibre count analyses in all models of Study III were also performed. Interestingly, hypoplasia was found in the Pln^{OE}/Sln^{KO} muscles, which could also contribute to the exacerbated soleus muscle atrophy found in these mice (Figure C3A). Correspondingly, deletion of *Sln* removed the expected myofibre hyperplasia (236) in response to mechanical overload (Figure C3B), which would suggest that SLN may have a role in maintaining total fibre counts. However, there were no differences in total fibre count in tenotomy experiments or *mdx* soleus muscles in the absence of SLN (Figure C3C and D).

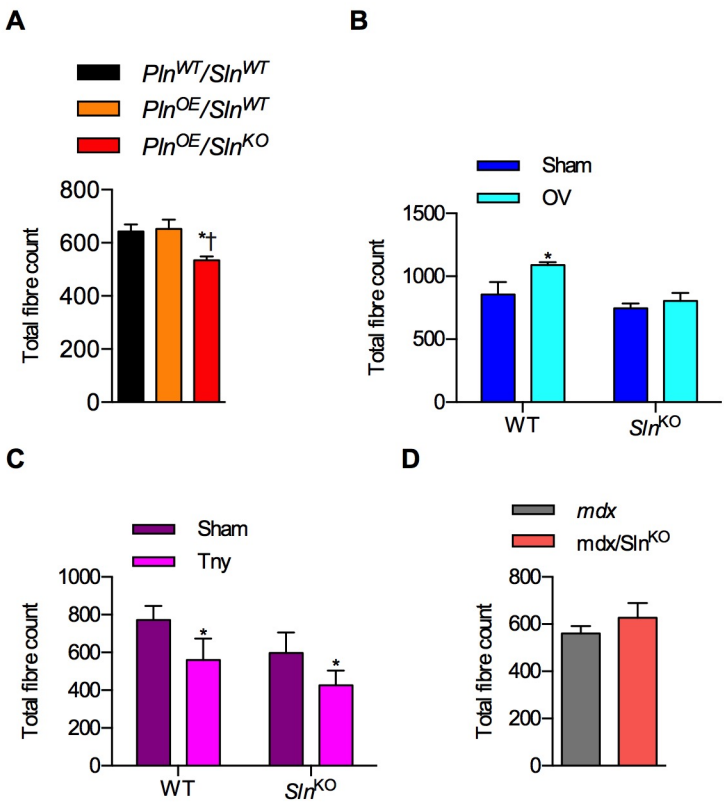

Figure C3. Total fibre count in Pln^{WT}/Sln^{WT}, Pln^{OE}/Sln^{WT}, and Pln^{OE}/Sln^{KO} soleus muscles (A), sham and mechanically overloaded WT and Sln^{KO} plantaris muscles (B), sham and tenotomized WT and Sln^{KO} muscles (C), and *mdx* and *mdx*/Sln^{KO} soleus muscles. For (A), *significantly different from Pln^{WT}/Sln^{WT}, † significantly different from Pln^{OE}/Sln^{WT} using a one-way ANOVA with a Tukey's post hoc test, $P \leq 0.05$. For (B) and (C), *significantly different from sham within a specific genotype using a paired (one-tailed) t-test, $P \leq 0.05$.

Appendix D

Protocols for genotyping mice

To genotype the Pln^{OE}, Sln^{WT} and Sln^{KO} mice, all mice were ear notched and tagged at 3-4 weeks of age. The DNA was then extracted from ear notches using a pureLink Genomic DNA mini kit (Invitrogen, Carslbad, CA). PCR was then performed to amplify the DNA of interest. Briefly, approximately 50 ng of DNA was added to a Taq DNA polymerase mix (EP0402, Thermo Scientific Fermentas, Canada) containing Taq Buffer with $(NH_4)_2S0_4$ buffer (diluted to 1X), 4 mM $MgCl_2$, 200 μM dNTP (R0192, Thermo Scientific Fermetas), 0.625 units of Taq DNA polymerase, and 0.4 μM of the appropriate forward and reverse primers (Table D1). Samples were then placed in a thermal cycler (MJ MINI, Bio-Rad Canada) and underwent their respective PCR reactions (Table D2). The amplified products were then separated on a 1% agarose gel (in 1X TBE) containing 0.01% ethidium bromide (Bioshop, Canada) for 40 min at 80V in 1xTBE buffer, and identified using a bio-imaging system (Syngene, Frederick, MD).

Table D1. Forward and reverse primers used to detect Pln^{OE}, Sln^{WT}, and Sln^{KO} mice.

Mouse	Sequence
Pln^{OE}	
forward, SK-1	5'-AAG GGG CGG GAA GGC ATA TAG-3'
reverse, PLB-RC	5'-GAT TCT GAC GTG CTT GCT GAGG-3'
Sln^{WT}	
forward	5'-TGT CCT CAT CAC CGT TCT CCT-3'
reverse	5'-GCT GGA GCA TCT TGG CTA ATC-3'
Sln^{KO}	
forward	5'-GTG GCC AGA GCT TTC CCA TA-3'
reverse	5'-CAA AAC CAA ATT AAG GGC CA-3'

Table D2. PCR cycles for Pln^{OE} Sln^{WT}, and Sln^{KO} mice.

Mouse	Temperature (°C)	Time	Number of cycles
Pln^{OE}			
1. Denaturation	95	3 min	1
2. Denaturation	94	30 s	
3. Annealing	70	30 s	34 cycles (ie. go to
4. Extension	72	1 min	2 34 times)
5. Final Extension	72	10 min	1
6. Hold	4	-	can hold here until ready to perform electrophoresis.
Pln^{OE}			
1. Denaturation	94	3 min	1
2. Denaturation	94	30 s	
3. Annealing	51	30 s	30 cycles (ie. go to
4. Extension	72	1 min	2 34 times)
5. Final Extension	72	7 min	1
6. Hold	4	-	can hold here until ready to perform electrophoresis.

To genotype the *mdx* mice, at 3-4 weeks of age all mice were ear notched and tagged. The DNA was then extracted using a high-purity/high-yield DNA extraction protocol (see below). Following this, 40 ng of DNA was added to a Taq DNA polymerase mix (EP0402, Thermo Scientific Fermentas, Canada) containing Taq Buffer with $(NH_4)_2S0_4$ buffer (diluted to 1X), 4 mM $MgCl_2$, 200 μM dNTP (R0192, Thermo Scientific Fermetas), 0.6 units of Taq DNA polymerase, and 0.66 μM of the appropriate forward and reverse primers (Table D3). The primers used in this assay were based from a competitive PCR reaction that uses a common forward primer, *mdx* reverse primer, and a WT reverse primer (237). The PCR reaction is detailed in Table D4. The amplified products were then separated on a 3% agarose gel (in 1x TBE) containing 0.01% ethidium bromide (Bioshop, Canada) for 80 min at 100V in 1xTBE buffer, and identified using a bio-imaging system (Syngene, Frederick, MD).

High DNA Extraction Protocol

Buffers:

Mouse Ear-notch/Tail DNA Isolation Buffer
0.5% SDS
0.1M NaCl
0.05M Tris base (pH 8.0)
2-4mM EDTA
Set final pH to 8.0.

8M Potassium Acetate
4g in 200mL dH20 (autoclaved water)

1. Add Proteinase K from pureLink Genomic DNA mini kit (Invitrogen, Carslbad, CA) to mouse ear-notch/tail DNA Isolation Buffer (see recipe below) at a concentration of 1.0 mg/ml and mix.
2. Add 400ul of solution to each Eppendorf tube with sample (ear notch/tail clip). Place tubes in a conical tube.
3. Immediately place tubes in a water bath set to 63°C. Let tissue digest overnight. NOTE: The digests are freezable after.
4. Add 75ul of 8M potassium acetate to each tube.
5. Add 500ul of chloroform to each tube. Vortex for 5-10 mins. Sample can be frozen overnight if needed.
6. Spin 5-8mins at 9,000 *g*.
7. Pipetter aqueous top layer in a new Eppendorf tube. There should be approximately 400ul.
8. Add 2 volumes (if you get 400ul from step 7 then you add 800ul) of 100% ethanol at room temperature. Mix by inverting.
9. Spin at 14000 rpm for 20min at 4°C.
10. Remove the supernatant and air dry for 2-3 mins.
11. Add 30 ul of Autoclaved Water.
12. Dilute to desired concentration with autoclaved water after determining concentration in a Nanodropper 2000 (for mdx genotyping protocol dilute to 20ng/ul).

Table D3. Forward and reverse primers used to detect *mdx* mice.

Primer name	Sequence
Common forward (DL1577)	5'GCG CGA AAC TCA AAT ATG CGT GTT AGT GT-3'
WT forward (DL1509) 134 bp	5'-GAT ACG CTG CTT TAA TGC CTT TAG TCA CTC AGA TAG TTG AAG CCA TTT TG-3'
mdx reverse (DL1573) 117 bp	5'-CGG CCT GTC ACT CAG ATA GTT GAA GCC ATT TTA-3'

Table D3. PCR cycle for *mdx* mice.

	Temperature (°C)	Time	Number of cycles
mdx			
1. Denaturation	94	5 min	1
2. Denaturation	94	30 s	
3. Annealing	60	30 s	34 cycles (ie. go to
4. Extension	72	30 s	2 34 times)
5. Final Extension	72	3 min	1
6. Hold	4	-	can hold here until ready to perform electrophoresis.

Appendix E

Breeding strategies for transgenic mice

Pln^{OE}/Sln^{KO} ($Pln^{OE}/Sln^{-/-}$) and Pln^{OE}/Sln^{WT} ($Pln^{OE}/Sln^{+/+}$) Breeding Strategy

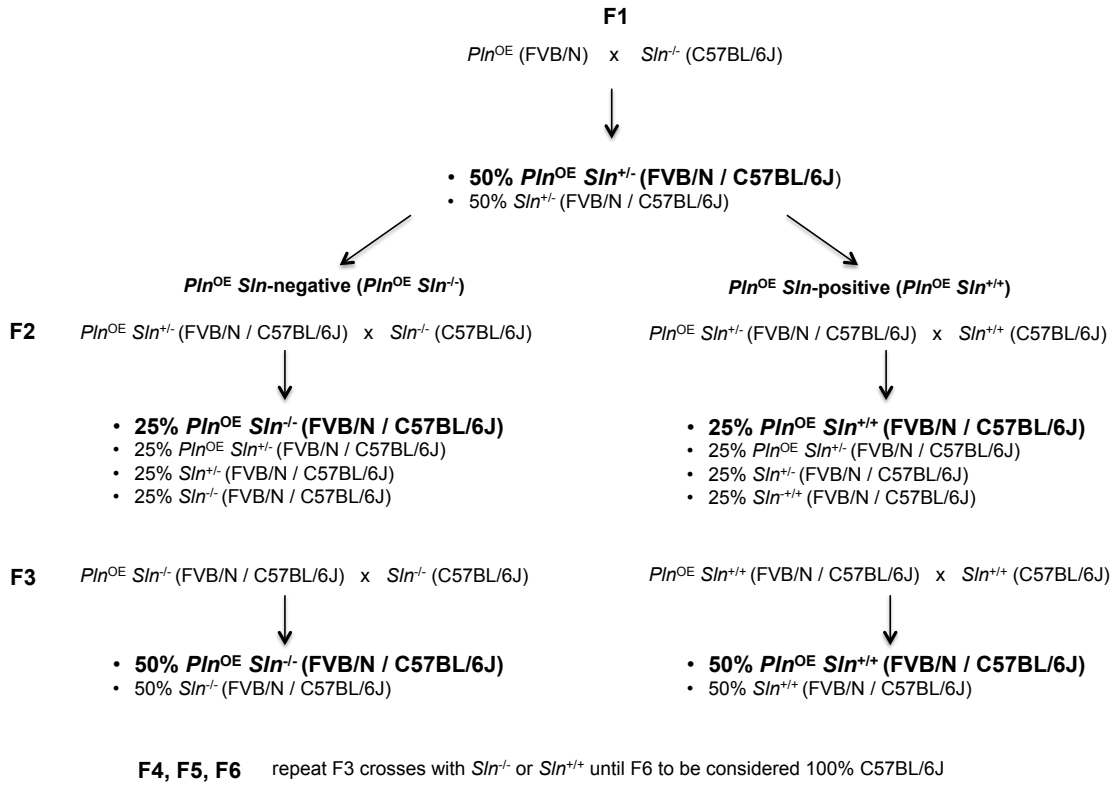

F1 - Pln^{OE} mice (AUPP 10-11) were mated with $Sln^{-/-}$ mice (11-03). As Pln^{OE} mice are heterozygous for the transgene F1 offspring are 50% Pln^{OE} and 50% without the transgene. Since Pln^{OE} mice are homozygous for *Sln*-positive ($Sln^{+/+}$) the F1 offspring will be 100% heterozygous for *Sln* ablation ($Sln^{-/+}$). At this point F1 progeny are 50:50 for FVB/N:C57BL/6J.

F2 - Progeny from F1 will be used to generate F2 progeny. Specifically, from here we decided to generate two subset colonies: 1) $Pln^{OE}Sln^{-/-}$ and 2) $Pln^{OE}Sln^{+/+}$. To do this, $Pln^{OE}Sln^{+/-}$ F1 progeny were crossed with either the $Sln^{-/-}$or the $Sln^{+/+}$ mice from AUPP 11-03. From this cross, we were able to generate the $Pln^{OE}Sln^{-/-}$ and the $Pln^{OE}Sln^{+/+}$ mice that were then used for the F3 cross. At this point F2 progeny are 25:75 for FVB/N:C57BL/6J.

F3 - The $Pln^{OE}Sln^{-/-}$ and the $Pln^{OE}Sln^{+/+}$ mice were then mated with $Sln^{-/-}$ and the $Sln^{+/+}$ mice, respectively. Again we were able to generate the $Pln^{OE}Sln^{-/-}$ and the $Pln^{OE}Sln^{+/+}$ mice that were then used for the F4 cross. At this point F3 progeny are 12.5:87.5 for FVB/N:C57BL/6J.

F4 – Repeat of F3 cross. Again we were able to generate the $Pln^{OE}Sln^{-/-}$ and the $Pln^{OE}Sln^{+/+}$ mice that were then used for the F4 cross. At this point F4 progeny are 6.25:93.75 for FVB/N:C57BL/6J. These mice were used for initial experiments under AUPP 13-01.

F5 – Repeat of F4 cross. Again we were able to generate the $Pln^{OE}Sln^{-/-}$ and the $Pln^{OE}Sln^{+/+}$ mice that were then used for the F6 cross. At this point F5 progeny are 3.125:96.875 for FVB/N:C57BL/6J. These mice will be used for experiments under AUPP 13-01.

F6 – Repeat of F5 cross. We will generate the $Pln^{OE}Sln^{-/-}$ and the $Pln^{OE}Sln^{+/+}$. At this point F6 progeny are 1.56:98.43 for FVB/N:C57BL/6J. Typically, this enough for these mice to be considered 100% C57BL/6J. These mice will be used for experiments under AUPP 13-01.

Since these mice are considered 100% C57BL/6J after F6 we will no longer need to backcross onto the $Sln^{-/-}$ or $Sln^{+/+}$ mice from AUPP 11-03. Instead, we can maintain these colonies by breeding the $Sln^{-/-}$ or $Sln^{+/+}$ mice generated from the F6 and future F generations. However, it is probably better practice to keep breeding to the $Sln^{-/-}$ or $Sln^{+/+}$ mice from AUPP 11-03, as this will completely eliminate the chances of getting a homozygous Pln^{OE} mouse (ie. the $Sln^{-/-}$ or $Sln^{+/+}$ mice from AUPP 11-03 never overexpressed PLN).

Mdx/*Sln*^{KO} mice

To generate our research animals for our *mdx*/*Sln*^{KO} and *mdx*/*Sln*^{WT} (*mdx*) colonies we first crossed homozygous female *mdx* animals with a male homozygous *Sln*^{KO} mouse.

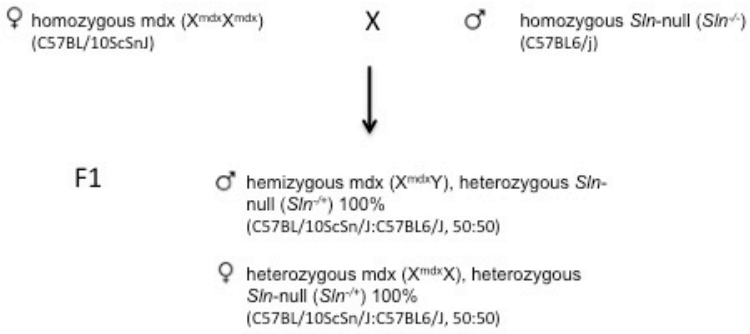

From this cross we obtained F1 offspring that are either female hemizgous *mdx* or male heterozygous *mdx*. All F1 offspring were heterozygous for *Sln*. Next, we crossed F1 offspring male and females together (from a separate breeding pair so that it is not inbred).

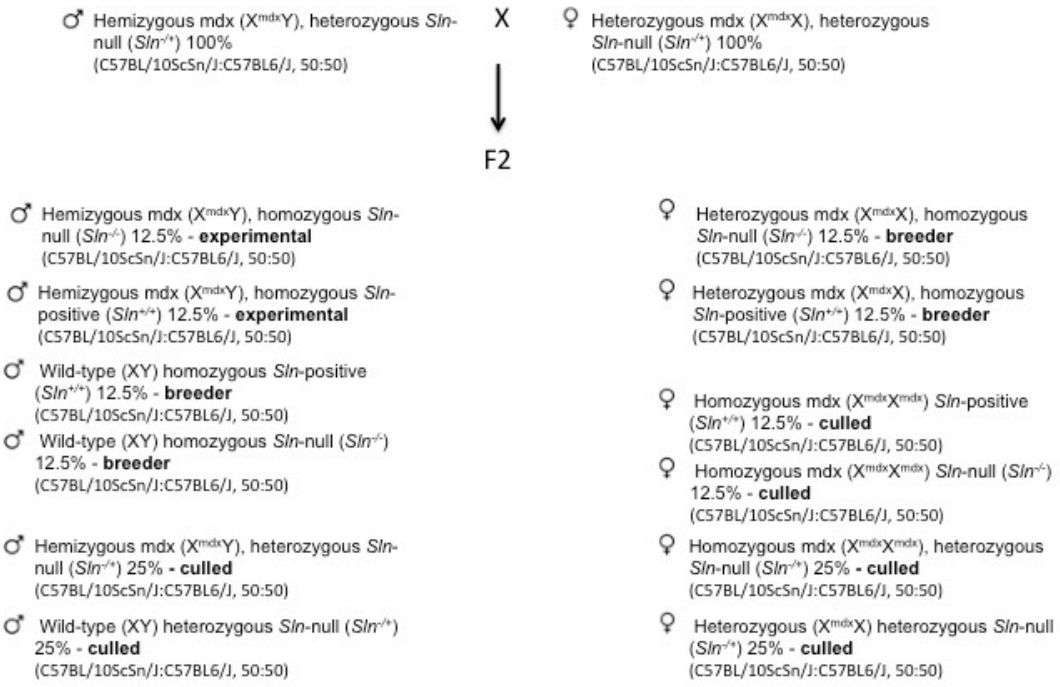

The resulting F2 offspring will be a variety of genotypes including our experimental animals, *mdx* and *mdx*/*Sln*^{KO}. To improve the odds at which we generate the experimental animals, we generated two subset colonies that independently gave rise to *mdx* mice and *mdx*/*Sln*^{KO} mice.

***mdx*/*Sln*^{KO}:** For this subset colony *dystrophin* positive male mice from F2 were bred with heterozygous *mdx* females from F2, and both sires and dams were homozygous for *Sln*^{KO}.

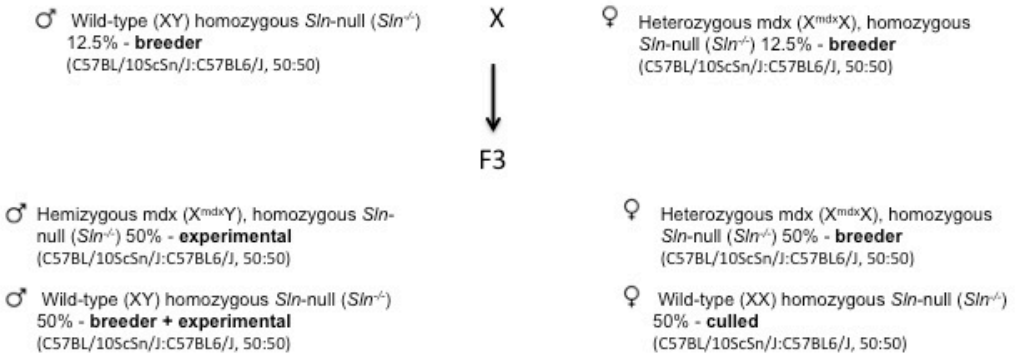

***mdx*:** For this subset colony *dystrophin* positive male mice from F2 were bred with heterozygous *mdx* females from F2, and both sires and dams were homozygous for *Sln*^{WT}.

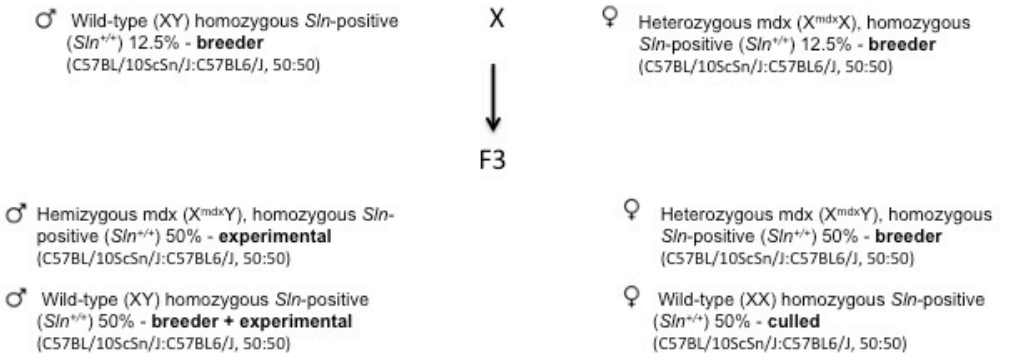

Note: Because crosses were bred from previous generations, the strain is a 50:50 mix of C57BL/10Scn:C57BL6/J). To prevent genetic drift, the *mdx* and *mdx*/*Sln*^{KO} subset colonies should be limited to 3 additional generations.

Appendix F

Protocol for SERCA activity assay

As per Duhamel et al. (137).

Buffers

Muscle Homogenizing Buffer

500 mM HEPES pH7.5
200 mM PMSF

SR Homogenate Ca^{2+}-ATPase buffer

	For 1L	For 200 ml
200 mM KCL	14.91 g	2.982 g
20 mM HEPES	4.766 g	953.2 mg
10 mM NaN_3	650 mg	130.02 mg
1 mM EGTA	380.4 mg	76.08 mg
15 mM $MgCl_2$	1.428 g	285.62 mg
5 mM ATP	3.026 g	605.2 mg
10 mM Phosphoenolpyruvate (PEP)	4.688 g	930.6 mg

Heat to 37°C and then pH to 7.0 with 2N KOH
Store at -20°C

Isolation Ca^{2+}-ATPase buffer

	For 1L	For 200 ml
100 mM KCL	7.45 g	1.491 g
20 mM HEPES	4.766 g	953.2 mg
10 mM NaN_3	650 mg	130.02 mg
1 mM EGTA	380.4 mg	76.08 mg
10 mM $MgCl_2$	952 mg	190.4 mg
5 mM ATP	3.026 g	605.2 mg
10 mM Phosphoenolpyruvate (PEP)	4.688 g	930.6 mg

Heat to 37°C and then pH to 7.0 with 2N KOH
Store at -20°C

Enzymes and reagents

18 $U^{\bullet}ml^{-1}$ pyruvate kinase (PK, 10-128-163-001, Roche)

18 $U^{\bullet}ml^{-1}$ lactate dehydrogenase (LDH, L2625-25 KU, Sigma)

1 $mg^{\bullet}ml^{-1}$ Calcium Ionophore (A23187, C-7522 Sigma; 10 mg in 10 ml of HPLC grade ethanol)

1.9 % (w/v) NADH (Divide mass by 19 to get volume of water needed) *only good for 6 hours.* (13348539, Roche)

10 mM $CaCl_2$

40 mM cyclopiazonic acid (CPA, 111258-00-5, Sigma) (50 mg in 3.71 ml chloroform)

Protocol

1. Pipette Ca^{2+} from 10 mM $CaCl_2$ stock into eppendorf tubes to get 16 different calcium concentrations. This will vary depending on muscle type and species.

   Example: Add to 16 different tubes:
   1. 12 µl
   2. 15 µl
   3. 18 µl
   4. 19.5 µl
   5. 21 µl
   6. 22 µl
   7. 23 µl
   8. 24 µl
   9. 25 µl
   10. 26 µl
   11. 27 µl
   12. 28 µl
   13. 29 µl
   14. 30 µl
   15. 31 µl
   16. 31 µl + 1 µl CPA (measure background ATPase)

2. Make reaction master mix:
   5 ml of ATPase Buffer
   13.5 µl LDH
   18 µl PK
   10.5 µl Ionophore
   20 µl of SR vesicles or homogenate
3. Transfer 300 µl of master mix to each of the 16 Eppendorf tubes. Transfer 4 at a time then vortex before the next 4 tubes and so on.
4. Vortex Eppendorf tubes and pipette 100 µl in duplicate to a clear 96 well-plate
5. Add 2 µl of NADH to each well immediately prior to reading the plate.
6. Place loaded plate into Spec Plate reader and complete a Path length correction read. *This corrects the path length to 1/3 of a cm.*
7. Then read plate on Spec Plate reader for kinetic assay
   Temp = 37°C
   Time = 30 min
   Wavelength = 340 nm

All data are then plotted against a negative logarithm of $[Ca^{2+}]_f$ (*p*Ca) using Graphpad™ Prism statistical software to determine $K_{Ca,}$ which is the concentration required to elicit half-maximal SERCA activity reported in *p*Ca units (ie. pCa_{50}). Specifically, K_{Ca} was determined by non-linear regression curve fitting using the sigmoidal dose response equation:

$$Y = Y_{bot} + (Y_{top} - Y_{bot})/(1 + {}^{(LogCa_{50} - x)} * n_H)$$

where Y_{bot} is the bottom of the plateau, Y_{top} is the top of the plateau, Log Ca_{50} is the logarithm of pCa_{50} and n_H is the hill coefficient. Note that the maximal SERCA activity is taken from the raw data and not the plateau estimated from Graphpad.

The accurate measurement of $[Ca^{2+}]_f$ used for the ATPase activity assay was measured using the Ca^{2+} fluorophore, indo-1 on a spectrophotometric plate reader (SPECTRAmax Gemini SX; Molecular Devices, Toronto, ON). The 16 different Ca^{2+} additions along with a zero Ca^{2+} and max Ca^{2+} (10 mM) were measured in triplicate as described below.

1. Pipette Ca^{2+} from 10 mM $CaCl_2$ stock into eppendorf tubes to get 17 different calcium concentrations. You will have to multiply the original additions for the assay by 4/3 to adjust for triplicate rather than duplicate (ie. working with 400 µl of reaction mix per tube rather than 300 µl).

   Example: Add to 16 different tubes:
   17. 12 µl x 4/3 = 16 µl
   18. 15 µl x 4/3 = 20 µl
   19. 18 µl x 4/3 = 24 µl
   20. 19.5 µl x 4/3 = 25.9 µl
   21. 21 µl x 4/3 = 27.9 µl
   22. 22 µl x 4/3 = 29.3 µl
   23. 23 µl x 4/3 = 30.6 µl
   24. 24 µl x 4/3 = 31.9 µl

25. 25 µl x 4/3 = 33.3 µl
26. 26 µl x 4/3 = 34.6 µl
27. 27 µl x 4/3 = 35.9 µl
28. 28 µl x 4/3 = 37.2 µl
29. 29 µl x 4/3 = 38.6 µl
30. 30 µl x 4/3 = 40 µl
31. 31 µl x 4/3 = 41.2 µl
32. 0 Ca^{2+}
33. max Ca^{2+}: 41.2 µl of 10 mM $CaCl_2$

2. Make reaction master mix:
   7 ml of ATPase Buffer
   18.9 µl LDH
   25.2 µl PK
   14.7 µl Ionophore
   8 µl INDO-1 (in the dark)
3. Transfer 400 µl of master mix into each of the Ca^{2+} addition tubes. Transfer 4 at a time then vortex before the next 4 tubes and so on.
4. Vortex Eppendorf tubes and load 100µl in triplicate onto black 96 well plate (Costar, Corning Incorporated, NY).
5. Read black plate on Fluor Plate reader (SPECTRAmax Gemini XS; Molecular Devices, Toronto, ON) for an end point assay.
   Temp = 37°C
   Excitation wavelength = 355 nm
   Emission wavelength Ca^{2+} bound indo-1 = 405 nm
   Emission wavelength Ca^{2+} free indo-1 = 485 nm
   Ratio = 405/485
6. Read plate for first reading, then wait 15 minutes to warm the plate at 37°C, then re-read the plate. Temperature does affect *p*Ca values so this step is required.
7. Calculate using equation for INDO-1

$$[Ca^{2+}]_f = K_d * (G_{max}G_{min}) * (R-R_{min})/(R_{max}-R)$$

where K_d is the equilibrium constant for the interaction between Ca^{2+} and indo-1, R_{min} is the minimum value of R with zero Ca^{2+}, G_{max} is the maximum value of G with zero Ca^{22+}, R_{max} is the maximum value of R at max Ca^{2+} (10 mM) and G_{min} is the minimum value of G at max Ca^{2+} (10 mM). The K_d value of indo-1 Ca^{2+} dye complex is 250 for muscle homogenates (238).

Appendix G

Protocol for Ca^{2+} uptake assay

This uptake assay was initially described by Tupling et al., 2002 (138). The indo-1 Ca^{2+} fluorophore is used to determine Ca^{2+} uptake in muscle homogenates and SR vesicles. Fluorescence signals produced by Indo-1 are collected on a dual emission wavelength spectrofluorometer (Ratiomaster^{TM} system, Photon Technology International, Birmingham, NJ). Measurements are based on the difference in Ca^{2+} bound Indo-1 and Ca^{2+} free Indo-1 complexes which have emission wavelengths of 405 and 485 nm upon excitation with a 355 nm wavelength, respectively. As Ca^{2+} uptake occurs, the $[Ca^{2+}]_f$ decreases which therefore increases the Ca^{2+} free Indo-1 causing the ratio between free/bound Indo-1 (R) to decrease. Measurements can be done with or without the Ca^{2+} precipitation anion, oxalate. Oxalate and phosphate can increase rates of Ca^{2+} uptake by precipitating calcium in the lumen of the SR, which prevents an excessive rise in lumenal Ca^{2+} and preventing back-inhibition (239).

Buffers and reagents

Uptake buffer

	For 200 ml
200 mM KCl	2.982 g
20 mM HEPES	953.2 mg
10 mM NaN_3	130.02 mg
5 μM TPEN	0.424 g
5 mM Oxalate	0.18 g
15 mM $MgCl_2$	0.29 g

Add reagents to 150 ml of water. Heat to 37°C and then pH to 7.0 with 2N KOH and then bring to a final volume of 200 ml. Store at -20°C

Other reagents

250 mM ATP

Stock EGTA: 50 mM EGTA, pH 7.0

Stock Ca^{2+}: 100 mM Ca^{2+} solution

2 mM Indo-1 in 50 mM glycine, pH 11

Protocol

1. Turn on water bath and make sure it is set to 42°C. Ensure that there is good flow in tubing to heat the jacket around the cuvette. The temperature in the cuvette should be at 37°C after ~1hr. *If the temperature is failing to reach 37°C clean the jacket and don't jack up the temperature setting above 42°C.*
2. Turn on a second water bath to about 40-42°C. This will heat up the Ca^{2+} uptake buffer and is higher than 37°C because when pipetting and transferring buffer to the cuvette it will cool down naturally.
3. Turn on Arc lamp. Then ignite by pressing start. Ensure that it is set at greater than 65.
4. Get an aliquot of 250 mM ATP, pH 7.0. *This must be fresh and not freeze-thawed more than once.*
5. Place INDO-1 and ATP on ice.
6. Prepare EGTA.
    - Stock EGTA: 50 mM EGTA, pH 7.0
    - Dilute 10x to 5 mM
    - 200 µl stock + 1800 µl dH_2O
7. Prepare low and high Ca^{2+}
    - High 100 mM stock in fridge. Pipette 1 ml into Eppendorf tube.
    - Low 10 mM (10x dilution of stock: 100 µl stock + 900 µl water)
8. Turn on power of Motor-Driver MD-5020
9. Turn on power of BryteBox
10. Open Felix32 program on computer.
11. Check photomultipliers (Left – 909, Right – 1000)
12. Calibration
    - Click configure
        - Hardware configuration
        - Open digital file (only file listed)
        - Initialize (lightning bolt)
        - Go around to the others side and note the number on the dial.
        - Place value into monochromater
        - OK
        - Save
13. Acquisition
    - Open acquisition
        - Click uptake

- Set duration
- Set view window
- Check excitation 355
- Check emission 1 405
- Check emission 2 485

14. Display
    - Clear background * Only when using a new batch of buffer
15. Acquire prep
    - Go around to ensure that the number is 355. If not then re-calibrate by pressing abort on acquisition.

16. Measure background fluorescence
    - In cuvette place stir bar
    - 1960 µl of buffer
    - 40 µl of ATP
    - 2 µl low calcium
    - 1 µl INDO-1
        - Start. Wait 1s then click Stop.
17. Click Math
    - Average
    - Select tool | | and highlight the whole area.
    - Note the average for D1 and D2.
18. Click Display
    - Type in background values (D1 & D2)
    - Click OK
    - Save on acquisition.

Now ready for data collection.

Replace with new cuvette. Working solution is always 2 ml and this solution contains:

1. Uptake buffer. Subtract sum of: sample volume + ATP volume + INDO-1 volume + low Ca^{2+} volume from 2000 to get buffer volume.
2. Sample (volume depends on sample type). Soleus is 80 µl and plantaris is 30 µl.
3. 40 µl ATP
4. Low Ca^{2+} volume (depends on sample – try 2 µl first)
5. 1 µl INDO-1

Order of pipetting:

1. Pipette buffer then place cuvette into jacket to stay warm.
2. Add sample with a positive displacement pipette.
3. Add low Ca^{2+}
4. Add INDO-1
5. Click start on acquisition
6. Add ATP through hole on the top of the box (or open and close the lid quickly) into the cuvette. **This starts the reaction.**

7. Wait for curves to plateau.
8. Add 145 µl EGTA (for min).
9. Wait 10s.
10. Add 30 µl high Ca^{2+} (for max).
11. Clean stir bar before next sample.

Data acquisition

1. Click transform
    - Concentration Map
    - Highlight Ratio on left
    - Equation
    - Edit/select
2. Zoom into EGTA and high Ca^{2+} part of the curves
3. Select the flat part of the EGTA
    - Capture Rmin
4. Select the flat part of the high Ca^{2+}
    - Capture Rmax
5. Select the flat part of the high Ca^{2+}
    - Highlight D2 on left
    - Capture Sb2
6. Select the flat part of the EGTA
    - Highlight D2 on left
    - Capture Sf
7. Click on Ratio-2 then click execute on transform box.
8. Highlight Ratio-2
    - Click Math
    - Click Smooth
    - Buffer size set to 21 points
    - Execute
    - Close

Check the curve for the ratio by zooming out. Click Axes and select fixed. Set min 0 and max to 5000. Counts should be between 3000-4000 at the start.

Analysis

The generate curve ($[Ca^{2+}]_f$ versus time) is then smoothed over 21 points using the Savitsky-Golay algorithm. The instantaneous tangents/slopes are then determined at 500 nM, 1000 nM, and 1500 nM to determine the rate of calcium uptake, which is then normalized to total protein content and expressed as µmoles/g protein/min. Note that to determine rates of Ca^{2+} at a higher free $[Ca^{2+}]_f$ a modified Indo-1 that is not easily saturated at high Ca^{2+} concentrations could be used.

Appendix H

Protocol for simultaneous mechanical overload and soleus tenotomy

This protocol, approved by the University of Waterloo's Animal Care Committee, described the procedure to mechanically overload plantaris muscles by performing soleus and gastrocnemius tenotomy. Since, soleus muscles are left intact in the muscle, the soleus muscle can then be analyzed as well, as a model of unloading and muscle degeneration.

UNIVERSITY OF WATERLOO
OFFICE OF RESEARCH ETHICS

STANDARD OPERATING PROCEDURES

SOP CAF MED 083: Synergistic ablation in rodents

Purpose: This SOP discusses the materials required and the method used to perform synergistic ablation of the soleus and gastrocnemius muscles in the rodent. This procedure is to be done in a surgery room and not in an animal room. This is a survival procedure.

Responsibility: Animal Health Technicians, Researchers

1.0 Material Required Before Starting Procedure

- Forceps
- Surgical scissors
- Betadine solution
- alcohol swabs
- 7-0 silk suture (CDMV: 104965)
- gauze
- Bead sterilizer

2.0 Anaesthesia and Analgesia

2.1 General anaesthesia (GA) is required for the synergistic ablation of the soleus and gastrocnemius muscles from rodents. Isofluorane can be used as an anesthetic agent with the anaesthesia machine (refer to SOP CAF MED 030:

Use of Rodent Anaesthesia Machine).

2.2 Meloxicam will be administered subcutaneously shortly after GA induction (rats and mice 1.0 mg/kg; refer to SOP CAF MED 059: Meloxicam use in Rodents).

3.0 Surgical Protocol: General

3.1 Place animal on top of a covered heating pad to prevent hypothermia in the animal (refer to SOP CAF MED 061: Preventing Hypothermia During Surgery and Recovery from Anaesthesia).

3.2 Apply Tear Gel to the eyes. Shave the hindlimbs. Wipe the incision site with the alcohol swab. Follow with a wipe of Betadine solution.

3.3. Extend the hindlimb and pinch the foot to ensure that the mouse is under full anaesthesia. A brief midline incision will be made in the skin on the hindlimbs (2013 Ito et al., 2013. *Nature Medicine*. 19(1): 101-106).

3.4 Perform blunt dissection (open and close forceps inside the incision) to expose the muscle and tendons.

3.5 Invert the foot (ie. facing towards the body). By doing this it will be easier to perform step 3.4.

3.6 Locate and transect the distal tendons of both the gastrocnemius and soleus muscles.

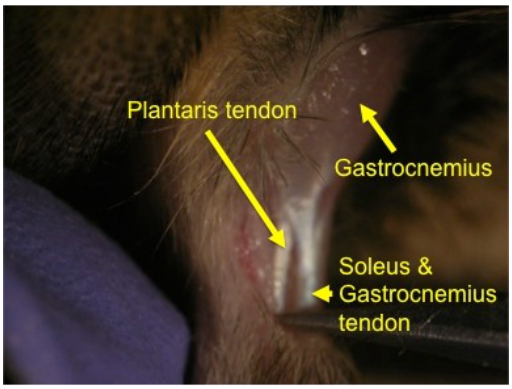

Figure H1. Photo illustrating the tendons involved in mechanically overloading the plantaris muscle and tenotomising the soleus. The soleus and gastrocnemius tendons from a mouse hind-limb are transected while the plantaris tendon is left intact. In the image is a right-hind limb with the foot inverted.

3.7 Close the incision/wound with a 7-0 silk suture.

3.8 The hindlimb from the other leg will serve as a sham control. Shave the hair from the incision site and wipe with alcohol followed by Betadine solution. Make a small incision and then close the wound with a 7-0 silk suture.

3.9 The animal will be returned to a recovery cage post-op and monitored. Following recovery, animal will be individually housed.

3.10 Meloxicam should be given up to 3 days post-operatively.

3.11 The animal should be carefully monitored for self injury to the hind limb or the removal of sutures.

3.12 If the animal will be kept for longer than 2 weeks post-surgery, then an absorbable suture should be considered.

Appendix I

Protocol for transmission electron microscopy

Fixing skeletal muscle for TEM analysis

Materials & Solutions

50% Glutaraldehyde solution (Electron Microscopy grade)
Reagent grade acetone
HPLC grade acetone
1 drum vials with black caps (4 mL vials)
BEEM capsules
Dissecting pins
Dissecting microscope with reticle
Blade

0.2 M Phosphate buffer pH 7.4

- Na_2HPO_4 10.9g
- NaH_2PO_4 3.2g
- Distilled water 400 mL
- pH to 7.4 with NaOH then top up to 500 mL

1% Osmium tetraoxide (OsO_4) in 0.2 M phosphate buffer

- 2 mL ampule of 4% OsO_4
    - Open very carefully in fumehood.
- Poor 2 mL of 4% OsO_4 into 6 mL of 0.2 M phosphate buffer
- Discard the ampule and any pipette into an appropriately labeled waste bucket.

Epon-Aldarite plastic resin

1. Weigh in a weigh boat the following chemicals and slowly pour into a plastic urine specimen bottle with lid
    - 30g dodecenylsuccinic anhydride (Canemco #031)
    - 11.1g of araldite 502 (Canemco #CA062)
    - 15.5g of TAAB 812 embedding resin (Canemco #CE001-3; previously called epon812)
2. Cover and stir well on a stir plate for 15-20 min
3. In the fumehood, add in 1.4 g of DMP-30 (2,4,6-tri-(dimethylaminoethyl)phenol) (Canemco #033)
4. Cover and stir well on a stir plate for 15-20 min
5. Degas for approx. 1 hr until bubbles subside. Put the solution (uncovered) inside a desiccator with side arm and attach to vacuum pump to degas. Line the bottom of the desiccator in case it bubbles over.
6. Get 2 new 30 mL syringes with a slip-tip and without the rubber gasket (NORM JECT eccentric lure slip Fisher #14-817034)
7. Attach approx. 2 inches of tygon tubing and clamp and label syringes.

8. Remove the syringe plungers and prop the syringes vertically.
9. After degassing, pour carefully to avoid further air introduction and pour the entire solution into the 2 syringes.
10. Remove the tube clamp and carefully put the plunger back into the syringes.
11. Re-attach clamps and freeze at -20 degrees for up to approx. 3 weeks.
12. Remove syringe from freezer approx. 1hr. before use. Can re-freeze unused portions.

Protocol

Day 1

1. Isolate mouse soleus tissue
2. Cut muscle tissue into 1 mm cubes using a dissecting scope with a reticle and a blade. Four or five of them to begin with.
3. Fix in 2.5% glutaraldehyde in 0.2 M phosphate buffer pH 7.4 overnight 4 deg in a 1-drum vial (200 uL of 50% glutaraldehyde in 3800 ul of 0.2 M phosphate buffer).

Day 2

1. Carefully pipette out 2.5% glutaraldehyde solution. Do not pipette out muscle cubes.
2. Wash in 0.2 M phosphate buffer for 20 min.
3. Discard and re-wash in new phosphate buffer for 20 min.
4. Discard and re-wash in new phosphate buffer for 20 min.
5. Fix in 250 ul of 1% OsO4 in phosphate buffer for 1 hr at room temperature in a fumehood. Sample should go black.
6. Replace OsO4 with water 2x (15 min each).
7. Dehydrate with 20% acetone (400 ul acetone + 1600 ul water; 10 min)
8. Dehydrate with 50% acetone (1000 ul acetone + 1000 ul water; 10 min)
9. Dehydrate with 70% acetone (1400 ul acetone + 600 ul water; 10 min)
10. Dehydrate with 70% acetone (1400 ul acetone + 600 ul water; 10 min)
11. Dehydrate with 90% acetone (1800 ul acetone + 200 ul water; 10 min)
12. Dehydrate with 90% acetone (1800 ul acetone + 200 ul water; 10 min)
13. Dehydrate with pure anhydrous acetone (100% acetone, HPLC grade) (10 min)
14. Dehydrate with pure anhydrous acetone (100% acetone, HPLC grade) (overnight room temperature)

Day 3

1. Thaw E/A plastics 1 hr RT.
2. With a sharpie and a ruler mark 4 obvious sections in the lower 2/3 of the vial.
3. Embed in 75% acetone + 25% E/A - rotate 1 hr room temperature (3 vols 100% acetone + 1 vol of E/A)
4. Embed in 50% E/A + 50% acetone - rotate 1 hr room temperature
5. 100% E/A rotate 1 hr room temperature
6. Fresh 100% E/A rotate overnight at room temperature

Day 4

1. Take syringe of E/A out of the freezer and warm to room temperature for 1 hr.

2. Place BEEM capsules in the special white tray in the storeroom on the shelves above the student lab dispenser pumps.
3. Use tiny font on the computer, make tiny labels on regular printer paper and cut them so that they are tall enough to go from the bottom of the tube to the top and wide enough so they don't interfere with the sample.
4. Put fresh E/A into each BEEM capsule to fill.
5. Aspirate the E/A from vials and turn vials upside down on individual pieces of foil to drain. Use dissection pins to get tissue into the BEEMS. Very carefully use the needle to poke the tissue all the way to the very bottom of the tube - TRAPPING NO AIR BUBBLES. The entire piece of tissue must be used for each BEEM capsule. Do not cut tissue down in size at this point or it won't be properly fixed.
6. Polymerize in 60deg oven 24-48 hrs or indefinitely.

Sectioning the Embedded Fixed Muscle

<u>Materials & Equipment</u>

Glass cutter
A strip of glass
Foil tape
Nail polish
Microtome
Blade
Xylene + wooden skewer stick
Distilled water
Tweezers
Copper mesh grids with 100 squares
Whatman filter paper (cut into small wedges)
Toludine blue
Microscope slides (#2)
Light microscope

Making the glass knife
These knives need to be made the day of sectioning as the moisture from the air can dull them.

1. Wash glass strip with soap and water. Then dry.
2. Place the rough edge against the white holder.
3. Push the glass through till it touches the silver bump.
4. Turn lever on the left towards you until the glass is clamped down. If the glass is not clamped down it will not cut properly, so clamp and unclamp until it is.
5. When the glass is sufficiently clamped ensure that the diamond cutter is set to the dial with 'two' lines.
6. Pull the knob for the diamond cutter towards you in a single smooth motion.
7. Turn the black knob on the bottom right clockwise to the silver line. This will break the glass where the diamond cutter made the score.

8. After the cut, turn the black knob back to its starting position. Release the clamp and push the diamond cutter back to its original position.
9. Remove the excess piece of glass and only work with the square.
10. Carefully turn the square into a diamond that fits the groove on the horizontal clamps. Pull the handle on the left to bring the clamps together.
11. Clamp the diamond down with the lever on the left, again keeping in mind that it has to be sufficiently clamped.
12. Using the diamond cutter, turn the dial to the 'diamond' 25. Then in a single smooth motion score the glass.
13. Turn the black knob on the bottom right to break the square into two triangles.
14. Turn each triangle so that the sharpest edge (1 and 2) are facing upwards.
15. Cut two pieces of foil tape, each approximately 2 inches long. Tape the foil tape at the top of the knife on one end and wrap it around to the other end leaving a gap to make a boat with the blade. This is important, as it will be filled with water so that when the blade cuts sections it falls into and floats atop the water.
16. Seal the edges of the tape with nail polish. Pay careful attention to the front; there should be not gap between the tape and the glass as will not serve well as a reservoir for water. Seal with thick nail polish.

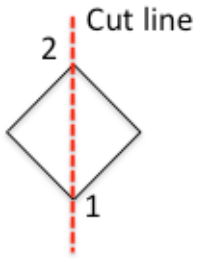

This figure shows the cutline of the square (diamond). The number 1 refers to that side being the primary blade (sharpest) and 2 being the secondary blade.

Sectioning the muscle sample into large trapezoids

1. Carefully remove your sample from the BEEM capsule using a blade to cut two strips along the edge.
2. Take the E/A embedded sample and place into vertical plane sample holder making sure that the sample is facing upwards.
3. Under the microscope and with a blade cut your sample into a small trapezoid. On the highest magnification it will be square wide at the top and 1.5-3 squares wide at the bottom. Always cut down on an angle.
4. Under the microscope, with an intermediate magnification, and with a blade cut your sample into a large trapezoid (ie. 3 squares on the top and 4 on the bottom). Always cut down on an angle.
5. Once the trapezoid is cut remove the sample from the vertical plane holder and place onto horizontal plane holder.

6. Place fresh glass knife into its holder and situate the knife close to the sample using the microscope for reference.
7. Fill the reservoir with distilled water until it gets a shiny silver metal car colour look.
8. Set the microtome to 0.74 um and a speed of 0.9.
9. Pull the lever down to start the microtome.
10. When sections become full trapezoids stop the microtome (only when the light green – never stop when it is red).
11. Collect a large trapezoid and place onto a drop of water on a microscope slide.
12. Place the slide on a block heater to dry.
13. Then add a few drops of toluidine blue while on the block heater.
14. Then rinse with water.
15. Under a light microscope check to see that the section is in the right orientation and which area you'd like to cut the small trapezoid for TEM.

Sectioning the muscle sample into small trapezoids

1. When you've decided which area of the sample to cut a small trapezoid place the sample back on the vertical plane holder.
2. Using a blade, cut the sample into a small trapezoid under the microscope at the highest magnification (1 square on top to 1.5-3 squares on the bottom).
3. Once the trapezoid is cut remove the sample from the vertical plane holder and place onto horizontal plane holder.
4. Place fresh glass knife into its holder and situate the knife close to the sample using the microscope for reference.
5. Fill the reservoir with distilled water until it gets a shiny silver metal car colour look.
6. Set the microtome to 90 nm and a speed of 0.9.
7. Pull the lever down to start the microtome.
8. When sections become full trapezoids stop the microtome (only when the light green – never stop when it is red).
9. Waft xylene over the reservoir with a skewer stick soaked in xylene with 3 passes.
10. Then using tweezers grab a copper mesh grid with the shiny side down and place it onto the trapezoid sections (ideally 6 per grid with 2 columns of 3).
11. The trapezoids should stick onto the grid. Place onto a wedge of Whatman paper to dry. Once dried place into a grid holder.
12. Repeat for 10-15 times per sample.

Staining the muscle sample with Lead Citrate (Pb Citrate) and Uranyl Acetate

Since the contrast in the electron microscope depends primarily on the differences in the electron density of the organic molecules in the cell, the efficiency of a stain is determined by the atomic weight of the stain attached to the biological structures. Consequently, the most widely used stains in electron microscopy are the heavy metals uranium and lead. Although the use of one of these stains alone could be quite practical for routine purposes, the highest contrast is obtained when both of these stains are used in sequences, "double contrasting", with uranyl acetate and lead citrate.

Uranyl acetate (negative stain)

The uranyl acetate (UA) enhances the contrast by interaction with lipids and proteins. The uranyl ions bind to proteins and lipids with sialic acid carboxyl groups such as glycoproteins and ganglioside and to nucleic acid phosphate groups of DNA and RNA. Gangliosides are glycolipids and are concentrated on cell surfaces. Glycoproteins are abundant in all membranes and part of the glycocalyx. Therefore UA delivers good contrasting results of membranes, nucleic acids and nucleic acids containing protein complexes such as ribosomes. ***UA is sensitive to light, especially UV and will precipitate if exposed. It also precipitates when ageing so all UA is made fresh and only used for ½ hour. In addition, UA is both radioactive and toxic (0.37-0.51 uCi/g). This is a very mild level of radioactivity and is not sufficient to be harmful while the material remains external to the body.***

For this protocol, we use alcoholic uranyl acetate, which has the advantage of penetrating more easily into the plastic embedded tissue and thus give a high contrast requiring only a short staining time (10 min).

Lead citrate

Lead citrate enhances the contrasting effect for a wide range of cellular structures such as ribosomes, lipid membranes, cytoskeleton and other compartments of the cytoplasm. The enhancement of the contrasting effect depends on the interaction with reduced osmium, since it allows the attachment of lead ions to the polar groups of molecules. Osmium, as in our protocol, is used routinely as a fixative. Lead citrate also interacts, to a weaker extent, with UA and therefore lead citrate staining is employed after UA staining. ***Lead citrate precipitates easily in the presence of carbon dioxide, either in air or in the water used for preparing the stain for rinsing. Lead carbonate is a water insoluble toxic white precipitate and accordingly will not dissolve in rinsing water. In general, all lead salts such as lead citrate are extremely toxic.***

The staining effect of lead solutions is highly dependent on the pH of the solution. Unlike uranyl acetate, it is possible to use lead based staining solutions at very high pH values (>12 pH). All alkaline lead stains can be considered to be stabilized solutions. Therefore, those solutions are suitable for commercial handling, provided they are made under conditions, which eliminate the formation of lead carbonate.

http://www.leica-microsystems.com/science-lab/brief-introduction-to-contrasting-for-em-sample-preparation/

Staining Protocol

Equipment and materials

Glass vials
Petri dishes
Parafilm
Filter paper
Syringe filters and small syringes (5cc)
Forceps

Pb Citrate
Uranyl Acetate
10N NaOH

Steps

1. Boil H_2O for 5 min (to release CO_2 from it) and cool the H_2O in a beaker covered with tin foil to room temp.
2. Make fresh 50% methanol (100 ml 50:50 with boiled water).
3. Dissolve a few crystals of uranyl acetate in 50% methanol. It takes about 10 min to get it into a bright yellow solution. This is light sensitive so cover in tin foil.
4. Using a small syringe with a syringe filter, place a few drops of uranyl acetate solution onto a piece of parafilm inside a petri dish.
5. With sections side up, place a TEM grid into a drop of uranyl acetate in the petri dish for 10 min.
6. Wash excess uranyl acetate with 50% methanol.
7. Place grid in a separate holding petri dish.
8. Weigh out 0.04 g of Pb citrate and put into 10 ml of boiled water. To get this into solution at 100 µl of 10 N NaOH. Close lid tightly and shake vigorously until Pb citrate is fully dissolved.
9. Using a small syringe with a syringe filter, place a few drops of Pb citrate solution onto another piece of parafilm inside a separate petri dish.
10. With sections side up, place a TEM grid into a drop of uranyl acetate in the petri dish for 10 min.
11. Wash excess uranyl acetate with boiled water.
12. Grids are now ready to be visualized using a Transmission Electron Microscope.

Note: You need fresh Pb citrate and uranyl acetate droplets for every time a new grid is stained.

References

1. Tupling AR (2009) Excitation-Contraction Coupling. *Encyclopedia of Neuroscience*, eds Binder M, Hirokawa N, & Windhorst U (Springer Berlin Heidelberg), pp 1479-1483.
2. Bombardier E*, et al.* (2013) Sarcolipin trumps beta-adrenergic receptor signaling as the favored mechanism for muscle-based diet-induced thermogenesis. *FASEB J* 27(9):3871-3878.
3. Bombardier E, Smith IC, Vigna C, Fajardo VA, & Tupling AR (2013) Ablation of sarcolipin decreases the energy requirements for Ca2+ transport by sarco(endo)plasmic reticulum Ca2+-ATPases in resting skeletal muscle. *FEBS Lett* 587(11):1687-1692.
4. Smith IC, Bombardier E, Vigna C, & Tupling AR (2013) ATP consumption by sarcoplasmic reticulum Ca(2)(+) pumps accounts for 40-50% of resting metabolic rate in mouse fast and slow twitch skeletal muscle. *PLoS One* 8(7):e68924.
5. Gailly P (2002) New aspects of calcium signaling in skeletal muscle cells: implications in Duchenne muscular dystrophy. *Biochim Biophys Acta* 1600(1-2):38-44.
6. Harr MW & Distelhorst CW (2010) Apoptosis and autophagy: decoding calcium signals that mediate life or death. *Cold Spring Harb Perspect Biol* 2(10):a005579.
7. Martonosi AN & Pikula S (2003) The network of calcium regulation in muscle. *Acta Biochim Pol* 50(1):1-30.
8. Schiaffino S & Reggiani C (2011) Fiber types in mammalian skeletal muscles. *Physiol Rev* 91(4):1447-1531.
9. Rasmussen H (1986) The calcium messenger system (2). *N Engl J Med* 314(18):1164-1170.
10. Rasmussen H (1986) The calcium messenger system (1). *N Engl J Med* 314(17):1094-1101.
11. Toyoshima C & Inesi G (2004) Structural basis of ion pumping by Ca2+-ATPase of the sarcoplasmic reticulum. *Annu Rev Biochem* 73:269-292.
12. Toyoshima C, Nakasako M, Nomura H, & Ogawa H (2000) Crystal structure of the calcium pump of sarcoplasmic reticulum at 2.6 A resolution. *Nature* 405(6787):647-655.
13. Clarke DM, Loo TW, Inesi G, & MacLennan DH (1989) Location of high affinity Ca2+-binding sites within the predicted transmembrane domain of the sarcoplasmic reticulum Ca2+-ATPase. *Nature* 339(6224):476-478.
14. Toyoshima C (2008) Structural aspects of ion pumping by Ca2+-ATPase of sarcoplasmic reticulum. *Arch Biochem Biophys* 476(1):3-11.
15. Periasamy M & Kalyanasundaram A (2007) SERCA pump isoforms: their role in calcium transport and disease. *Muscle Nerve* 35(4):430-442.
16. East JM (2000) Sarco(endo)plasmic reticulum calcium pumps: recent advances in our understanding of structure/function and biology (review). *Mol Membr Biol* 17(4):189-200.
17. Murphy RM (2011) Enhanced technique to measure proteins in single segments of human skeletal muscle fibers: fiber-type dependence of AMPK-alpha1 and -beta1. *J Appl Physiol* 110(3):820-825.

18. Tupling AR (2004) The sarcoplasmic reticulum in muscle fatigue and disease: role of the sarco(endo)plasmic reticulum Ca2+-ATPase. *Can J Appl Physiol* 29(3):308-329.
19. Wu KD & Lytton J (1993) Molecular cloning and quantification of sarcoplasmic reticulum Ca(2+)-ATPase isoforms in rat muscles. *Am J Physiol* 264(2 Pt 1):C333-341.
20. Fajardo VA*, et al.* (2013) Co-Expression of SERCA Isoforms, Phospholamban and Sarcolipin in Human Skeletal Muscle Fibers. *PLoS One* 8(12):e84304.
21. Babu GJ*, et al.* (2007) Ablation of sarcolipin enhances sarcoplasmic reticulum calcium transport and atrial contractility. *Proc Natl Acad Sci U S A* 104(45):17867-17872.
22. Vangheluwe P*, et al.* (2005) Sarcolipin and phospholamban mRNA and protein expression in cardiac and skeletal muscle of different species. *Biochem J* 389(Pt 1):151-159.
23. Bhupathy P, Babu GJ, & Periasamy M (2007) Sarcolipin and phospholamban as regulators of cardiac sarcoplasmic reticulum Ca2+ ATPase. *J Mol Cell Cardiol* 42(5):903-911.
24. Babu GJ, Bhupathy P, Carnes CA, Billman GE, & Periasamy M (2007) Differential expression of sarcolipin protein during muscle development and cardiac pathophysiology. *J Mol Cell Cardiol* 43(2):215-222.
25. Damiani E, Sacchetto R, & Margreth A (2000) Variation of phospholamban in slow-twitch muscle sarcoplasmic reticulum between mammalian species and a link to the substrate specificity of endogenous Ca(2+)-calmodulin-dependent protein kinase. *Biochim Biophys Acta* 1464(2):231-241.
26. Tupling AR*, et al.* (2011) Enhanced Ca2+ transport and muscle relaxation in skeletal muscle from sarcolipin-null mice. *Am J Physiol Cell Physiol* 301(4):C841-849.
27. Wawrzynow A*, et al.* (1992) Sarcolipin, the "proteolipid" of skeletal muscle sarcoplasmic reticulum, is a unique, amphipathic, 31-residue peptide. *Arch Biochem Biophys* 298(2):620-623.
28. Gorski PA, Glaves JP, Vangheluwe P, & Young HS (2013) Sarco(endo)plasmic reticulum calcium ATPase (SERCA) inhibition by sarcolipin is encoded in its luminal tail. *J Biol Chem* 288(12):8456-8467.
29. Simmerman HK, Collins JH, Theibert JL, Wegener AD, & Jones LR (1986) Sequence analysis of phospholamban. Identification of phosphorylation sites and two major structural domains. *J Biol Chem* 261(28):13333-13341.
30. Sahoo SK, Shaikh SA, Sopariwala DH, Bal NC, & Periasamy M (2013) Sarcolipin protein interaction with sarco(endo)plasmic reticulum Ca2+ ATPase (SERCA) is distinct from phospholamban protein, and only sarcolipin can promote uncoupling of the SERCA pump. *J Biol Chem* 288(10):6881-6889.
31. Morita T*, et al.* (2008) Interaction sites among phospholamban, sarcolipin, and the sarco(endo)plasmic reticulum Ca(2+)-ATPase. *Biochem Biophys Res Commun* 369(1):188-194.
32. Asahi M*, et al.* (2003) Sarcolipin regulates sarco(endo)plasmic reticulum Ca2+-ATPase (SERCA) by binding to transmembrane helices alone or in association with phospholamban. *Proc Natl Acad Sci U S A* 100(9):5040-5045.

33. Asahi M, Kurzydlowski K, Tada M, & MacLennan DH (2002) Sarcolipin inhibits polymerization of phospholamban to induce superinhibition of sarco(endo)plasmic reticulum Ca2+-ATPases (SERCAs). *J Biol Chem* 277(30):26725-26728.
34. Luo W*, et al.* (1994) Targeted ablation of the phospholamban gene is associated with markedly enhanced myocardial contractility and loss of beta-agonist stimulation. *Circ Res* 75(3):401-409.
35. Slack JP, Grupp IL, Luo W, & Kranias EG (1997) Phospholamban ablation enhances relaxation in the murine soleus. *Am J Physiol* 273(1 Pt 1):C1-6.
36. Bhupathy P, Babu GJ, Ito M, & Periasamy M (2009) Threonine-5 at the N-terminus can modulate sarcolipin function in cardiac myocytes. *J Mol Cell Cardiol* 47(5):723-729.
37. Simmerman HK & Jones LR (1998) Phospholamban: protein structure, mechanism of action, and role in cardiac function. *Physiol Rev* 78(4):921-947.
38. Tada M & Katz AM (1982) Phosphorylation of the sarcoplasmic reticulum and sarcolemma. *Annu Rev Physiol* 44:401-423.
39. Tada M, Yamada M, Inui M, & Ohmori F (1982) [Regulation of Ca2+-dependent ATPase of cardiac sarcoplasmic reticulum by cAMP- and calmodulin-dependent phosphorylation of phospholamban]. *Tanpakushitsu Kakusan Koso* 27(15):2350-2364.
40. Gramolini AO*, et al.* (2006) Cardiac-specific overexpression of sarcolipin in phospholamban null mice impairs myocyte function that is restored by phosphorylation. *Proc Natl Acad Sci U S A* 103(7):2446-2451.
41. Song Q*, et al.* (2004) Overexpression of phospholamban in slow-twitch skeletal muscle is associated with depressed contractile function and muscle remodeling. *FASEB J* 18(9):974-976.
42. Autry JM*, et al.* (2011) Oligomeric interactions of sarcolipin and the Ca-ATPase. *J Biol Chem* 286(36):31697-31706.
43. Toyofuku T, Kurzydlowski K, Tada M, & MacLennan DH (1994) Amino acids Glu2 to Ile18 in the cytoplasmic domain of phospholamban are essential for functional association with the Ca(2+)-ATPase of sarcoplasmic reticulum. *J Biol Chem* 269(4):3088-3094.
44. Bal NC*, et al.* (2012) Sarcolipin is a newly identified regulator of muscle-based thermogenesis in mammals. *Nat Med* 18(10):1575-1579.
45. Frank K, Tilgmann C, Shannon TR, Bers DM, & Kranias EG (2000) Regulatory role of phospholamban in the efficiency of cardiac sarcoplasmic reticulum Ca2+ transport. *Biochemistry* 39(46):14176-14182.
46. Briggs FN, Lee KF, Wechsler AW, & Jones LR (1992) Phospholamban expressed in slow-twitch and chronically stimulated fast-twitch muscles minimally affects calcium affinity of sarcoplasmic reticulum Ca(2+)-ATPase. *J Biol Chem* 267(36):26056-26061.
47. Mall S*, et al.* (2006) The presence of sarcolipin results in increased heat production by Ca(2+)-ATPase. *J Biol Chem* 281(48):36597-36602.
48. Smith WS, Broadbridge R, East JM, & Lee AG (2002) Sarcolipin uncouples hydrolysis of ATP from accumulation of Ca2+ by the Ca2+-ATPase of skeletal-muscle sarcoplasmic reticulum. *Biochem J* 361(Pt 2):277-286.

49. Tupling AR, Asahi M, & MacLennan DH (2002) Sarcolipin overexpression in rat slow twitch muscle inhibits sarcoplasmic reticulum Ca2+ uptake and impairs contractile function. *J Biol Chem* 277(47):44740-44746.
50. Bönnemann CG & Voermans NC (2012) Chapter 70 - ECM-Related Myopathies and Muscular Dystrophies. *Muscle*, eds Hill JA & Olson EN (Academic Press, Boston/Waltham), pp 979-994.
51. Bertrand AT, Ben Yaou R, & Bonne Gl (2012) Chapter 72 - Diseases of the Nucleoskeleton. *Muscle*, eds Hill JA & Olson EN (Academic Press, Boston/Waltham), pp 1003-1012.
52. Cannon SC (2012) Chapter 73 - Channelopathies of Skeletal Muscle Excitability. *Muscle*, eds Hill JA & Olson EN (Academic Press, Boston/Waltham), pp 1013-1022.
53. Haller RG & DiMauro S (2012) Chapter 75 - Metabolic and Mitochondrial Myopathies. *Muscle*, eds Hill JA & Olson EN (Academic Press, Boston/Waltham), pp 1031-1041.
54. Ochala J & Larsson L (2012) Chapter 74 - Thick and Thin Filament Proteins: Acquired and Hereditary Sarcomeric Protein Diseases. *Muscle*, eds Hill JA & Olson EN (Academic Press, Boston/Waltham), pp 1023-1030.
55. Thornton C (2012) Chapter 68 - Myotonic Dystrophy. *Muscle*, eds Hill JA & Olson EN (Academic Press, Boston/Waltham), pp 955-968.
56. Altamirano F*, et al.* (2012) Increased resting intracellular calcium modulates NF-kappaB-dependent inducible nitric-oxide synthase gene expression in dystrophic mdx skeletal myotubes. *J Biol Chem* 287(25):20876-20887.
57. Gehrig SM*, et al.* (2012) Hsp72 preserves muscle function and slows progression of severe muscular dystrophy. *Nature* 484(7394):394-398.
58. Goonasekera SA*, et al.* (2011) Mitigation of muscular dystrophy in mice by SERCA overexpression in skeletal muscle. *J Clin Invest* 121(3):1044-1052.
59. Zvaritch E*, et al.* (2009) Ca2+ dysregulation in Ryr1(I4895T/wt) mice causes congenital myopathy with progressive formation of minicores, cores, and nemaline rods. *Proc Natl Acad Sci U S A* 106(51):21813-21818.
60. Cardamone M, Darras BT, & Ryan MM (2008) Inherited myopathies and muscular dystrophies. *Semin Neurol* 28(2):250-259.
61. Nance JR, Dowling JJ, Gibbs EM, & Bonnemann CG (2012) Congenital myopathies: an update. *Curr Neurol Neurosci Rep* 12(2):165-174.
62. Sharma MC, Jain D, Sarkar C, & Goebel HH (2009) Congenital myopathies--a comprehensive update of recent advancements. *Acta neurologica Scandinavica* 119(5):281-292.
63. Tubridy N, Fontaine B, & Eymard B (2001) Congenital myopathies and congenital muscular dystrophies. *Curr Opin Neurol* 14(5):575-582.
64. Romero NB (2010) Centronuclear myopathies: a widening concept. *Neuromuscul Disord* 20(4):223-228.
65. Sewry CA (2008) Pathological defects in congenital myopathies. *J Muscle Res Cell Motil* 29(6-8):231-238.
66. Sewry CA, Jimenez-Mallebrera C, & Muntoni F (2008) Congenital myopathies. *Curr Opin Neurol* 21(5):569-575.
67. Jungbluth H & Gautel M (2014) Pathogenic mechanisms in centronuclear myopathies. *Frontiers in aging neuroscience* 6:339.

68. Maclennan DH & Zvaritch E (2011) Mechanistic models for muscle diseases and disorders originating in the sarcoplasmic reticulum. *Biochim Biophys Acta* 1813(5):948-964.
69. Ottenheijm CA*, et al.* (2008) Sarcoplasmic reticulum calcium uptake and speed of relaxation are depressed in nebulin-free skeletal muscle. *FASEB J* 22(8):2912-2919.
70. Emery AE (2002) The muscular dystrophies. *Lancet* 359(9307):687-695.
71. Rybakova IN, Patel JR, & Ervasti JM (2000) The dystrophin complex forms a mechanically strong link between the sarcolemma and costameric actin. *J Cell Biol* 150(5):1209-1214.
72. Millay DP*, et al.* (2009) Calcium influx is sufficient to induce muscular dystrophy through a TRPC-dependent mechanism. *Proc Natl Acad Sci U S A* 106(45):19023-19028.
73. Gailly P (2012) TRP channels in normal and dystrophic skeletal muscle. *Curr Opin Pharmacol* 12(3):326-334.
74. Spencer MJ, Croall DE, & Tidball JG (1995) Calpains are activated in necrotic fibers from mdx dystrophic mice. *J Biol Chem* 270(18):10909-10914.
75. Millay DP*, et al.* (2008) Genetic and pharmacologic inhibition of mitochondrial-dependent necrosis attenuates muscular dystrophy. *Nat Med* 14(4):442-447.
76. Allen DG, Gervasio OL, Yeung EW, & Whitehead NP (2010) Calcium and the damage pathways in muscular dystrophy. *Can J Physiol Pharmacol* 88(2):83-91.
77. Turner PR, Westwood T, Regen CM, & Steinhardt RA (1988) Increased protein degradation results from elevated free calcium levels found in muscle from mdx mice. *Nature* 335(6192):735-738.
78. Tantral L*, et al.* (2004) Intracellular calcium release is required for caspase-3 and -9 activation. *Cell Biochem Funct* 22(1):35-40.
79. Brookes PS, Yoon Y, Robotham JL, Anders MW, & Sheu SS (2004) Calcium, ATP, and ROS: a mitochondrial love-hate triangle. *Am J Physiol Cell Physiol* 287(4):C817-833.
80. Schneider JS*, et al.* (2013) Increased sarcolipin expression and decreased sarco(endo)plasmic reticulum Ca uptake in skeletal muscles of mouse models of Duchenne muscular dystrophy. *J Muscle Res Cell Motil*.
81. Tupling AR*, et al.* (2004) HSP70 binds to the fast-twitch skeletal muscle sarco(endo)plasmic reticulum Ca2+ -ATPase (SERCA1a) and prevents thermal inactivation. *J Biol Chem* 279(50):52382-52389.
82. Mazala DA*, et al.* (2015) SERCA1 overexpression minimizes skeletal muscle damage in dystrophic mouse models. *Am J Physiol Cell Physiol* 308(9):C699-709.
83. Morine KJ, Sleeper MM, Barton ER, & Sweeney HL (2010) Overexpression of SERCA1a in the mdx diaphragm reduces susceptibility to contraction-induced damage. *Hum Gene Ther* 21(12):1735-1739.
84. Douglass JA*, et al.* (1992) Myopathy in severe asthma. *Am Rev Respir Dis* 146(2):517-519.
85. Leatherman JW, Fluegel WL, David WS, Davies SF, & Iber C (1996) Muscle weakness in mechanically ventilated patients with severe asthma. *Am J Respir Crit Care Med* 153(5):1686-1690.
86. Nava S*, et al.* (1996) Effects of acute steroid administration on ventilatory and peripheral muscles in rats. *Am J Respir Crit Care Med* 153(6 Pt 1):1888-1896.

87. Gayan-Ramirez G, Vanzeir L, Wuytack F, & Decramer M (2000) Corticosteroids decrease mRNA levels of SERCA pumps, whereas they increase sarcolipin mRNA in the rat diaphragm. *J Physiol* 524 Pt 2:387-397.
88. Schneider JS*, et al.* (2013) Increased sarcolipin expression and decreased sarco(endo)plasmic reticulum Ca2+ uptake in skeletal muscles of mouse models of Duchenne muscular dystrophy. *J Muscle Res Cell Motil* 34(5-6):349-356.
89. Nakagawa O*, et al.* (2005) Centronuclear myopathy in mice lacking a novel muscle-specific protein kinase transcriptionally regulated by MEF2. *Genes Dev* 19(17):2066-2077.
90. Liu N*, et al.* (2011) Mice lacking microRNA 133a develop dynamin 2-dependent centronuclear myopathy. *J Clin Invest* 121(8):3258-3268.
91. Calvo AC*, et al.* (2012) Genetic biomarkers for ALS disease in transgenic SOD1(G93A) mice. *PLoS One* 7(3):e32632.
92. Osborne RJ*, et al.* (2009) Transcriptional and post-transcriptional impact of toxic RNA in myotonic dystrophy. *Hum Mol Genet* 18(8):1471-1481.
93. Campanaro S*, et al.* (2002) Gene expression profiling in dysferlinopathies using a dedicated muscle microarray. *Hum Mol Genet* 11(26):3283-3298.
94. Sciote JJ & Kentish JC (1996) Unloaded shortening velocities of rabbit masseter muscle fibres expressing skeletal or alpha-cardiac myosin heavy chains. *J Physiol* 492 (Pt 3):659-667.
95. Pattison JS*, et al.* (2008) Phospholamban overexpression in transgenic rabbits. *Transgenic Res* 17(2):157-170.
96. Bloemberg D & Quadrilatero J (2012) Rapid determination of myosin heavy chain expression in rat, mouse, and human skeletal muscle using multicolor immunofluorescence analysis. *PLoS One* 7(4):e35273.
97. MacLennan DH & Kranias EG (2003) Phospholamban: a crucial regulator of cardiac contractility. *Nat Rev Mol Cell Biol* 4(7):566-577.
98. Young HS, Ceholski DK, & Trieber CA (2015) Deception in simplicity: hereditary phospholamban mutations in dilated cardiomyopathy. *Biochemistry and cell biology = Biochimie et biologie cellulaire* 93(1):1-7.
99. Gamu D, Bombardier E, Smith IC, Fajardo VA, & Tupling AR (2014) Sarcolipin provides a novel muscle-based mechanism for adaptive thermogenesis. *Exercise and sport sciences reviews* 42(3):136-142.
100. Rindt H, Gulick J, Knotts S, Neumann J, & Robbins J (1993) In vivo analysis of the murine beta-myosin heavy chain gene promoter. *J Biol Chem* 268(7):5332-5338.
101. Knotts S, Rindt H, Neumann J, & Robbins J (1994) In vivo regulation of the mouse beta myosin heavy chain gene. *J Biol Chem* 269(49):31275-31282.
102. Rindt H, Knotts S, & Robbins J (1995) Segregation of cardiac and skeletal muscle-specific regulatory elements of the beta-myosin heavy chain gene. *Proc Natl Acad Sci U S A* 92(5):1540-1544.
103. Murphy RM, Verburg E, & Lamb GD (2006) Ca2+ activation of diffusible and bound pools of mu-calpain in rat skeletal muscle. *J Physiol* 576(Pt 2):595-612.
104. Dubowitz V, Sewry C, & Oldfors A (2013) *Muscle Biopsy: A Practical Approach* (Oxford : Saunders)4th Ed p 592.
105. Folker ES & Baylies MK (2013) Nuclear positioning in muscle development and disease. *Front Physiol* 4:363.

106. Charge SB & Rudnicki MA (2004) Cellular and molecular regulation of muscle regeneration. *Physiol Rev* 84(1):209-238.
107. DiMario JX, Uzman A, & Strohman RC (1991) Fiber regeneration is not persistent in dystrophic (MDX) mouse skeletal muscle. *Dev Biol* 148(1):314-321.
108. Grady RM*, et al.* (1997) Skeletal and cardiac myopathies in mice lacking utrophin and dystrophin: a model for Duchenne muscular dystrophy. *Cell* 90(4):729-738.
109. Sartore S, Gorza L, & Schiaffino S (1982) Fetal myosin heavy chains in regenerating muscle. *Nature* 298(5871):294-296.
110. Jungbluth H, Wallgren-Pettersson C, & Laporte J (2008) Centronuclear (myotubular) myopathy. *Orphanet J Rare Dis* 3:26.
111. Dowling JJ, Lawlor MW, & Dirksen RT (2014) Triadopathies: an emerging class of skeletal muscle diseases. *Neurotherapeutics : the journal of the American Society for Experimental NeuroTherapeutics* 11(4):773-785.
112. Laporte J*, et al.* (1996) A gene mutated in X-linked myotubular myopathy defines a new putative tyrosine phosphatase family conserved in yeast. *Nat Genet* 13(2):175-182.
113. Bitoun M*, et al.* (2005) Mutations in dynamin 2 cause dominant centronuclear myopathy. *Nat Genet* 37(11):1207-1209.
114. Bohm J*, et al.* (2014) Adult-onset autosomal dominant centronuclear myopathy due to BIN1 mutations. *Brain*.
115. Nicot AS*, et al.* (2007) Mutations in amphiphysin 2 (BIN1) disrupt interaction with dynamin 2 and cause autosomal recessive centronuclear myopathy. *Nat Genet* 39(9):1134-1139.
116. Wilmshurst JM*, et al.* (2010) RYR1 mutations are a common cause of congenital myopathies with central nuclei. *Ann Neurol* 68(5):717-726.
117. Jungbluth H*, et al.* (2007) Centronuclear myopathy due to a de novo dominant mutation in the skeletal muscle ryanodine receptor (RYR1) gene. *Neuromuscul Disord* 17(4):338-345.
118. Ceyhan-Birsoy O*, et al.* (2013) Recessive truncating titin gene, TTN, mutations presenting as centronuclear myopathy. *Neurology* 81(14):1205-1214.
119. Cowling BS*, et al.* (2014) Reducing dynamin 2 expression rescues X-linked centronuclear myopathy. *J Clin Invest* 124(3):1350-1363.
120. Cowling BS*, et al.* (2011) Increased expression of wild-type or a centronuclear myopathy mutant of dynamin 2 in skeletal muscle of adult mice leads to structural defects and muscle weakness. *Am J Pathol* 178(5):2224-2235.
121. Demonbreun AR & McNally EM (2014) Dynamin 2 the rescue for centronuclear myopathy. *J Clin Invest* 124(3):976-978.
122. Minamisawa S*, et al.* (2003) Mutation of the phospholamban promoter associated with hypertrophic cardiomyopathy. *Biochem Biophys Res Commun* 304(1):1-4.
123. Haghighi K*, et al.* (2006) A mutation in the human phospholamban gene, deleting arginine 14, results in lethal, hereditary cardiomyopathy. *Proc Natl Acad Sci U S A* 103(5):1388-1393.
124. Schmitt JP*, et al.* (2003) Dilated cardiomyopathy and heart failure caused by a mutation in phospholamban. *Science* 299(5611):1410-1413.

125. DeWitt MM, MacLeod HM, Soliven B, & McNally EM (2006) Phospholamban R14 deletion results in late-onset, mild, hereditary dilated cardiomyopathy. *J Am Coll Cardiol* 48(7):1396-1398.
126. Agrawal PB*, et al.* (2014) SPEG interacts with myotubularin, and its deficiency causes centronuclear myopathy with dilated cardiomyopathy. *American journal of human genetics* 95(2):218-226.
127. Gal A*, et al.* (2015) The coexistence of dynamin 2 mutation and multiple mitochondrial DNA (mtDNA) deletions in the background of severe cardiomyopathy and centronuclear myopathy. *Clinical neuropathology* 34(2):89-95.
128. Al-Qusairi L & Laporte J (2011) T-tubule biogenesis and triad formation in skeletal muscle and implication in human diseases. *Skelet Muscle* 1(1):26.
129. Al-Qusairi L*, et al.* (2009) T-tubule disorganization and defective excitation-contraction coupling in muscle fibers lacking myotubularin lipid phosphatase. *Proc Natl Acad Sci U S A* 106(44):18763-18768.
130. Gibbs EM, Davidson AE, Telfer WR, Feldman EL, & Dowling JJ (2014) The myopathy-causing mutation DNM2-S619L leads to defective tubulation in vitro and in developing zebrafish. *Dis Model Mech* 7(1):157-161.
131. Anderson DM*, et al.* (2015) A Micropeptide Encoded by a Putative Long Noncoding RNA Regulates Muscle Performance. *Cell*.
132. Mazala DA*, et al.* (2015) SERCA1 overexpression minimizes skeletal muscle damage in dystrophic mouse models. *Am J Physiol Cell Physiol*:ajpcell 00341 02014.
133. Horowitz JD, Rosenson RS, McMurray JJ, Marx N, & Remme WJ (2011) Clinical Trials Update AHA Congress 2010. *Cardiovascular drugs and therapy / sponsored by the International Society of Cardiovascular Pharmacotherapy* 25(1):69-76.
134. Jessup M*, et al.* (2011) Calcium Upregulation by Percutaneous Administration of Gene Therapy in Cardiac Disease (CUPID): a phase 2 trial of intracoronary gene therapy of sarcoplasmic reticulum Ca2+-ATPase in patients with advanced heart failure. *Circulation* 124(3):304-313.
135. Zsebo K*, et al.* (2014) Long-term effects of AAV1/SERCA2a gene transfer in patients with severe heart failure: analysis of recurrent cardiovascular events and mortality. *Circ Res* 114(1):101-108.
136. Tarnopolsky MA, Pearce E, Smith K, & Lach B (2011) Suction-modified Bergstrom muscle biopsy technique: experience with 13,500 procedures. *Muscle Nerve* 43(5):717-725.
137. Duhamel TA*, et al.* (2007) Muscle metabolic, SR Ca(2+) -cycling responses to prolonged cycling, with and without glucose supplementation. *J Appl Physiol (1985)* 103(6):1986-1998.
138. Tupling R & Green H (2002) Silver ions induce Ca2+ release from the SR in vitro by acting on the Ca2+ release channel and the Ca2+ pump. *J Appl Physiol (1985)* 92(4):1603-1610.
139. Zubrzycka-Gaarn E, MacDonald G, Phillips L, Jorgensen AO, & MacLennan DH (1984) Monoclonal antibodies to the Ca2+ + Mg2+-dependent ATPase of sarcoplasmic reticulum identify polymorphic forms of the enzyme and indicate the presence in the enzyme of a classical high-affinity Ca2+ binding site. *J Bioenerg Biomembr* 16(5-6):441-464.

140. Schiaffino S*, et al.* (1989) Three myosin heavy chain isoforms in type 2 skeletal muscle fibres. *J Muscle Res Cell Motil* 10(3):197-205.
141. Lucas CA, Kang LH, & Hoh JF (2000) Monospecific antibodies against the three mammalian fast limb myosin heavy chains. *Biochem Biophys Res Commun* 272(1):303-308.
142. Nguyen thi M*, et al.* (1990) Monoclonal antibodies against defined regions of the muscular dystrophy protein, dystrophin. *FEBS Lett* 262(2):237-240.
143. McMillan EM & Quadrilatero J (2011) Differential apoptosis-related protein expression, mitochondrial properties, proteolytic enzyme activity, and DNA fragmentation between skeletal muscles. *Am J Physiol Regul Integr Comp Physiol* 300(3):R531-543.
144. Bloemberg D, McDonald E, Dulay D, & Quadrilatero J (2014) Autophagy is altered in skeletal and cardiac muscle of spontaneously hypertensive rats. *Acta Physiol (Oxf)* 210(2):381-391.
145. Szasz G, Gruber W, & Bernt E (1976) Creatine kinase in serum: 1. Determination of optimum reaction conditions. *Clin Chem* 22(5):650-656.
146. Lannergren J, Bruton JD, & Westerblad H (2000) Vacuole formation in fatigued skeletal muscle fibres from frog and mouse: effects of extracellular lactate. *J Physiol* 526 Pt 3:597-611.
147. Smith BK, Goddard M, & Childers MK (2014) Respiratory assessment in centronuclear myopathies. *Muscle Nerve* 50(3):315-326.
148. Schiaffino S & Serrano A (2002) Calcineurin signaling and neural control of skeletal muscle fiber type and size. *Trends in pharmacological sciences* 23(12):569-575.
149. Rumi-Masante J*, et al.* (2012) Structural basis for activation of calcineurin by calmodulin. *J Mol Biol* 415(2):307-317.
150. Olson EN & Williams RS (2000) Remodeling muscles with calcineurin. *BioEssays : news and reviews in molecular, cellular and developmental biology* 22(6):510-519.
151. Michel RN, Dunn SE, & Chin ER (2004) Calcineurin and skeletal muscle growth. *The Proceedings of the Nutrition Society* 63(2):341-349.
152. Dolmetsch RE, Lewis RS, Goodnow CC, & Healy JI (1997) Differential activation of transcription factors induced by Ca2+ response amplitude and duration. *Nature* 386(6627):855-858.
153. Flanagan WM, Corthesy B, Bram RJ, & Crabtree GR (1991) Nuclear association of a T-cell transcription factor blocked by FK-506 and cyclosporin A. *Nature* 352(6338):803-807.
154. Chin ER*, et al.* (1998) A calcineurin-dependent transcriptional pathway controls skeletal muscle fiber type. *Genes Dev* 12(16):2499-2509.
155. Dunn SE, Burns JL, & Michel RN (1999) Calcineurin is required for skeletal muscle hypertrophy. *J Biol Chem* 274(31):21908-21912.
156. Musaro A, McCullagh KJ, Naya FJ, Olson EN, & Rosenthal N (1999) IGF-1 induces skeletal myocyte hypertrophy through calcineurin in association with GATA-2 and NF-ATc1. *Nature* 400(6744):581-585.
157. Dunn SE, Chin ER, & Michel RN (2000) Matching of calcineurin activity to upstream effectors is critical for skeletal muscle fiber growth. *J Cell Biol* 151(3):663-672.

158. Ehlers ML, Celona B, & Black BL (2014) NFATc1 controls skeletal muscle fiber type and is a negative regulator of MyoD activity. *Cell reports* 8(6):1639-1648.
159. Shen T, Cseresnyes Z, Liu Y, Randall WR, & Schneider MF (2007) Regulation of the nuclear export of the transcription factor NFATc1 by protein kinases after slow fibre type electrical stimulation of adult mouse skeletal muscle fibres. *J Physiol* 579(Pt 2):535-551.
160. Liu Y, Cseresnyes Z, Randall WR, & Schneider MF (2001) Activity-dependent nuclear translocation and intranuclear distribution of NFATc in adult skeletal muscle fibers. *J Cell Biol* 155(1):27-39.
161. Tothova J*, et al.* (2006) NFATc1 nucleocytoplasmic shuttling is controlled by nerve activity in skeletal muscle. *Journal of cell science* 119(Pt 8):1604-1611.
162. Fajardo VA*, et al.* (2015) Phospholamban overexpression in mice causes a centronuclear myopathy-like phenotype. *Dis Model Mech*.
163. Green HJ, Reichmann H, & Pette D (1984) Inter- and intraspecies comparisons of fibre type distribution and of succinate dehydrogenase activity in type I, IIA and IIB fibres of mammalian diaphragms. *Histochemistry* 81(1):67-73.
164. Talmadge RJ*, et al.* (2004) Calcineurin activation influences muscle phenotype in a muscle-specific fashion. *BMC Cell Biol* 5:28.
165. Mendez J K, A (1960) Density and composition of mammalian muscle. *Metabolism* 9:184-188.
166. Buj-Bello A*, et al.* (2002) The lipid phosphatase myotubularin is essential for skeletal muscle maintenance but not for myogenesis in mice. *Proc Natl Acad Sci U S A* 99(23):15060-15065.
167. Odermatt A*, et al.* (1998) Sarcolipin regulates the activity of SERCA1, the fast-twitch skeletal muscle sarcoplasmic reticulum Ca2+-ATPase. *J Biol Chem* 273(20):12360-12369.
168. Timmerman LA, Clipstone NA, Ho SN, Northrop JP, & Crabtree GR (1996) Rapid shuttling of NF-AT in discrimination of Ca2+ signals and immunosuppression. *Nature* 383(6603):837-840.
169. Semsarian C*, et al.* (1999) Skeletal muscle hypertrophy is mediated by a Ca2+-dependent calcineurin signalling pathway. *Nature* 400(6744):576-581.
170. Frey N*, et al.* (2008) Calsarcin-2 deficiency increases exercise capacity in mice through calcineurin/NFAT activation. *J Clin Invest* 118(11):3598-3608.
171. Polla B, D'Antona G, Bottinelli R, & Reggiani C (2004) Respiratory muscle fibres: specialisation and plasticity. *Thorax* 59(9):808-817.
172. Chin ER (2005) Role of Ca2+/calmodulin-dependent kinases in skeletal muscle plasticity. *J Appl Physiol (1985)* 99(2):414-423.
173. Bigard X*, et al.* (2000) Calcineurin Co-regulates contractile and metabolic components of slow muscle phenotype. *J Biol Chem* 275(26):19653-19660.
174. Selsby JT, Morine KJ, Pendrak K, Barton ER, & Sweeney HL (2012) Rescue of dystrophic skeletal muscle by PGC-1alpha involves a fast to slow fiber type shift in the mdx mouse. *PLoS One* 7(1):e30063.
175. Chakkalakal JV*, et al.* (2004) Stimulation of calcineurin signaling attenuates the dystrophic pathology in mdx mice. *Hum Mol Genet* 13(4):379-388.

176. Chakkalakal JV*, et al.* (2003) Expression of utrophin A mRNA correlates with the oxidative capacity of skeletal muscle fiber types and is regulated by calcineurin/NFAT signaling. *Proc Natl Acad Sci U S A* 100(13):7791-7796.
177. Chakkalakal JV, Michel SA, Chin ER, Michel RN, & Jasmin BJ (2006) Targeted inhibition of Ca2+ /calmodulin signaling exacerbates the dystrophic phenotype in mdx mouse muscle. *Hum Mol Genet* 15(9):1423-1435.
178. Stupka N, Michell BJ, Kemp BE, & Lynch GS (2006) Differential calcineurin signalling activity and regeneration efficacy in diaphragm and limb muscles of dystrophic mdx mice. *Neuromuscul Disord* 16(5):337-346.
179. Stupka N, Schertzer JD, Bassel-Duby R, Olson EN, & Lynch GS (2007) Calcineurin-A alpha activation enhances the structure and function of regenerating muscles after myotoxic injury. *Am J Physiol Regul Integr Comp Physiol* 293(2):R686-694.
180. Stupka N, Schertzer JD, Bassel-Duby R, Olson EN, & Lynch GS (2008) Stimulation of calcineurin Aalpha activity attenuates muscle pathophysiology in mdx dystrophic mice. *Am J Physiol Regul Integr Comp Physiol* 294(3):R983-992.
181. Long YC, Glund S, Garcia-Roves PM, & Zierath JR (2007) Calcineurin regulates skeletal muscle metabolism via coordinated changes in gene expression. *J Biol Chem* 282(3):1607-1614.
182. Sandri M*, et al.* (2006) PGC-1alpha protects skeletal muscle from atrophy by suppressing FoxO3 action and atrophy-specific gene transcription. *Proc Natl Acad Sci U S A* 103(44):16260-16265.
183. Abbott KL, Friday BB, Thaloor D, Murphy TJ, & Pavlath GK (1998) Activation and cellular localization of the cyclosporine A-sensitive transcription factor NF-AT in skeletal muscle cells. *Molecular biology of the cell* 9(10):2905-2916.
184. Maurya SK*, et al.* (2015) Sarcolipin Is a Key Determinant of the Basal Metabolic Rate, and Its Overexpression Enhances Energy Expenditure and Resistance against Diet-induced Obesity. *J Biol Chem* 290(17):10840-10849.
185. Paran CW*, et al.* (2015) Reduced efficiency of sarcolipin-dependent respiration in myocytes from humans with severe obesity. *Obesity* 23(7):1440-1449.
186. Liu YW, Lukiyanchuk V, & Schmid SL (2011) Common membrane trafficking defects of disease-associated dynamin 2 mutations. *Traffic* 12(11):1620-1633.
187. Fajardo VA*, et al.* (2015) Phospholamban overexpression in mice causes a centronuclear myopathy-like phenotype. *Dis Model Mech* 8(8):999-1009.
188. Ito N, Ruegg UT, Kudo A, Miyagoe-Suzuki Y, & Takeda S (2013) Activation of calcium signaling through Trpv1 by nNOS and peroxynitrite as a key trigger of skeletal muscle hypertrophy. *Nat Med* 19(1):101-106.
189. Briguet A, Courdier-Fruh I, Foster M, Meier T, & Magyar JP (2004) Histological parameters for the quantitative assessment of muscular dystrophy in the mdx-mouse. *Neuromuscul Disord* 14(10):675-682.
190. Baker JH & Poindextor CE (1991) Muscle regeneration following segmental necrosis in tenotomized muscle fibers. *Muscle Nerve* 14(4):348-357.
191. McMinn RM & Vrbova G (1964) The Effect of Tenotomy on the Structure of Fast and Slow Muscle in the Rabbit. *Quarterly journal of experimental physiology and cognate medical sciences* 49:424-429.

192. Shenkman BS & Nemirovskaya TL (2008) Calcium-dependent signaling mechanisms and soleus fiber remodeling under gravitational unloading. *J Muscle Res Cell Motil* 29(6-8):221-230.
193. Radley-Crabb HG, Fiorotto ML, & Grounds MD (2011) The different impact of a high fat diet on dystrophic mdx and control C57Bl/10 mice. *PLoS currents* 3:RRN1276.
194. McPherron AC & Lee SJ (2002) Suppression of body fat accumulation in myostatin-deficient mice. *J Clin Invest* 109(5):595-601.
195. Guo T*, et al.* (2009) Myostatin inhibition in muscle, but not adipose tissue, decreases fat mass and improves insulin sensitivity. *PLoS One* 4(3):e4937.
196. Hamrick MW, Pennington C, Webb CN, & Isales CM (2006) Resistance to body fat gain in 'double-muscled' mice fed a high-fat diet. *International journal of obesity* 30(5):868-870.
197. Argiles JM, Busquets S, Stemmler B, & Lopez-Soriano FJ (2015) Cachexia and sarcopenia: mechanisms and potential targets for intervention. *Curr Opin Pharmacol* 22:100-106.
198. Drescher C, Konishi M, Ebner N, & Springer J (2015) Loss of muscle mass: Current developments in cachexia and sarcopenia focused on biomarkers and treatment. *Int J Cardiol* 202:766-772.
199. Dowling JJ*, et al.* (2009) Loss of myotubularin function results in T-tubule disorganization in zebrafish and human myotubular myopathy. *PLoS Genet* 5(2):e1000372.
200. Cowling BS, Toussaint A, Muller J, & Laporte J (2012) Defective membrane remodeling in neuromuscular diseases: insights from animal models. *PLoS Genet* 8(4):e1002595.
201. Praefcke GJ & McMahon HT (2004) The dynamin superfamily: universal membrane tubulation and fission molecules? *Nat Rev Mol Cell Biol* 5(2):133-147.
202. Chin YH*, et al.* (2015) Dynamin-2 mutations associated with centronuclear myopathy are hypermorphic and lead to T-tubule fragmentation. *Hum Mol Genet* 24(19):5542-5554.
203. Durieux AC*, et al.* (2010) A centronuclear myopathy-dynamin 2 mutation impairs skeletal muscle structure and function in mice. *Hum Mol Genet* 19(24):4820-4836.
204. Taghibiglou C*, et al.* (2009) Role of NMDA receptor-dependent activation of SREBP1 in excitotoxic and ischemic neuronal injuries. *Nat Med* 15(12):1399-1406.
205. Thorpe LM, Yuzugullu H, & Zhao JJ (2015) PI3K in cancer: divergent roles of isoforms, modes of activation and therapeutic targeting. *Nat Rev Cancer* 15(1):7-24.
206. Al-Qusairi L*, et al.* (2013) Lack of myotubularin (MTM1) leads to muscle hypotrophy through unbalanced regulation of the autophagy and ubiquitin-proteasome pathways. *FASEB J* 27(8):3384-3394.
207. Fetalvero KM*, et al.* (2013) Defective autophagy and mTORC1 signaling in myotubularin null mice. *Mol Cell Biol* 33(1):98-110.
208. Teng AC*, et al.* (2015) Metformin increases degradation of phospholamban via autophagy in cardiomyocytes. *Proc Natl Acad Sci U S A* 112(23):7165-7170.
209. Zhao XS, Gallardo TD, Lin L, Schageman JJ, & Shohet RV (2002) Transcriptional mapping and genomic analysis of the cardiac atria and ventricles. *Physiol Genomics* 12(1):53-60.

210. Potthoff MJ, *et al.* (2007) Histone deacetylase degradation and MEF2 activation promote the formation of slow-twitch myofibers. *J Clin Invest* 117(9):2459-2467.
211. Mao Z & Wiedmann M (1999) Calcineurin enhances MEF2 DNA binding activity in calcium-dependent survival of cerebellar granule neurons. *J Biol Chem* 274(43):31102-31107.
212. Li J, Vargas MA, Kapiloff MS, & Dodge-Kafka KL (2013) Regulation of MEF2 transcriptional activity by calcineurin/mAKAP complexes. *Experimental cell research* 319(4):447-454.
213. Wu H, *et al.* (2001) Activation of MEF2 by muscle activity is mediated through a calcineurin-dependent pathway. *EMBO J* 20(22):6414-6423.
214. Wu H, *et al.* (2000) MEF2 responds to multiple calcium-regulated signals in the control of skeletal muscle fiber type. *EMBO J* 19(9):1963-1973.
215. Lu J, McKinsey TA, Nicol RL, & Olson EN (2000) Signal-dependent activation of the MEF2 transcription factor by dissociation from histone deacetylases. *Proc Natl Acad Sci U S A* 97(8):4070-4075.
216. Liu N, *et al.* (2014) Requirement of MEF2A, C, and D for skeletal muscle regeneration. *Proc Natl Acad Sci U S A* 111(11):4109-4114.
217. Tidball JG & Rinaldi C (2012) Chapter 63 - Immunological Responses to Muscle Injury. *Muscle*, ed Joseph H (Academic Press, Boston/Waltham), pp 899-909.
218. Zhao M, *et al.* (1999) Regulation of the MEF2 family of transcription factors by p38. *Mol Cell Biol* 19(1):21-30.
219. Fajardo VA, *et al.* (2015) Sarcoplasmic Reticulum Phospholipid Fatty Acid Composition and Sarcolipin Content in Rat Skeletal Muscle. *The Journal of membrane biology* 248(6):1089-1096.
220. Ballak SB, *et al.* (2015) Blunted hypertrophic response in old mouse muscle is associated with a lower satellite cell density and is not alleviated by resveratrol. *Experimental gerontology* 62:23-31.
221. Lee JD, *et al.* (2015) Aged Muscle Demonstrates Fiber-Type Adaptations in Response to Mechanical Overload, in the Absence of Myofiber Hypertrophy, Independent of Satellite Cell Abundance. *The journals of gerontology. Series A, Biological sciences and medical sciences*.
222. Oh M, *et al.* (2005) Calcineurin is necessary for the maintenance but not embryonic development of slow muscle fibers. *Mol Cell Biol* 25(15):6629-6638.
223. Horsley V & Pavlath GK (2003) Prostaglandin F2(alpha) stimulates growth of skeletal muscle cells via an NFATC2-dependent pathway. *J Cell Biol* 161(1):111-118.
224. Rosenblatt JD, Yong D, & Parry DJ (1994) Satellite cell activity is required for hypertrophy of overloaded adult rat muscle. *Muscle Nerve* 17(6):608-613.
225. Phelan JN & Gonyea WJ (1997) Effect of radiation on satellite cell activity and protein expression in overloaded mammalian skeletal muscle. *The Anatomical record* 247(2):179-188.
226. Horsley V, *et al.* (2001) Regulation of the growth of multinucleated muscle cells by an NFATC2-dependent pathway. *J Cell Biol* 153(2):329-338.
227. Sotiropoulos A, *et al.* (2006) Growth hormone promotes skeletal muscle cell fusion independent of insulin-like growth factor 1 up-regulation. *Proc Natl Acad Sci U S A* 103(19):7315-7320.

228. Rodriguez J*, et al.* (2014) Myostatin and the skeletal muscle atrophy and hypertrophy signaling pathways. *Cellular and molecular life sciences : CMLS* 71(22):4361-4371.
229. Sopariwala DH*, et al.* (2015) Sarcolipin overexpression improves muscle energetics and reduces fatigue. *J Appl Physiol (1985)* 118(8):1050-1058.
230. Dufresne S, Dumont, N., Piette, A., Fajardo, V.A., Gamu, D., Kake-Guena, S., David, R., Bouchard, P., Lavergne, E., Penninger, J., Pape, P., Tupling, A.R., Frenette, J. (Muscle RANK is a key regulator of calcium storage, SERCA activity, and function of fast-twitch skeletal muscles. *American Journal of Physiology.* In submission, Sept. 30, 2015(C-00285-2015R1).
231. Beals CR, Sheridan CM, Turck CW, Gardner P, & Crabtree GR (1997) Nuclear export of NF-ATc enhanced by glycogen synthase kinase-3. *Science* 275(5308):1930-1934.
232. Maurya SK & Periasamy M (2015) Sarcolipin is a novel regulator of muscle metabolism and obesity. *Pharmacol Res* 102:270-275.
233. Stupka N, Gregorevic P, Plant DR, & Lynch GS (2004) The calcineurin signal transduction pathway is essential for successful muscle regeneration in mdx dystrophic mice. *Acta Neuropathol* 107(4):299-310.
234. Horsley V, Jansen KM, Mills ST, & Pavlath GK (2003) IL-4 acts as a myoblast recruitment factor during mammalian muscle growth. *Cell* 113(4):483-494.
235. Williams RS, Caron MG, & Daniel K (1984) Skeletal muscle beta-adrenergic receptors: variations due to fiber type and training. *Am J Physiol* 246(2 Pt 1):E160-167.
236. Ferry A*, et al.* (2015) Mechanical Overloading Increases Maximal Force and Reduces Fragility in Hind Limb Skeletal Muscle from Mdx Mouse. *Am J Pathol* 185(7):2012-2024.
237. Shin JH, Hakim CH, Zhang K, & Duan D (2011) Genotyping mdx, mdx3cv, and mdx4cv mice by primer competition polymerase chain reaction. *Muscle Nerve* 43(2):283-286.
238. Grynkiewicz G, Poenie M, & Tsien RY (1985) A new generation of Ca2+ indicators with greatly improved fluorescence properties. *J Biol Chem* 260(6):3440-3450.
239. Inesi G & de Meis L (1989) Regulation of steady state filling in sarcoplasmic reticulum. Roles of back-inhibition, leakage, and slippage of the calcium pump. *J Biol Chem* 264(10):5929-5936.